FUJIFILM

ISSN : 0915-1478
CODEN : FFRDEK 55, 1-156 (2010)

FUJIFILM RESEARCH & DEVELOPMENT

No.55−2010

富士フイルム研究報告

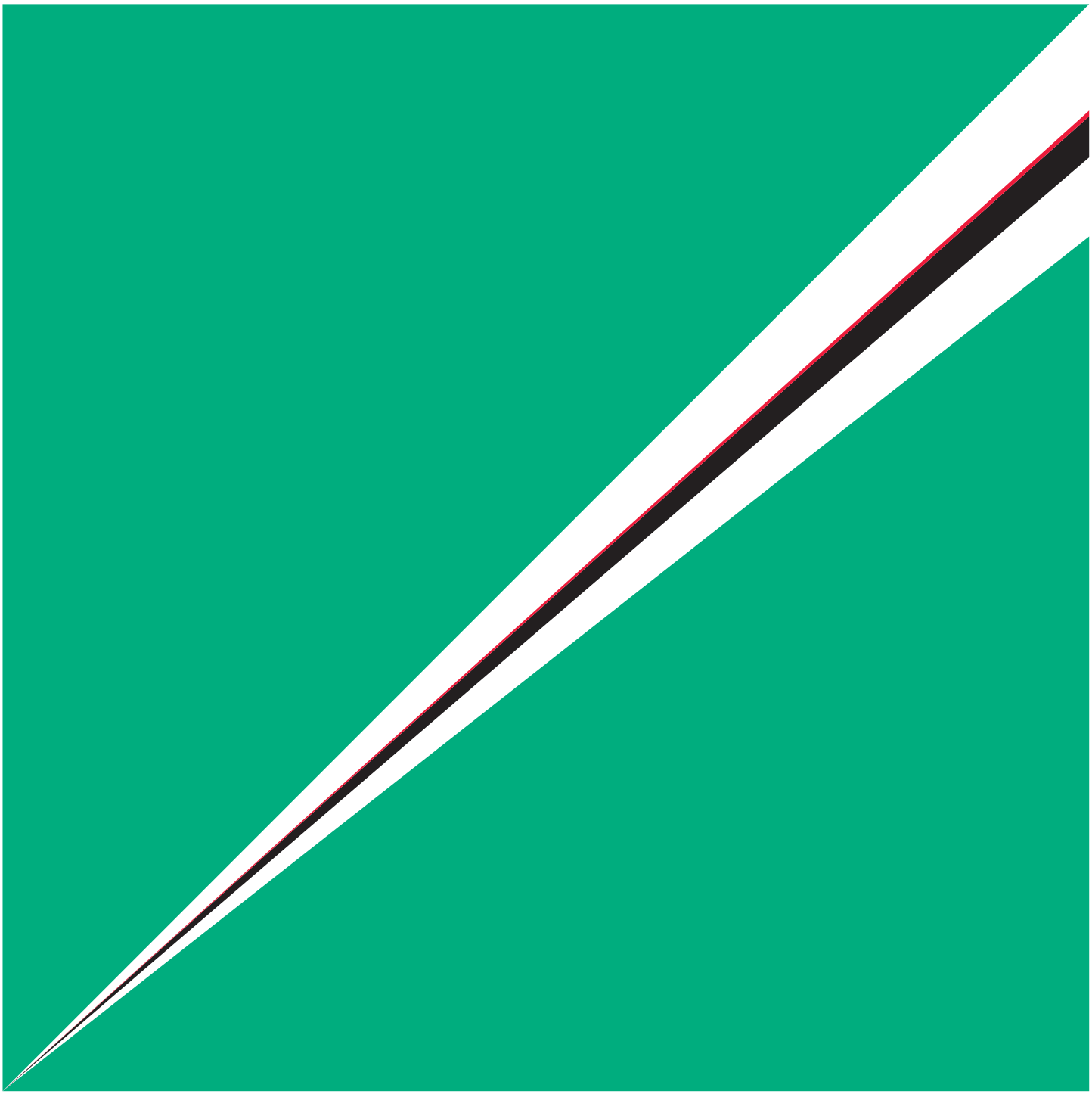

PURPOSE OF PUBLICATION

This publication incorporates the results of research and development carried on in the laboratories and subsidiaries of FUJIFILM Corporation. It includes papers and reviews related to imaging technologies such as silver halide photographic materials, printing materials and electronic cameras, data recording technologies such as magnetic recording media and optical discs, organic material design technologies such as materials for display and electronic device, optical design technologies, medical and life science technoligies, information system and software development techinologies, and so on. Original papers submitted to this journal are published in the Japanese language with an opening English language abstract, and papers which have already been printed in other scientific journals are reproduced from said journals in unmodified form. After the main texts listed are printed papers which have been found in the JDreamII-JSTPlus file and our company's own file until November, 2009.

Editorial policy intends that content be accurately provided to the reader. Indulgence is begged for character usage and entry methodologies in materials not directly related to the subject at hand which may result in some lack of unity in expression.

Published by Intellectual Property Administration Group,
Intellectual Property Division,
Research & Development Management Headquarters,
FUJIFILM Corporation
Minamiashigara, Kanagawa 250-0193 Japan

FOREWORD

Nobuaki Inoue
Director, Executive Vice President,
General Manager,
R&D Management Headquarters
FUJIFILM Corporation

As the collapse of Lehman in September 2008 triggered a worldwide recession, the economies of Japan and many other developed countries in North America and Europe were hit hard in fiscal 2009. Although there are some signs of recovery, they are not yet definite. Even if the economies recover, experts predict, existing businesses in advanced countries will not be able to restore the previous level due to shrinking demand.

To conquer the unfavorable environment and put the business back onto a growth path, the entire company, research and development (R&D), production and sales, must seek innovation. Especially, innovation in R&D, which creates new values (new products), means a lot. We have divided our mid-term and long-term growth fields into three categories. FUJIFILM Group will put all-out efforts to R&D for these categories. The first category is imaging and printing, such as digital photography, graphics and documenting, and the medical field, such as diagnostic radiography. We aim to keep providing high-value added products and services that keep up with the progress in digital and information technology. The second category is the pharmaceutical and health care. We define them as growth fields in the future and aim to foster this category and ensure the growth in the future. The third category is highly functional materials. We aim to focus on this field to create new businesses like the optical films for LCD by further enhancing our organic material technology we have developed for silver halide photography, film forming technology and thin film coating technology.

Success of Japanese businesses has mostly come from developed countries and the wealthy people in emerging countries. Japan has fallen behind Korea and China in emerging countries, such as BRICs, which are huge markets. In developed countries, Japan is now much less competitive in the fields of flat panel TV, cell phones and other electronic products, which once were Japan's specialties. People are seriously debating "Why does Japan, superior in technology, lose in business?" (written by Kenichiro Senoo). The importance of building a business model is drawing attention. For example, Japanese manufacturers are still keeping an overwhelming competitive edge in semiconductor materials essential for production of electronic devices, e.g., wafers and resists, and highly functional materials making up devices for LCD, e.g., optical films. The progress in those devices is continuing to create market needs. We will try to detect market potential needs early and create new businesses in the highly functional material field.

Innovation in a corporate R&D is said to be successful only when it provides society with added values that lead to growth of the company (economic success). People say that what is required for a creative person to become more creative is an environment where many different diversified people and things meet. FUJIFILM Advanced Research Laboratories, established to "put our heads together and create something new", are a community of scientists and engineers with expertise in diversified fields. The laboratories provide an environment where these experts can enhance their creativity further and strive to accomplish innovation. Now, humans are facing various problems, namely the environmental disruption, depletion of fossil fuel, aging society and pandemic diseases. Our corporate philosophy says, "We will use leading-edge, proprietary technologies to help enhance the quality of life of people worldwide". We will pay attention to these problems and help solve them.

FUJIFILM RESEARCH & DEVELOPMENT

No. 55

CONTENTS

Originals

* Co-researcher outside FUJIFILM Corporation

UDC 621.397.422+778.42+771.315

Development of "3D Digital Camera System"

Hirofumi HORII*, Koichi TANAKA*, Kazuya ODA*,
Hitoshi SATO*, and Toru NISHIMURA*

Abstract

FUJIFILM has developed revolutionary 3D digital imaging system "FINEPIX REAL 3D system". The system incorporates a 3D digital camera "FINEPIX REAL 3D W1", a 3D viewer "FINEPIX REAL 3D V1", and 3D printing service. The FINEPIX REAL 3D W1 has two 10 megapixel CCDs, two 3× optical zoom lenses, newly developed 2D/3D LCD monitor (2.8inch), and newly developed 3D processor "Real Photo Processor 3D". The camera can take both 3D still images and movies by just pressing the shutter button, and allows you to view the 3D images on the LCD monitor without special glasses. Everyone can enjoy high-quality 3D still images and movies with this camera.

1. Introduction

The history of 3D vision technology is old and surprisingly it dates back to the early 19th century, about the same time as the daguerreotype was invented. Some trace the origin of 3D vision technology back to the stereoscope invented by a British scientist Sir Charles Wheatstone in 1838. The stereoscope provides different images to the left and right eyes using mirrors. The process uses the so-called "binocular parallax". Basically, the principle is the same as that of the present technology.

Over a hundred and several tens of years since the invention of the stereoscope, buffs have enjoyed 3D display technology with silver halide photography or 3D movies, and the 3D display technology development has been accelerated dramatically in the 21st century. These days we hear about 3D very often. Commercial 3D PC displays and mobile phones have been launched. BS channels have started broadcasting 3D programs. A new HDMI standard, HDMI 1.4, has been established to support 3D broadcasting. Electronics companies have announced their launch of 3D TVs and 3D recorders. People say the age of 3D vision is dawning.

Our company has been working on 3D technology development for some time. In the mid 1990s, we launched a film with lens, "3D adapter for Utsurundesu (QuickSnap)", and "3D print viewer". We have also been tackling 3D technology development for digital camera since we started digital camera development. In 2007, when we concluded that the fundamental technology and the market were ready, we have decided to develop "FINEPIX REAL 3D system", the first of its kind in the world, aiming at creating and expanding a 3D market. In 2008, we announced the technology at the Photokina. In summer 2009, we launched the new system. The conceptual diagram of this system is shown in Fig. 1.

This 3D system consists of three products: 3D digital camera W1, a 3D photo viewer V1, and 3D print service. The system allows the user to take a picture, view the image, and keep it on paper. It allows the user to enjoy 3D vision without special skills. Since its launch, the system has been well received both at home and abroad. This report describes FINEPIX REAL 3D W1, a 3D camera and viewer all in one.

Fig. 1 FINEPIX REAL 3D system.

Original paper (Received December 29, 2009)
* Electronic Imaging Products Development Center
Research & Development Management Headquarters
FUJIFILM Corporation
Matsusakadaira Taiwa-cho, Kurokawa-gun, Miyagi
981-3496, Japan

2. FINEPIX REAL 3D system

This section provides (1) the appearance, (2) main specifications, (3) block diagram and (4) features of the W1 camera.

2.1 Main Specifications of the Camera

The main specifications are shown in Table 1. As the storage format, the Multi Picture Format established by CIPA for still images was adopted. For movie images, the widely-used AVI, expending it for 3D was adopted.

Table 1 Specifications of FINEPIX REAL 3D W1.

Item	Specifications
Model	FINEPIX REAL 3D W1
Shooting element	1/2.3-inch CCD with 10 million pixels × 2
3D storage format	Still image : Multi Picture Format [MPO+JPEG], [MPO] Movie : Stereo AVI with 2 image channels
Lens	Fujinon 3× optical zoom lens × 2 Equivalent to foal length of 35 mm to 105 mm
Shooting distance	[2D] Approximately 8 cm to infinity [3D] Approximately 60 cm to infinity
Recommended 3D shooting distance	[Wide] 1.3 m to infinity [Telephoto] 4.1 m to infinity
LCD monitor	2.8-inch 3D/2D color LCD with light direction control, Approximately 230,000 dots (Approximately 100% coverage)
Number of movie recording pixels	VGA (640 × 480) / QVGA (320 × 240)
Photography functions	[2D] Face detection, red-eye removal, and more [3D] Auto parallax control, and more
Playback functions	[2D] Face detection, red-eye removal, and more [3D] Parallax adjustment, and more
Number of shots	230 shots for 3D (compliant with CIPA)
Dimensions	123.6 × 68.0 × 25.6 mm
Weight	Approximately 300 g (including battery and memory)

Other specifications:
http://fujifilm.jp/personal/3d/camera/finepixreal3dW1/index.html

2.2 Appearance

The camera has two (left and right) lens units spaced 77 mm apart on the front. Under the units is a slide barrier used as the lens cover and the power switch. On the back of the camera is the naked-eye stereoscopic LCD in the center flanked by operation keys. The 3D-related keys, i.e., 3D/2D button and parallax control button, are all placed on the left.

Fig. 2 System configuration of FINEPIX REAL 3D W1.

2.3 Block Diagram

The shooting system consists of two lens units comprising Fujinon 3× optical zoom lens and 10 M-pixel CCD. The signal processor has the Real Photo Engine 3D that receives image data from the left and right lens units and process the data to merge the two images into a 3D image. The display unit is the 2D/3D LCD with light direction control. Showing different images to the left and right eyes creates the perception of depth.

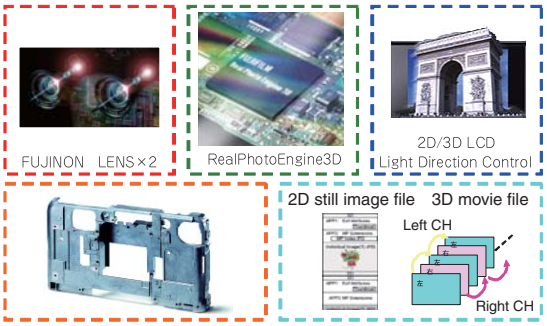

Fig. 3 Key technologies of FINEPIX REAL 3D W1.

2.4 Features of FINEPIX REAL 3D W1

The W1 has two main features. One is the easiness to shoot images in 3D and view them in 3D. It does not require special skills. The other is the capability of shooting 3D images of subjects close to or far from the camera, which is difficult just by shooting with two lenses.

(1) It is easy to shoot and view 3D images.

In the past, shooting and viewing 3D images required a lot of equipment and highly advanced techniques. We wanted every one to enjoy 3D images. And we came up with the W1. The W1 does not require any complicated setting or technique. Just pressing the release button, the camera automatically sets itself into the optimum conditions and the user can easily take a 3D still image or movie. The images can also be reviewed on the spot.

(2) The macro photography and landscape photography are capable of taken in 3D.

As binocular parallax is used, stereoscopy is not suitable for macro photography, in which the parallax is too large, or for landscape photography, in which the parallax is too small. In order to shoot such subjects, the W1 has the advanced 3D modes: the individual shutter 3D shooting and the interval 3D shooting. These modes allow the user to change the stereo base and expand possibilities of 3D shooting.

** 3D shooting of a subject in a close range is possible (Fig. 4)*

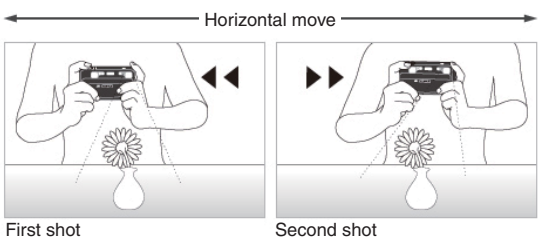

Fig. 4 Individual Shutter 3D Shooting (Macro photography).

The parallax is too large when a subject is close to the camera. The individual shutter 3D shooting allows the user to reduce the stereo base to several centimeters to enable 3D shooting of such subjects.

** 3D shooting of a subject in the distance is possible (Fig. 5)*

The parallax is too small when a subject is far from the camera. The individual shutter 3D shooting allows the user to increase the stereo base thereby enhancing the stereoscopic effect.

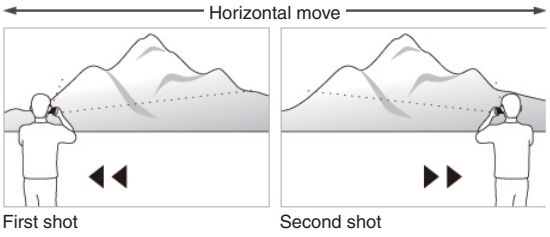

Fig. 5 Individual Shutter 3D Shooting (Landscape Photography).

3. Comfortable 3D Viewing[1)]

Although the W1 had many problems before put onto the market, we had especially the following major problems. This section describes what we did to solve these problems.

1) Binocular parallax control (parallax design and optical axis fixing)
2) Alignment of the property differences between right and left images
3) Development of a naked-eye 3D display monitor

3.1 Binocular Parallax Design

3.1.1 Parallax Design

The human mind perceives 3D by creating a feeling of depth based on such information as binocular parallax, motion parallax, binocular convergence and focal point (Fig. 6)[2)]. Among the information, the W1 uses binocular parallax (to produce a stereoscopic effect by displaying different 2D images to the right and left eyes) to provide a 3D image. Specifically, an object is shot at different angles with the right and left lenses. Those images are input to the right and left eyes separately to provide 3D vision.

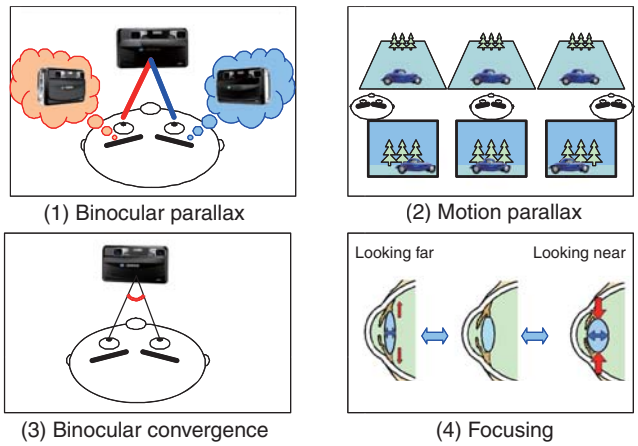

Fig. 6 Depth perception factors (Physiological factors).

How much an object looks protruding or distant varies according to the degree of parallax. Fig. 7 shows the outline.

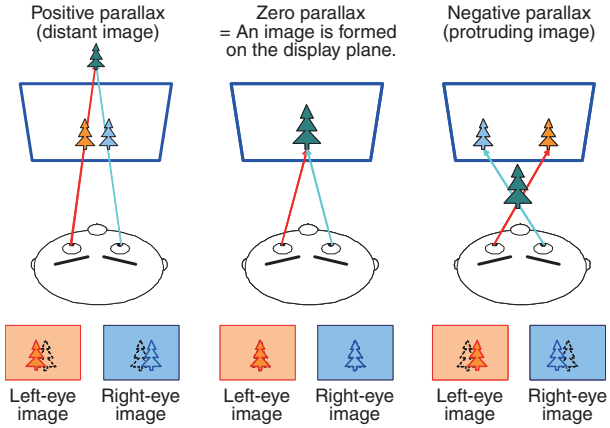

Fig. 7 Depth perception effects from binocular parallax.

When there is no parallax between the right and left eyes, the 3D image is formed on the display plane. When the object appears to the right in the left-eye image compared with the right-eye image, the 3D image is formed in front of the display surface. On the contrary, when the object appears to the left in the left-eye image compared with the right-eye image, the 3D image is formed behind the display surface. The larger the parallax becomes, the larger the depth or protrusion (stereoscopic effect) will be. But, there is a limit. If the parallax is too large or too small, the two images cannot be fused into a single 3D image (Fig. 8)[3)]. This often happens when objects in an image have vastly different parallaxes.

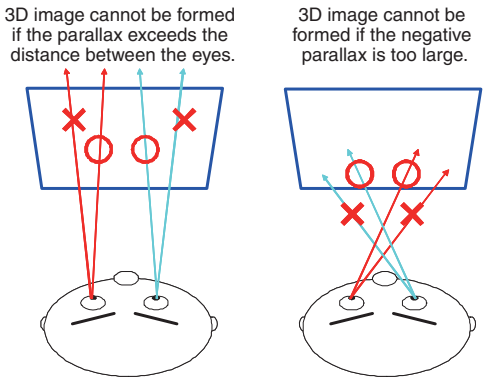

Fig. 8 Fusional limit of stereopsis.

Therefore, for maximum 3D effect, we want to increase the parallax. For eye-friendly image, we donot want the parallax to be too large. It is necessary to control the parallax to balance the 3D effect and the eye-friendliness. However, there are many factors that determine the parallax (Fig. 9). Considering these situation, we have thought of many occasions in which customers would use the camera and designed the parameters.

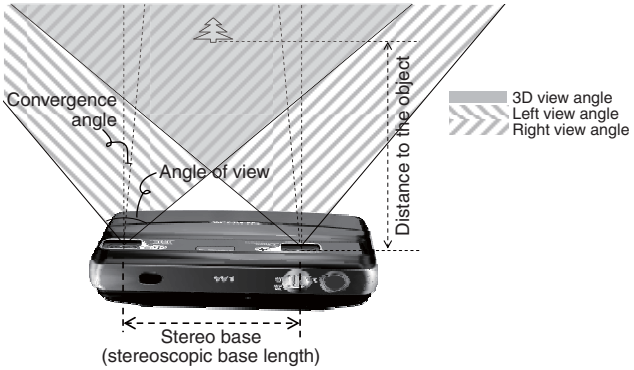

Fig. 9 Elements of binocular parallax.

3.1.2 Fixing Optical Axis

To produce comfortable 3D vision using binocular parallax, the optical axes of the right and left shooting systems must be aligned and kept stationary with high precision.

To solve the problem, the W1 employs (1) Fujinon lens fabricated with high precision, (2) an aluminum die-cast frame to keep the optical axes of the lenses stationary (Fig. 10) and (3) the highly advanced production technology to align the optical axes with high precision.

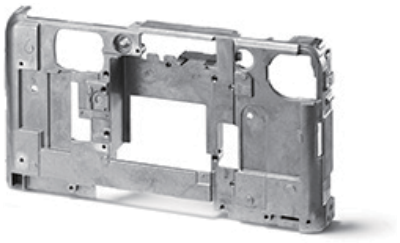

Fig. 10 Aluminum die casting to fix lenses firmly.

3.2 Two-lens Shooting

Property differences between right and left images, such as vertical parallax, time lag, differences in color and brightness, are major obstructive factors[3]. The W1 employs a new signal processor, “Real Photo Engine 3D”. The processor irons out the property differences. Time lag between right and left images distorts a 3D effect and often ruins 3D imaging. This problem was solved by fully synchronizing the right and left shooting units below microsecond for both still images and movies. Consequently this enables comfortable 3D viewing of live-view images, movies and images shot with flash.

3.3 Naked-eye 3D Display[4]

Because of the nature of a digital camera, it was essential to develop a 3D LCD that could be viewed by the naked eye. So we have developed the light direction control system LCD. This system has two backlights for left eye and right eye. These backlights blink alternately at high speed. In synchronization with the blinking, images for left eye and right eye are displayed alternately. To display a 2D image, the same image is provided to the right and left eyes. One of the features of the system is that the horizontal resolution does not have to be sacrificed to produce a 3D effect as the right and left images are displayed with time division. Fig. 11 and Fig. 12 show the conceptual diagrams.

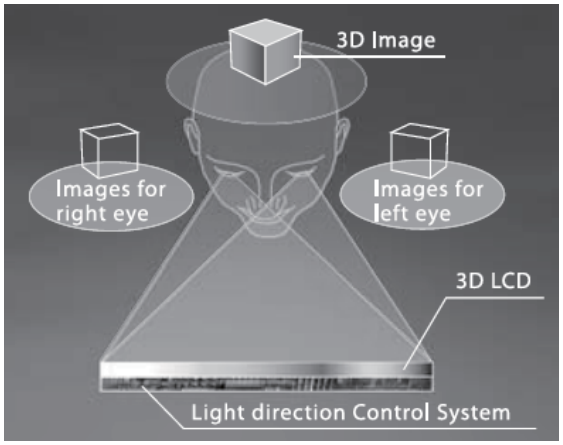

Fig. 11 Conceptual diagram of light direction control system.

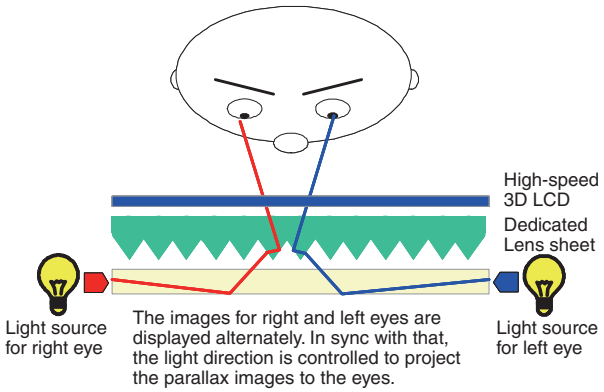

Fig. 12 Principle of operation of light direction control system.

4. Conclusion

We have worked on development of a digital camera easy to shoot and view a 3D image. Stereoscopic parallax control and elimination of property differences were two major problems. These problems were solved with our newly developed Real Photo Engine 3D and our high-precision production technology and lens technology. We finally succeeded in completing the W1 that provides comfortable viewing of 3D images. After 2010, it is expected that more and more 3D products, such as movies and TV, are spreading in the market. Making the most of the technology that enabled the development of the world's first 3D imaging system "FINEPIX REAL 3D system" and the knowledge gained through the development, we will continuously make our efforts to improve the system and to expand the market.

References

1) 3-D Display Technologies: New Trends of Space Expression. Honda, Toshio, supervising ed., Tokyo, CMC Publishing, 2008.
2) Inoue, Tetsuri. Introduction to 3-D imaging: Mechanism of 3-D imaging and applications, Rittai Expo'08 Technical Seminar, 2008-12-4.
3) 3D Consortium Safety Guidelines Subcommittee. Safety guidelines for the diffusion of human-friendly 3D (revised on 2008-12-1).
4) Horii, Horifumi. Development of 3D Digital Camera System. the 17th Camera Technology Seminar, Society of Photographic Science and Technology of Japan, 2009-11-20.

UDC 616-073.75+771.537+546.23

Development of High-image quality and High-durability Direct Conversion Digital Radiography System "FDR AcSelerate"

Hirotaka WATANO*, Fumito NARIYUKI*, Shinji IMAI**, Toshiyuki NABETA*, Yuichi HOSOI*, Tetsuya TSUJI*, Keita WATANABE*, Jun ENOMOTO*, and Masaru SATO*

Abstract

FUJIFILM's newly-developed "AcSelerate", a digital radiography system, simultaneously realizes high-image quality, low-dose image acquisition and highly improvement on durability. "AcSelerate" contains a new direct conversion detector using a fullerene (C_{60})-doped polymer layer added on a thick amorphous selenium (a-Se) layer coupled to an amorphous silicon thin film transistor (a-Si TFT) array. The C_{60}-doped polymer layer changes the electronic junction between a-Se and the electron-transporting layer smoothly, leading to the improved lag reduction characteristics. This polymer layer also improves the durability of the detector. The crystallization of a-Se which causes the pixel defects is drastically prevented by the polymer layer. With respect to low dose examination, the preview image is available on the Console Advance screen in only 2 seconds, allowing quick review of the image. Additionally, cycle time between exposures is approximately 4 seconds, allowing the technologist to work efficiently and make the process smoother for the patient. Moreover, "AcSelerate" can relieve the technologist of calibration work.

1. Introduction

We have succeeded in developing a new X-ray image detector. The detector "directly converts" the X-ray signals that have passed through a patient to electric signals using amorphous selenium (a-Se). The detector reads the electric signals using a-Si TFT to produce a digital image while keeping the high image quality which is characteristic of a direct-conversion a-Se detector. In addition, we have reduced the image lag and enhanced durability of a-Se semiconductor layer. The FDR AcSelerate (Fig. 1) equipped with this detector is a digital radiography system which realizes high image quality and low radiation dose, as well as high throughput. The background of development, the configuration, features of the system and the capabilities will be outlined in this report.

1.1 Background of Development

In recent years, more and more digital radiography (DR) systems are being used in the diagnostic radiography as a medical field is going digital. FUJIFILM pioneered digitalization of diagnostic X-ray imaging using computed radiography (CR). Since then, we have been providing digital diagnostic X-ray imaging systems. These systems are well received; existing X-ray systems can be easily digitized by combining with our digital products.

Fig. 1 System configuration of AcSelerate (FDR200).

Original paper (Received November 25, 2009)

* Medical Systems Research & Development Center
Research & Development Management Headquarters
FUJIFILM Corporation
Miyanodai, Kaisei-machi, Ashigarakami-gun, Kanagawa 258-8538, Japan

** Frontier Core-Technology Laboratories
Research & Development Management Headquarters
FUJIFILM Corporation
Ushijima, Kaisei-machi, Ashigarakami-gun, Kanagawa 258-8577, Japan

Compared with the conventional screen/film (S/F) system or CR system, digital radiography has a higher efficiency in X-ray use and that leads to high image quality and radiation dose reduction. Especially, the "direct-conversion" flat panel detector (FPD) using a-Se is high in both image sharpness and sensitivity. On the other hand, in connection with FPDs using a-Se, the improvement of the throughput by reducing lag and the reduction of pixel defects resulting from a-Se crystallization have been required.

Solving these problems, we have developed the AcSelerate (Model: FDR200). The diagnostic capabilities are improved with high sensitivity and high sharpness. Good workflow, such as comfortable throughput, and high reliability are also achieved.

1.2 AcSelerate System Configuration

As shown in Fig. 1, the AcSelerate consists of the imaging unit (X-ray source unit and image detector unit) and the console. The imaging unit comes in one-tube two-panel (upright and supine positions) system or one-tube one-panel (upright or supine position) system. The images captured by the imaging unit are processed and displayed on the console. The images then can be sent to an external server, stored on a PC or edited on an application program. The imaging unit consists of the X-ray source unit that emits X-rays and the newly developed image detector that detects an image of X-rays passing through a patient's body. The following sections describe the image detector that features in the AcSelerate and provide the capabilities of the system equipped with the detector.

2. Image Detector

The AcSelerate is equipped with a high image quality X-ray detector characterized by the amorphous selenium and the polymer protective layer used for image lag reduction and high reliability. Fig. 2 shows the overview of the image detector. The detector has layers, which are formed with hole-transporting layer, X-ray photoconductive layer (PCL), protective layer, electron-transporting layer and top electrode, on the TFT for reading out signals. The following sections will explain each function of the individual layers and the principle of imaging.

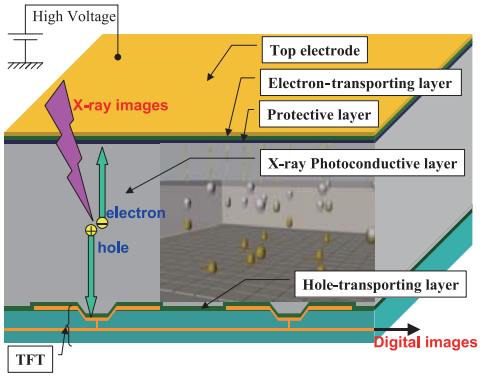

Fig. 2 Schematic view of the image sensor.

2.1 Principle of Imaging

When X-rays enter the energized semiconductor layer, the X-ray quantum is absorbed in the layer, and the electrons and holes which are finally produced are transported along the electric field. The "direct conversion" system uses this photoconductive effect to convert X-ray signals to electric signals. As shown by the cross section of the detector in Fig. 2, if X-rays enter when a positive voltage is applied to the top electrode, the produced holes are carried to the pixel electrodes. Then by controlling the TFT device, the detector reads out the charge of each pixel, and converts them to digital signals via the amplifier circuit and the ADC circuit, thereby acquiring image data.

2.2 Enhancing Reliability

As a-Se is a semiconductor, the glass transition point is as low as 40 °C, and for this reason, it crystallizes at room temperature gradually into crystalline selenium which is a conductor. An FPD using a-Se requires a cooling mechanism, such as water-cooling. The operating ambient temperature range is also limited.

The AcSelerate employs the protective layer containing polymer to improve the temperature resistance of a-Se. That provides air cooling and expands the operating ambient temperature range. The polymer protective layer bonded to the a-Se surface prevent from the crystallization of a-Se[1].

2.3 Reducing Image Lag

A direct-conversion FPD is liable to image lag resulting from a delay in transportation of free charges produced in the X-ray PCL. An energy barrier in the interface between the layers is pointed out as one of the causes of the delay.

To improve the transportation of free electrons, the AcSelerate uses a fullerene (C_{60})-doped layer as the protective layer. Fig. 3 shows the energy level diagram of the device.

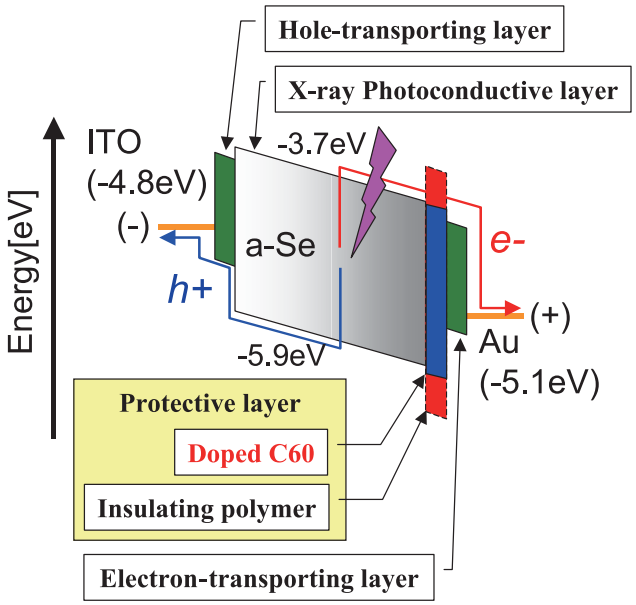

Fig. 3 Proposed energy level diagram of the detector stack.

The C_{60}-doped polymer protective layer improves connection between the X-ray PCL and the electron-transporting layer to enhance the transportation of free electrons produced in the X-ray PCL. The hole flow by the bias applied to the top electrode is also minimized and that helps to reduce dark current. With these electric characteristics, the AcSelerate achieves stable image lag reduction[1].

3. System Capabilities

3.1 Image Quality

DQE and MTF are widely used as comprehensive indices for image quality evaluation. DQE and MTF of the AcSelerate and our conventional model "FCR VELOCITY" are shown in Fig. 4. We used RQA5 as a beam quality in accordance with the IEC standard[2]. As shown in Fig. 4, the AcSelerate has a high MTF compared with the VELOCITY. It demonstrates the effect of the direct conversion using amorphous selenium. About DQE, the AcSelerate is higher than VELOCITY with 1 mR, which is a standard dose for general radiography (2.5 times higher at 1 cyc/mm and 5 times at 2 cyc/mm). Additionally, the DQE of the AcSelerate is also high with 0.3 mR which is in a low dose range, and these indicate the potential of the AcSelerate for radiation dose reduction.

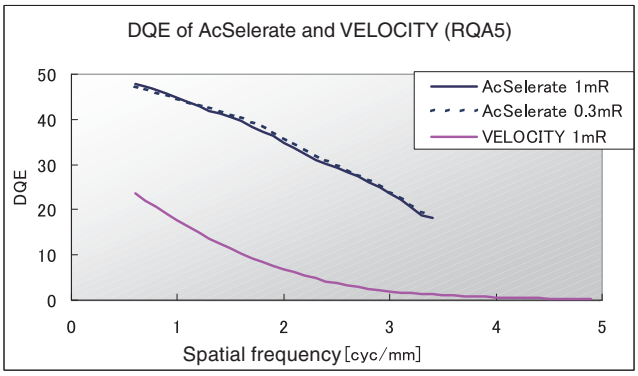

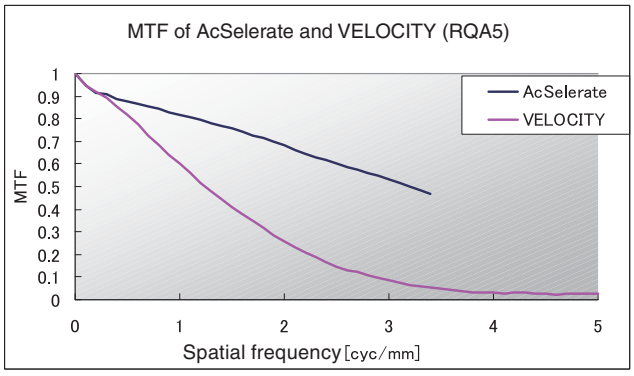

Fig. 4 DQE and MTF of AcSelerate and VELOCITY.

3.2 Workflow

The AcSelerate has the following functions and provide comfortable workflow which enhances the efficiency of examinations.

(1) Comfortable throughput

We have optimized time to accumulate charges and time to read out the accumulated charges for low-dose radiography that requires short radiation time. As a result, the preview will appear in two seconds and the processed image will appear in four seconds. That allows quick review of images and reduces the examination time.

(2) No calibration by user is needed

(3) CR/DR common console

For the console to operate the DR and do image processing, we have employed the favorably received CR console for FCR, "Console Advance", with some improvements. If an operator is using an FCR, he or she can still operate the examination with DR in the same way. The console is also intuitive and it is easy to operate for an unfamiliar user. In addition, the AcSelerate and a digital FCR reader (models specified by us) can be operated on one "Console Advance" and the image processing work will be integrated. When several imaging machines are working in one room, the Console Advance will simplify the workflow without redundancy in distribution from the RIS (Radiography Information System) or transmission of images to the PACS (Picture Archiving and Communication Systems) (Fig. 5).

Fig. 5 Possible system configuration.

(4) Auto positioning functions

The ceiling suspension system with a 5-axis motor works in conjunction with the radiography menu and automatically moves the X-ray tube to the predetermined position.

(5) Tilting functions

The flat panel for upright position can be tilted from minus 20 to plus 90 degrees.

(6) Dose-Area-Product (DAP) meter ※ option functions

The DAP meter keeps a record of the area dose of every image. It is used for patient dose management.

(7) Grid replacement direction is selectable (both right and left)

The installation location in the room is not restricted.

4. Conclusion

The digital radiography system "AcSelerate" is high in both image sensitivity and sharpness, thanks to its image detector, which is characterized by direct conversion with amorphous selenium. The conventional problems of image lag and pixel defects due to crystallization have been resolved. The MTF remains high at high frequencies and the system is expected to have higher visibility of very fine bone trabeculae. The DQE remains high in a low dose range and the system is expected to reduce the radiation dose. At the moment, no other radiography systems provide both high image quality and throughput as this system. We expect AcSelerate will help improve the precision and efficiency of examinations and diagnoses and reduce patients' exposure to radiation.

References

1) Nariyuki, F. : Imai, S. : Watano, H. : Nabeta, T. : Hosoi, Y. New development of large-area direct conversion detector for digital radiography using amorphous selenium with C_{60}-doped polymer layer. Proc. SPIE, **7622**, 762240-1 – 762240-7 (2010).
2) IEC62220-1 : Medical electrical equipment – Characteristic of digital X-ray imaging devices – Part1: Determination of the detective quantum efficiency, Ed. 1.0 (2003).

(In this paper, "FCR" is a registered trademark of FUJIFILM Corporation.)

UDC 616-073.75+771.537

Development of "CALNEO", an Indirect-conversion Digital Radiography System with High-conversion Efficiency

Keiichiro SATO*, Fumito NARIYUKI*, Takeshi KUWABARA*, Shinichiro FUKUI*, Yoshihiro OKADA*, Toshiyuki NABETA*, Yuichi HOSOI*, Jun ENOMOTO*, Masanori SASAO*, and Yoshinori SEGUCHI*

Abstract

We have developed a new digital radiography system "CALNEO" which has realized dose reduction, a faster workflow, and space saving. Newly developed detection technology "Irradiation Side Sampling" and an optimized scintillator made it possible to utilize a signal from the scintillator without attenuation and spreading of the emission. DQE of the Irradiation Side Sampling system detector is 1.2 times higher than that of conventional Pentration Side Sampling system detectors, and 1.7 times that of our existing model of FCR VELOCITY. The combination of a thin and durable imaging unit and a newly developed console "Console Advance" enables a quick review of the image, making it highly suitable for any X-ray rooms or examination vehicles.

1. Introduction

We have developed radiographic modalities in diagnosis, which have evolved from screen/film (S/F) to FCR (Fuji computed radiography) and to DR (digital radiography). We are seeking to reduce radiation dose by raising image quality, enhance the diagnostic capabilities, and improve the workflow in the X-ray room. In the field of DR, we have succeeded in enhancing the image quality further by developing the ISS system, the first of its kind in the world. With the ISS system, the layers of the flat panel detector (FPD) are in reverse order of the conventional FPD. The FUJIFILM CALNEO (Fig. 1) which is equipped with this detector was launched in September 2009. This DR system provides 1.7 times higher quality images than the conventional FCR. It is space saving. It is high in throughput. In addition, the newly developed Console Advance helps create a comfortable workflow. The operator can operate the system on the console similar way to that of FCR. The features and capabilities of the FUJIFILM DR CALNEO (DR-ID 300) as well as the technology used in FPD for enhancing image quality will be described in this paper.

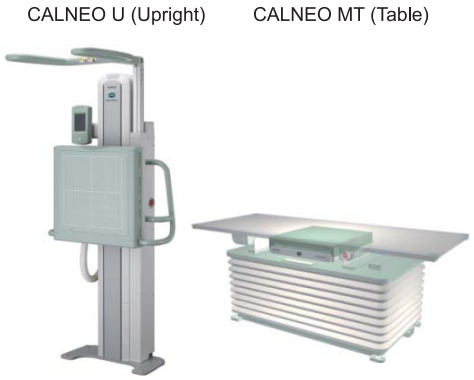

Fig. 1 External view of digital radiograph system FUJIFILM DR CALNEO.

2. Enhancing Image Quality

2.1 Features of FPD used for CALNEO

The FPD used for the CALNEO is an indirect-conversion FPD. It consists of a phosphor that converts X-rays to light and photodiode equipped with a TFT that converts light to electric charges. By driving TFT, charges produced in the photodiode are read out. And, the charges are converted to a digital image via the amplifier circuit and the analog-to-digital converter. An indirect-conversion FPD, as the phosphor layer and the photodiode are made into one panel, has several advantages. For example, loss of light, *i.e.*, loss of X-ray data is small, the display response is fast, and it helps build a thinner system. The conventional indirect-conversion FPD employs the PSS (Penetrated Side Sampling) system[1]. X-rays enter the phosphor layer and come out of the photodiode. It is the other way round with the FPD used for

Original paper (Received November 25, 2009)

* Medical System Equipment Research & Development Center
Research & Development Management Headquarters
FUJIFILM Corporation
Miyanodai, Kaisei-machi, Ashigarakami-gun, Kanagawa 258-8538, Japan

the CALNEO. It is called ISS (Irradiation Side Sampling) system (Fig. 2) which is the first of its kind in the world.

We use GOS (Gd_2O_2S:Tb) for the phosphor, considering efficiency in X-ray conversion and stability of performance. GOS is high in X-ray conversion efficiency and slow in deterioration with age or by X-rays. It will help provide stable image quality over a long period of time. GOS has been widely used for the intensifying screens of screen/film (S/F) systems. So even the users who are familiar with S/F systems will not feel strangeness resulting from difference in X-ray absorbance between materials used as phosphor.

As well as employing the ISS system, we have designed the phosphor suitable for the ISS system. That makes it possible to drastically enhance the image quality. The following sections provide detailed description of the technology.

2.2 ISS System and PSS System

The key point to raising the image quality of X-ray detectors is to increase the efficiency in use of X-ray energy and to reduce the spread of the X-ray input. For an indirect-conversion FPD, that means increasing X-ray absorption by the phosphor layer, enhancing the efficiency in detection of light emission (reducing the attenuation), and reducing the spread (blurring) of the emission.

In order to increase the X-ray absorption, the thickness and density of the phosphor layer must be increased, and in order to enhance the efficiency in detection of light emission, attenuation of the emission must be reduced until the X-rays reach the photodiode. X-rays are absorbed in the phosphor layer and they move on while being attenuated. The emission in the direction of the thickness of the phosphor layer is large on the surface X-rays enter and small at the surface X-rays come out. GOS phosphor is made of phosphor particles packed densely. As the phosphor particles scatter light, attenuation in the phosphor layer is not negligible. Fig. 3 (simplified Lubberts effect[2]) shows differences in intensity of received light and blurring depending on attenuation of X-rays in the direction of the phosphor thickness and scattering of light. The differences in detection efficiency and spread of light by system will be explained with reference to Fig. 3.

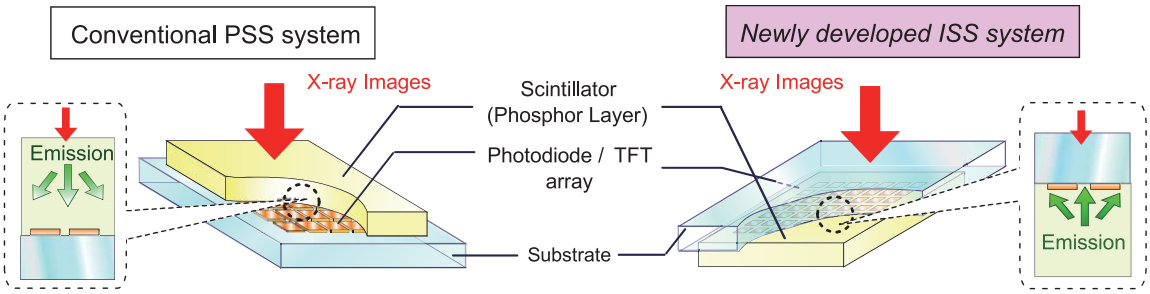

Fig. 2 Schematic view and cross section of conventional and newly developed flat panel detectors.

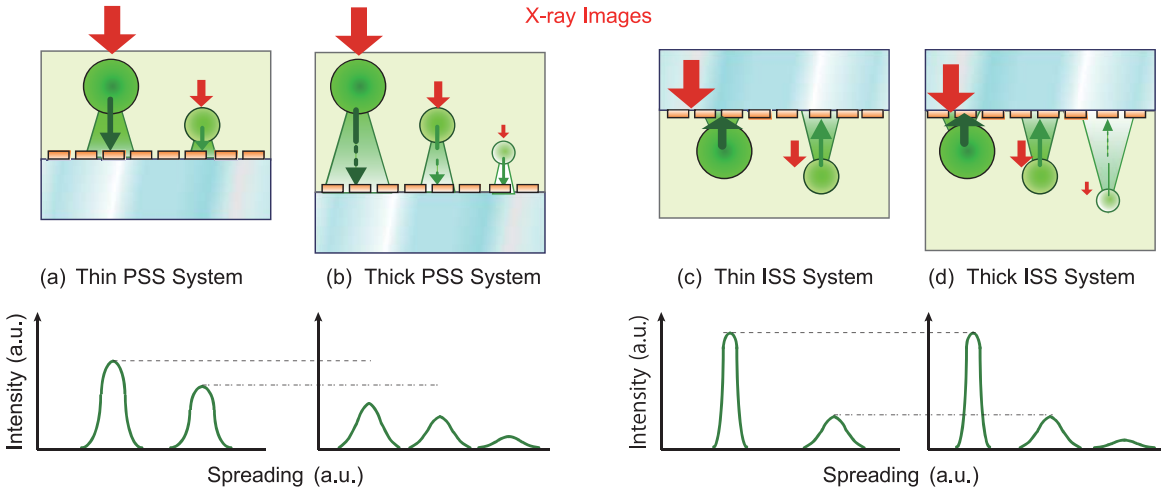

Fig. 3 Schematic diagram of intensity and blur of detected light signals.

The changes in sensitivity according to the phosphor layer thickness are shown in Fig. 4. With the PSS, the sensitivity

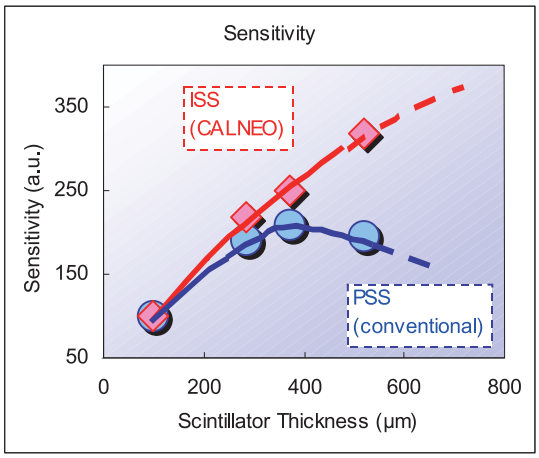

Fig. 4 Relation between scintillator thickness and sensitivity.

increases in proportion to the phosphor thickness while the thickness is small. The X-ray absorption can be increased. But, when the phosphor is too thick, the sensitivity falls. A thicker phosphor layer means that the emission is attenuated over a longer distance before reaching the photodiode. This adverse effect exceeds the effect of increasing the emission (Fig. 3 (a) and (b)). In the PSS system, there is a limit in the amount of effective X-ray absorption increased by thickening the phosphor layer. In the ISS system, the sensitivity does not fall even if the layer thickness is increased. Even if the layer thickness is increased, that does not change the intensity of the emission from the phosphors located on the X-ray entrance side or the attenuation distance to the photodiode. Only the phosphors located at the exit of X-rays and corresponding to the increase in thickness will be smaller in emission intensity and longer in attenuation distance. But, that does not affect the phosphors on the entrance side (Fig. 3 (c) and (d)). In the ISS system, although X-rays are slightly attenuated before entering the phosphor layer, the X-ray absorbance of the photodiode is relatively small and the sensitivity will not fall below that of the PSS system (Fig. 4). For this reason, in the ISS system, it is possible to increase the X-ray absorption exceeding the limit of the PSS system.

The ISS system is also advantageous compared with the PSS system in the point of the spread of emission. The emission of phosphor is scattered within the layer. In the PSS system, if the layer thickness is increased, the spread expands by the time the light is detected in the photodiode (Fig. 3 (b)). Especially, the phosphors at the X-ray entrance are high in emission intensity and scattered light is also detected with relatively high intensity, thereby resulting in blurring of the image. In the ISS system, the spread of the emission from the phosphors at the X-ray entrance will not change even if the layer is thickened (Fig. 3 (c) and (d)). Although the emission of the phosphors far from the photodiode and corresponding to the increase in thickness tends to spread, the contribution to image blurring will be relatively small on the reason that the emission intensity is small compared with the X-ray entrance side (Fig. 3 (d)).

The dependence of MTF on phophor layer thickness is shown in Fig. 5. In the whole thickness range, the ISS system is higher in MTF than the PSS system. That indicates the ISS system has an advantage about image blurring.

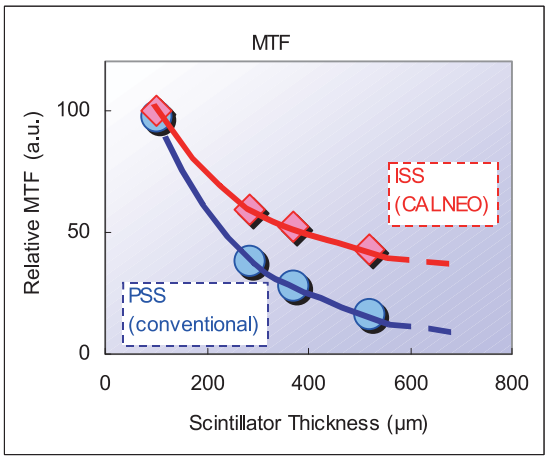

Fig. 5 Relation between scintillator thickness and spatial resolution.

2.3 Original Phosphor layer Design

Thanks to the ISS system, the phosphor of the CALNEO stands a drastic increase in thickness while maintaining the image quality. To use as much X-ray data as possible, it is effective to increase the phosphor layer thickness and density and enhance the emission efficiency of the phosphor particles. When increasing the density, the spaces between the phosphor particles must be minimized. When enhancing the emission efficiency, the optimum particle size must be selected. That is because of a trade-off. If the phosphor particle size decreases, the emission efficiency falls. If the particle size increases, the spread of emission increases. For the CALNEO, we applied our high-density particle filling technology we have developed for IP (imaging plate) to the GOS phosphor. We mixed large particles and small particles in an appropriate ratio (Fig. 6). Large particles are large in

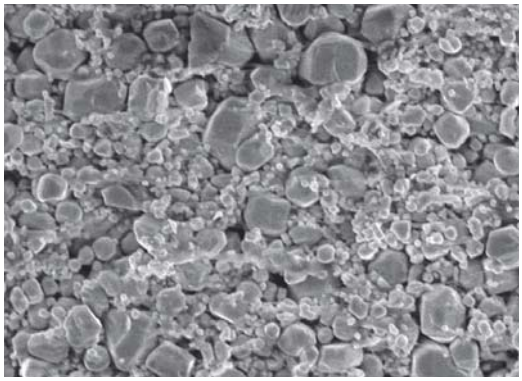

Fig. 6 A cross-sectional image of a GOS scintillator.

emission. The emission of small particles does not blur very much. As a result, we have achieved the volume filling density of 75%. It is a very high percentage for the density of phosphor particles. We have succeeded in increasing the X-ray absorption per unit thickness and balancing the emission intensity and image blurring.

3. Features of FUJIFILM DR CALNEO System

3.1 Image Quality

Fig. 7 and Fig. 8 show DQE and MTF of the ISS-system FPD (CALNEO), PSS-system FPD and our conventional model FCR VELOCITY. The beam quality is RQA5 as specified in the IEC standard[3] and the radiation dose is 1 mR. DQE of the CALNEO is about 1.2 times larger than that of the PSS-system FPD and 1.7 times the VELOCITY's. In principle, it is possible to reduce the radiation dose to lower than those of these systems. MTF of the CALNEO is higher than those of other systems in the frequency range higher than 1.5 cyc/mm. This indicates that the CALNEO will be good at showing fine parts of the anatomy, such as bone trabeculae and pulmonary blood vessels.

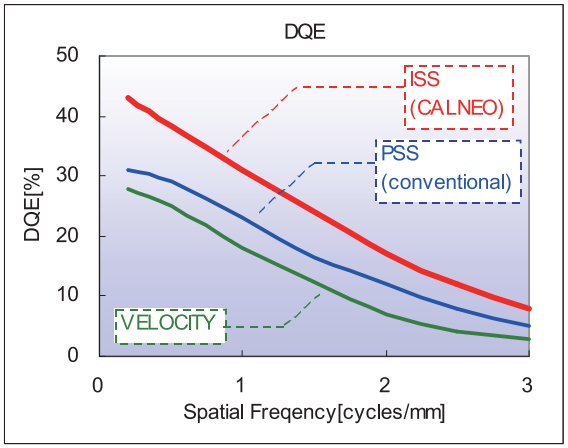

Fig. 7 DQE.

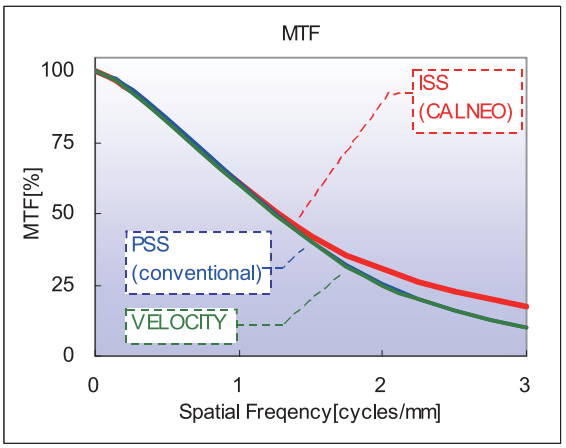

Fig. 8 MTF.

3.2 Compact Design

The CALNEO system is compact in size and simplified in configuration so that it will fit in various installation environments.

The imaging unit is more than 50% thinner than that of the FCR VELOCITY. As well as reducing the thickness of the FPD, we have increased the density using the mechanical design technology. The slim imaging unit will fit into a small space in an X-ray room. It is suitable for medical examination cars, which have limited space.

The console is the Console Advance, the same as the FDR AcSelerate. Several tasks can be done on one console. There is no need to install several PCs in one room. The space required for operation is also designed compact.

3.3 High Throughput

The CALNEO provides a high throughput similar to that of the FDR AcSelerate, thanks to the image lag reduction of the FPD and high-speed reading. It will create a stress-free workflow even in a very busy x-ray room.

4. Conclusion

This report has explained the technology for enhancing image quality used in the FUJIFILM DR CALNEO and its features and capabilities. This system and the developed technologies make it possible to reduce radiation dose and improve the workflow. We hope this system will be widely used.

We will continue to develop new technologies and provide high-performance products to advance the quality of medical care, and the quality of life.

References

1) Beutel, J. et al. Handbook of medical imaging, Volume.1. Physics and Psychophysics, chapter 4, SPIE (2000).
2) Nishikawa, R.M. et al. Effect of finite phosphor thickness on detective quantum efficiency. Med. Phys., **16** (5), 773-780 (1989).
3) IEC62220-1-1 : Medical electrical equipment- Characteristics of digital X-ray imaging devices- Part1: Determination of the detective quantum efficiency Ed. 1.0 (2003).

Proposal of New Organic CMOS Image Sensor for Reduction in Pixel Size

Mikio IHAMA*, Tetsurou MITSUI*, Kimiatsu NOMURA**, Yoshiki MAEHARA*,
Hiroshi INOMATA*, Takashi GOTOU*, and Yutaka TAKEUCHI*

Abstract

We proposed a new CMOS image sensor with a thin overlaid panchromatic organic photoelectric conversion layer as the best candidate for sensors with reduced pixel size. We experimentally made trial products of the proposed sensor, verified their potential capability, and proved the validity of the organic CMOS sensor.

1. Introduction

The history of imaging science and technology encompasses the history of Fujifilm, running together with that of Eastman Kodak. However, more than a hundred and a half years of history of silver halide photography based on organic materials has been replaced by several decades of history of the silicon technology based on inorganic materials. It is not unreasonable to assume that as we charge toward the future, the next historical chapter will consist of a hybrid technology of organic and inorganic materials that will overcome the present limits of each technology.

Silicon technology has been developing dramatically, and the smallest pixel size of 1.4 μm, which is nearly equal to 1/1000 of 1 mm, has now been achieved. Nevertheless, to meet the successive and strong demand of the market requiring an increasingly greater number of pixels within a limited chip area, it is necessary to continuously reduce the size of a pixel. Despite the tireless efforts to improve technologies for achieving smaller pixel size, the light capture efficiency and sensitivity of CCD and CMOS image sensors have been decreasing. Recently, many manufacturers have announced their development of back-illuminated CMOS image sensors[1] based on state-of-the-art silicon technologies, and the competition for achieving smaller pixel size is becoming fiercer and fiercer. However, the situation where many manufactures are faced with the major challenge in attaining higher sensitivity within smaller pixel size, has not changed.

We have been exploring the possibilities of developing a new image sensor which is not based on conventional technologies, by utilizing the features of an organic photoelectric conversion layer[2-4]. Fig. 1 shows a schematic cross section of the new organic CMOS image sensor, which we consider the most suitable structure for reducing pixel size. The sensor consists of a thin panchromatic organic photoelectric conversion layer and a CMOS signal read-out substrate. It is a hybrid structure comprising two layers: the upper layer for capturing light and converting it to electrical signals consists of organic materials, and the lower layer for outputting electrical signals consists of inorganic materials. In principle, the aperture for capturing incident light is 100%. The photoelectric conversion layer consists of a thin panchromatic organic photoelectric conversion layer sandwiched between a transparent counter electrode and pixel electrodes. Since the organic photoelectric conversion layer can be laid over the CMOS signal read-out substrate as a continuous film, it does not need any of the expensive micro-fabrication processes which are necessary for conventional silicon technology, and is suitable for reducing pixel size. Incident light is separated into three primary colors of blue, green and red by the micro-color filters, and signal charges generated by the absorption of each primary color in the thin panchromatic organic photoelectric conversion layer are read out by the signal charge read-out circuits in the CMOS substrate through via-plugs.

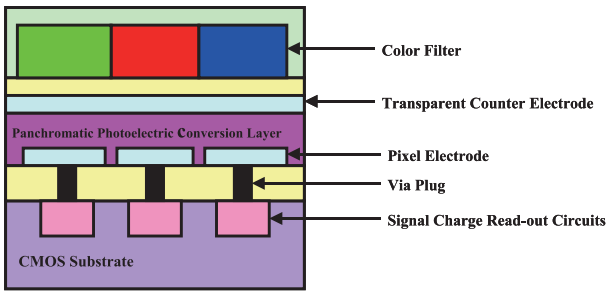

Fig. 1 Structure of the proposed image sensor with a thin overlaid panchromatic organic photoelectric conversion layer.

Original paper (Received November 25, 2009)

* Frontier Core-Technology Laboratories
Research & Development Management Headquarters
FUJIFILM Corporation
Ushijima, Kaisei-machi, Ashigarakami-gun, Kanagawa
258-8577, Japan

** Synthetic Organic Chemistry Laboratories
Research & Development Management Headquarters
FUJIFILM Corporation
Ushijima, Kaisei-machi, Ashigarakami-gun, Kanagawa
258-8577, Japan

As the organic photoelectric conversion layer has a large absorption coefficient in principle, it can absorb enough light in spite of its extreme thinness. Therefore, it is free from spectral cross-talk between tiny pixels when capturing slanting rays of light and does not need any micro-lenses conventionally used for gathering incident light. The spectral sensitivity of the organic photoelectric conversion layer can be freely controlled by designing organic materials and it is possible to achieve a panchromatic property which does not have sensitivity to infrared light but only to blue, green and red light as shown in Fig. 2. Therefore, it is not necessary to use a conventional infrared light cut filter and we can eliminate its problem, a change of infrared cut wavelength and color hue caused by a change of the angle of light incidence.

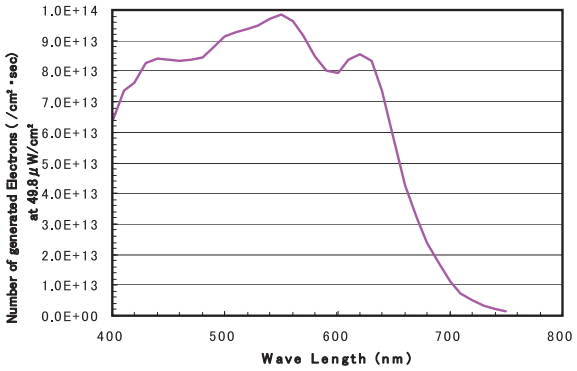

Fig. 2 Spectral sensitivity of the panchromatic organic photoelectric conversion layer.

We have made a trial product of the CMOS image sensor with an overlaid thin panchromatic organic photoelectric conversion layer in order to verify the potential capability of the new organic CMOS image sensor. The results of the evaluation are reported in this paper.

2. Experiments

Table 1 shows the specifications of the trial product of a new organic CMOS image sensor, which has a structure as shown in Fig. 1. The CMOS signal read-out substrate was made by a 0.18 μm, 2-poly/4-metal CMOS process. The pixel size is 3 μm and the number of pixels is 360 × 256 (QVGA). Each pixel has a signal read-out circuit with a 3-transistor mechanism, which operates at 50 frames/sec as shown in Fig. 3. The ratio of the pixel electrode size to the pixel size is equivalent to the apparent aperture for capturing incident light. Fig. 4 shows an electron micrograph of the pixel electrodes on the CMOS signal read-out substrate of the trial product. The size of pixel is 3 μm and the size of pixel electrode is 2.76 μm, accordingly, the apparent aperture for capturing incident light is 85%.

The panchromatic organic photoelectric conversion layer, color filters and other materials were overlaid on the CMOS signal read-out substrate, and it was assembled as a package. We evaluated the S/N ratio, degree of image lag and other characteristics of an image sensor. Fig. 5 shows a photograph of an assembled chip of the new organic CMOS image sensor.

Table 1 Specifications of a trial product of the proposed organic CMOS sensor.

Process	0.18 μm, 2-Poly/4-Metal
Pixel Number	360 × 256 (QVGA)
Pixel Size	3 μm
Read-out Speed	50 frames/second
Signal Read-out Circuit	3-Transistor Mechanism
Photoelectric Conversion Layer	Panchromatic Organic Materials

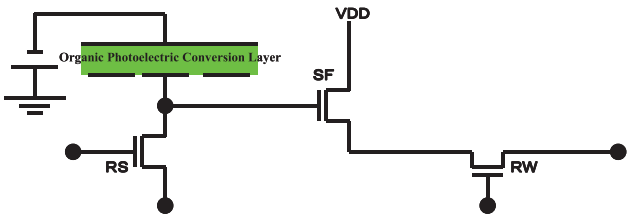

Fig. 3 Outline of signal charge read-out circuit with three-transistor mechanism for the proposed organic CMOS sensor.

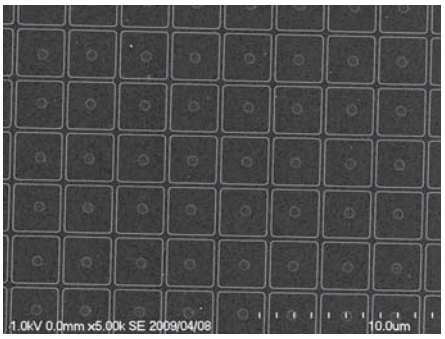

Fig. 4 Electron micrograph of pixel electrodes.

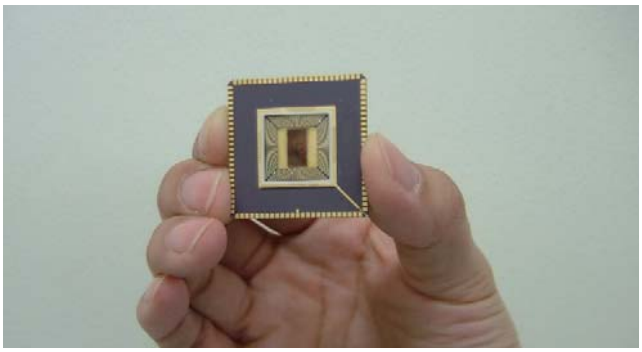

Fig. 5 Photograph of a trial product of the assembled organic CMOS sensor proposed in this study.

3. Results and Discussion

Fig. 6 shows an electron micrograph of a cross section of the trial product of a new organic CMOS image sensor. The thickness of the panchromatic organic photoelectric conversion layer is only 0.5 μm and extreme thinness is apparent when compared with the size of a pixel. Since the thin layer can absorb incident light well enough and convert it to electric signals, spectral cross-talk between pixels when capturing slanting rays of light can be reduced efficiently without using any micro-lenses.

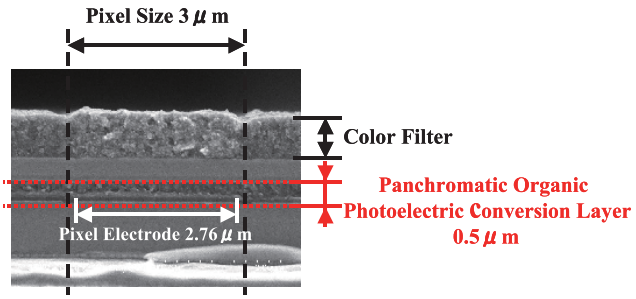

Fig. 6 Electron micrograph of the cross section of a trial product of the proposed organic CMOS sensor.

Fig. 7 shows a photograph of a resolution chart taken by the trial product of a new organic CMOS sensor without micro-color filters. Although the organic photoelectric conversion layer was laid over the CMOS signal read-out substrate as a continuous film without any structures, a resolution of 250 TV lines, which is the theoretical limit of resolution determined by the number of pixels in a column, was attained. This indicates that the new organic CMOS image sensor can achieve a resolution corresponding to the number of pixels without using any expensive and complicated micro-fabrication processes and be the best candidate for sensors with fine pixel size.

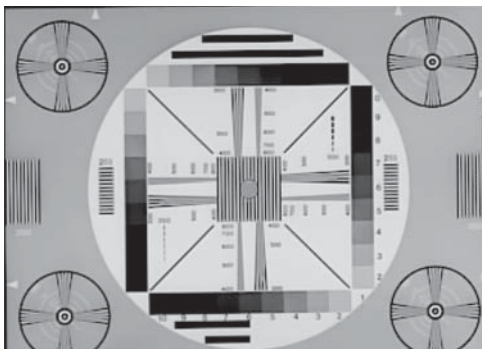

Fig. 7 Photograph of a resolution chart, which was taken by the trial product of the proposed organic CMOS sensor without micro color filters.

Fig. 8 shows a photograph under an intense spotlight approximately 300 times greater than standard light. There are no false signals due to the excessive light, such as smear and blooming, demonstrating that the new organic CMOS image sensor is free from these problems.

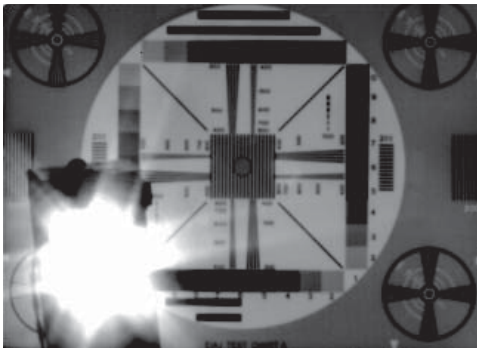

Fig. 8 Photograph of a resolution chart under intense light from a spotlight, which was taken by the trial product of the proposed organic CMOS sensor without micro color filters.

Fig. 9 shows one movie frame of operating metronome taken at 50 frames/sec. The moving pendulum is clearly taken and no image lag was observed.

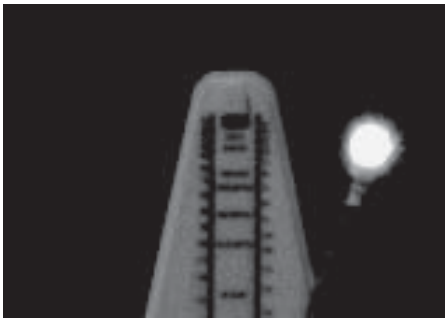

Fig. 9 Photograph of an operating metronome, which was taken by the trial product of the proposed organic CMOS sensor without micro color filters.

Fig. 10 shows a skin color comparison photograph taken by the trial product of a new organic CMOS image sensor with micro-color filters. This is the first color image in the world, which was taken by a single-board image sensor utilizing an organic photoelectric conversion layer. In a photograph of the 24 colors of Macbeth color chart, the average color difference from actual ones is 0.64, which can hardly be recognized by human eyes. Since the panchromatic organic photoelectric conversion layer is designed to be sensitive to only visible light, namely blue, green and red light, it can achieve such a negligible color difference without requiring any infrared light cut filters.

Fig. 10 Photograph of a skin color chart, which was taken by the trial product of the proposed organic CMOS sensor with micro color filters.

Table 2 shows the characteristics of the trial product of a new organic CMOS image sensor. The external quantum efficiency of photoelectric conversion is 65% at the wavelength of 550 nm corresponding to green light, and can be increased by adopting an anti-reflection layer for incident light. The number of saturation electrons is 40,000 per pixel and a wide dynamic range corresponding to 60 dB is achieved. The large number of saturation electrons gives a great advantage to the new organic CMOS image sensor with pixels of smaller size and contributes to the creation of images with rich gradation. Although the random noise per pixel is considerable (38 electrons), it is nearly equal to the kTC-reset noise inherent in principle of a 3-transistor signal read-out circuit. This random noise should be reduced by developing a new signal read-out circuit, which could decrease the kTC-reset noise for a 3-transistor mechanism. Although the dark current of the organic photoelectric conversion layer at 60°C is equal to about 7 electrons, it should be decreased further by the progress of research on the materials used for organic photoelectric conversion layer in the future.

Table 2 Characteristics of a trial product of the proposed organic CMOS sensor.

External Quantum Efficiency (550 nm)	65%
Conversion Gain	56 μV/e
Number of Saturation Electrons	40,000e
Smear & Blooming	Below Detection Limit
Lag	Below Detection Limit
Random Noise (RMS)	38e
Dynamic Range	60 dB
Dark Current of Organic Photoelectric Conversion Layer at 50 frame/second (60°C)	7e

4. Conclusion

We proposed a new organic CMOS image sensor, in which a thin panchromatic organic photoelectric conversion layer was overlaid upon a signal read-out CMOS substrate, as the best candidate for sensors with pixels of reduced size. This image sensor has a hybrid structure consisting of organic materials and inorganic materials. We have made the trial product in order to verify the potential capability of the sensor, and succeeded in experimentally proving that the panchromatic organic photoelectric conversion layer without requiring any expensive micro-fabrication processes could achieve high external quantum efficiency. We will continue our efforts to improve and develop this technology of a new organic CMOS image sensor, wishing to create a new milestone in the history of imaging science and technology.

References

1) 2009 International Image Sensor Workshop Symposium on Backside Illumination of Solid-State Image Sensors, Bergen, Norway (2009).
2) Takada, S.; Ihama, M.; Inuiya, M. Proc. SPIE, **6068**, 60680A-1−60680A-8 (2006).
3) Ihama, M.; Hayashi, M.; Maehara, Y.; Mitsui, T.; Takada, S. Proc. SPIE, **6656**, 66560A-1−66560A-9 (2007).
4) Takada, S.; Ihama, M.; Inuiya, M.; Komatsu, T.; Saito, T. Proc. SPIE, **6502**, 650207-1−650207-11 (2007).

UDC 655.226.26

Development of Photopolymer-type Simple-Process CTP Systems, "PRO-V" and "PRO-VN"

Toshifumi INNO*, Keiichi ADACHI*, and Chikashi OISHI*

Abstract

We have newly developed unique environmentally friendly photopolymer-type simple-process CTP systems "PRO-V" and "PRO-VN", which use a single solution/single-bath without requiring replenishment, along with a new CTP suitable for this process. These systems integrate the conventional four-step process into a single-step process and offer customers a variety of advantages, like reducing the running cost, reducing processor maintenance, saving the space and protecting environment.

1. Introduction

With the increasing concern of society about the global environment, the momentum towards ecologically friendly products is increasing in Japan's printing industry, thanks to the industry's various efforts. The Japan Federation of Printing Industries (JFPI) has established the green printing (GP) certification program. The Environment Pollution Prevention Printing Association (E3PA) has set up the environment pollution prevention printing mark (Clione Mark) certification system.

On the other hand, as printing is going digital, as a system for making printing plates, demand for CTP (computer to plate) is increasing. In CTP technology, an image on computer is output directly to a printing plate without requiring a photographic film. Although the current CTP systems enhance efficiency of the plate making process, save time and stabilize the quality, as for plate processing, the mainstream systems still require high-alkali developers. These systems require management of automatic processors and developers to maintain quality and disposal of waste solutions, which are a heavy burden in cost and labor.

Considering the above situation, we have developed next-generation CTP technology for two types of CTP systems in order to simplify or eliminate the plate processing process and thereby reducing the environmental impact and cost,. One is thermal CTP that uses infrared laser. The other is visible CTP that uses visible-light violet laser).

For thermal CTP, we developed processless thermal plate PRO-T (ET-S in Japan)[1)] and put it on the market in 2006. The PRO-T has been well received. It provides the same level of sensitivity (productivity) and printing capability as the conventional thermal plates using high-alkali developers. Still, the new plate requires no processing at all, which means no developers or waste solution.

For visible CTP, we have simplified the processing because of the aptitude for the safelight during printing process. And, we have come up with a simple-process photopolymer CTP system. We launched the system in 2008. The system for commercial printing comes with the plate PRO-V, the plate processing solution LC-V, and automatic processor FCF-85V or FCF-125V (Photo 1). The system for newspaper printing comes with the plate PRO-VN, the processing solution LC-VN and the automatic processor FCF-NEWS. This report mainly focuses on the newly developed technology on the high-alkali-free processing solutions for simplifying the process and CTP plate materials suitable for the solutions.

Photo 1 Plate: PRO-V, Treatment solution: LC-V, Processor: FCF-125V.

Original paper (Received November 19, 2009)
* Graphic Materials Research Laboratories
Research & Development Management Headquarters
FUJIFILM Corporation
Kawashiri, Yoshida-cho, Haibara-gun, Shizuoka 421-0396
Japan

2. Development Concept and Problems of the Simple-process Photopolymer CTP System

As shown in Fig. 1, the plate processing of the conventional photopolymer CTP system after the laser exposure and the preheating consists of the following four steps (four baths): pre-washing, developing, rinse and finishing. The developer is highly alkaline (pH = approx. 12 to 13). The developer is susceptible to fatigue due to repeated use for many plates or fatigue with age by carbon dioxide generated during operation/stand-by hours of the automatic processor. For stable processing, a replenishment system is required to counter the fatigue. This makes the automatic processor big and complicated, and the maintenance is difficult, and the machine takes up a lot of space. Moreover, the process uses a large amount of solutions, including a developer, finisher and rinse water. All the steps produce waste solutions, which are an impact on the environment and a strain on the costs.

To solve these problems and create benefits to customers, we have started technological development for simplifying the photopolymer CTP processing system.

<Benefits for customers by simplified processing>

(1) Reduction in the running cost (reduction in processing solutions and waste solutions)
(2) Reduction in maintenance loads of the automatic processor (reduction in workloads for solution management and cleaning)
(3) Reduction in space required by the automatic processor
(4) Reduction in the impact on the environment (in print production)

As shown in Fig. 1, simplifying process we have sought is integrating the four steps of the processing process into a single step process. Specifically, we need to remove the oxygen barrier layer (overcoat layer = OC layer), remove the unexposed part of the photosensitive layer and form the hydrophilic protective layer in one process (one solution and one bath). In the conventional process, these are done in separate steps. We also need to configure a stable processing system using a high-alkali-free solution that does not require replenishment to reduce the impact on environment and the amount of processing solutions.

<Problems for simplifying the process>

(1) Processing with one solution
(2) Developing with high-alkali-free solution
(3) No replenishment

We have solved these problems and developed new high-alkali-free solutions and new CTP plates suitable for the solutions. The following sections provide the detailed descriptions about the main technologies we have developed for the solutions and plates.

3. Development Technology

3.1 Development of Processing Solutions

3.1.1 Dispersing Photosensitive Layer

In the conventional processing system, if some sludge is left on the plate, it will be fully removed during the rinse and finishing process subsequent to developing. In our new system, on the otherhand, there is no rinse or finishing process and processing is carried out in one process with one solution. The sludge may often remain on the plate. In order to solve the problem, the photosensitive components need to be dispersed completely in the processing solution.

Among the photosensitive components, pigments and polymerizable monomers are especially hard to disperse. Pigments released into a processing solution will not stably disperse and they are prone to remain as sludge. Monomers gradually hydrolyze and dissolve completely in a high-alkali developer. In our high-alkali-free solution, the hydrolysis is still slow, resulting in sludge with time. Dispersion of

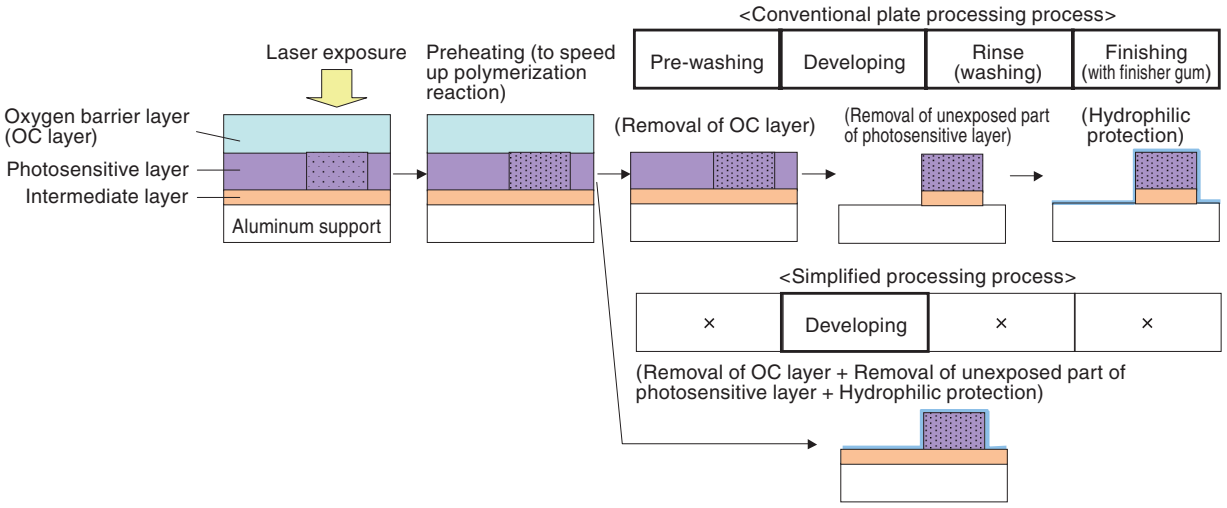

Fig. 1 Comparison between the conventional process and simplified process.

pigments and monomers is the key in processing with one solution without sludge of photosensitive components.

Considering the above situation, we have tried stabilizing the dispersion using a surfactant to disperse pigments and monomers uniformly. As shown in Fig. 2, we have found that several types of ampholytic surfactants increase the dispersion of pigments and monomers satisfactorily. These surfactants help disperse photosensitive components including pigments and monomers and stabilize the dispersion of photosensitive components.

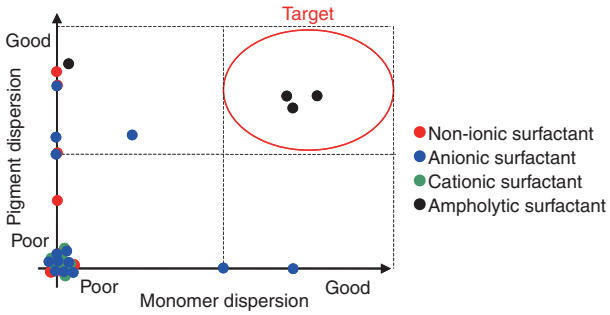

Fig. 2 Dispersion ability of monomer and pigment.

In the first place, a processing solution needs the developing function, that is, removal of the non-imaged area of the photosensitive layer. In the conventional system, the developing function is provided mostly by the high alkaline property of a developer. High-alkali free solutions will not have an adequate developing function. However, as described above, our system employs a surfactant excellent in dispersion of photosensitive components and the surfactant helps remove the photosensitive layer sufficiently and stably. That makes possible a processing solution free of strong alkali.

3.1.2 Stabilizing Processing Solution

In order to realize the stable processing, it is essential to stabilize the pH of the processing solution. The conventional high-alkali developer is liable to fatigue resulting from consumption of the alkali. The alkali is consumed by carbon dioxide in the atmosphere and by the photosensitive components during their processing. To solve this problem, the conventional systems make up for the consumption by adding a high-pH alkali.

In general, the higher the pH of an alkaline solution is the more it takes in carbon dioxide, which reduces the pH. Compared with the conventional high-alkali developers, the high-alkali-free solutions are insusceptible to carbon dioxide and fall in the pH is small. But, the pH needs to be more stable to eliminate the need of replenishment. We have added a buffer function to the processing solutions. We tried several types of buffer agents that work between neutral and low alkaline (pH10 or less). Finally, we have decided on a carbonate buffer for the pH stability and impact on the environment. By adding a buffer function, we have succeeded in stabilizing the pH of processing solutions reducing the effects of the fatigue without replenishment (Fig. 3).

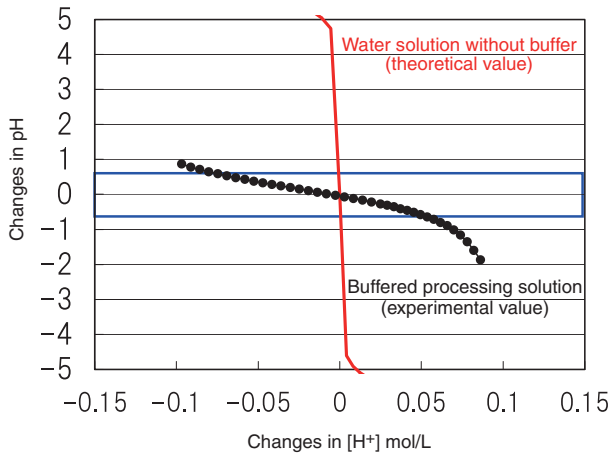

Fig. 3 pH stability range of sodium carbonate.

3.2 Development of Plates

3.2.1 High-solubility Overcoat Layer

Photopolymer plates use polymerization reaction to form an image. They need an oxygen barrier layer as an overcoat layer to prevent oxygen, which hinders polymerization reaction, from entering into the photosensitive layer. For the conventional overcoat layer, it was common that the polyvinyl alcohol is used as a hydrophilic polymer to reduce oxygen permeability. In the conventional plate processing process, the overcoat layer is removed in the pre-washing process before the unexposed part of the photosensitive layer is dissolved and removed with a high-alkali developer in the developing process. However, our system does not have the pre-washing process and the overcoat layer material, not only the components of the photosensitive layer, is dissolved into the processing solution. The overcoat layer material, i.e., polyvinyl alcohol, dissolved into the processing solution affects the printing capability. It increases the viscosity of the solution, hinders the dissolution of the photosensitive layer, and causes sludge due to gelation. Moreover, it increases loads on washing by the automatic processor. Therefore, for one-solution processing, it is necessary to reduce the loads of the overcoat layer material on the processing solution. On this account, we have sought ways of enhancing the solubility of polyvinyl alcohol and reducing the thickness of the overcoat layer. To enhance the solubility of polyvinyl alcohol, the acid-denatured polyvinyl alcohol using sulfonate group have been employed by us. The flat particles high in aspect ratio have been added in order to reduce the thickness of the overcoat layer. Adding the particles increases the length of the oxygen permeation pathway in the overcoat layer and that makes it possible to reduce the thickness of the layer without reducing the

oxygen barrier property (Fig. 4).

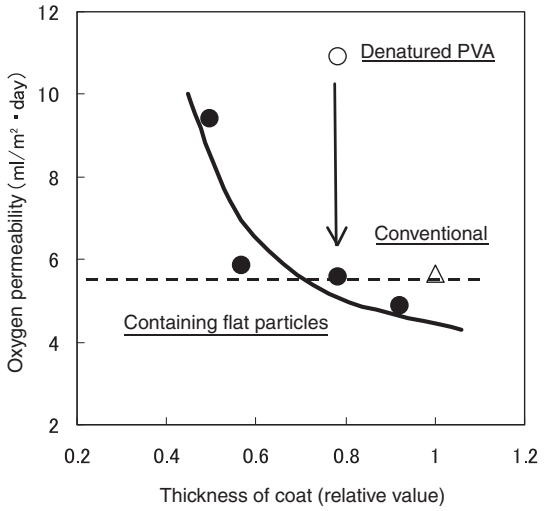

Fig. 4 Control for oxygen permeation of overcoat layer.

3.2.2 Control of the Interface Adhesion

Between the photosensitive layer and the support, an intermediate layer is placed to ensure adhesion of the image area and hydrophilicity of the non-image area. In the conventional high-alkali developing CTP, the intermediate layer material is hydrophobic and soluble in the high-alkali developers. In our system using a high-alkali-free solution, it is difficult to remove the hydrophobic intermediate layer. We need a hydrophilic intermediate layer that ensures adhesion of the image area and hydrophilicity of the non-image area. We have decided to leave the intermediate layer and started development of a hydrophilic intermediate layer that can control the adhesion of the interface with the photosensitive layer. The adhesion of the image area is achieved by adding to the intermediate layer a functional group that electrostatically interacts with the polar functional group of the photosensitive layer components. The hydrophilicity of the non-image area is achieved by reversing the electrostatic interaction in the processing solution, which ensures the solubility of the photosensitive layer and the hydrophilicity of the intermediate layer (Fig. 5).

4. Features of the System

4.1 System Specifications

Table 1 shows the specifications of the new system. The system has practically the same level of capabilities as those of the conventional violet laser CTP systems using high-alkali developers (FUJIFILM "Brillia LP-NV" and "Brillia LP-NNW"). That means that the light exposure settings are also the same. And, the present violet CTP setter can be used with the new system. The high productivity of photopolymer CTP will be maintained. The plates made by this system will cause as little toning in printing as the conventional CTP plates. In printing, they can be handled exactly the same way as the conventional plates.

Table 1 Specifications of "PRO-V" and "PRO-VN".

	PRO-V system for commercial printing	PRO-VN system for newspaper printing
Plate	Polymerized photopolymer (negative)	Polymerized photopolymer (negative)
Exposed Light source	Violet laser (wavelength: 405 nm)	Violet laser (wavelength: 405 nm)
Plate/processing solution (name)	PRO-V/LC-V	PRO-VN/LC-VN
Automatic processor (name)	FCF-85V, FCF-125V	FCF-NEWS
Processing time	19 seconds (28 °C)	21 seconds (25 °C)
Sensitivity (standard)	65 μJ/cm^2	30 μJ/cm^2
Resolution	2-98% (200 lpi)	2-98% (100 lpi)
Runlength	200,000 prints (depending on printing conditions)	200,000 prints (depending on printing conditions)
Capability of processing	20m^2/L	20m^2/L

As the process is simplified, the automatic processor of the new system is reduced in size. It is approximately 35% smaller than the automatic processors for the conventional CTP

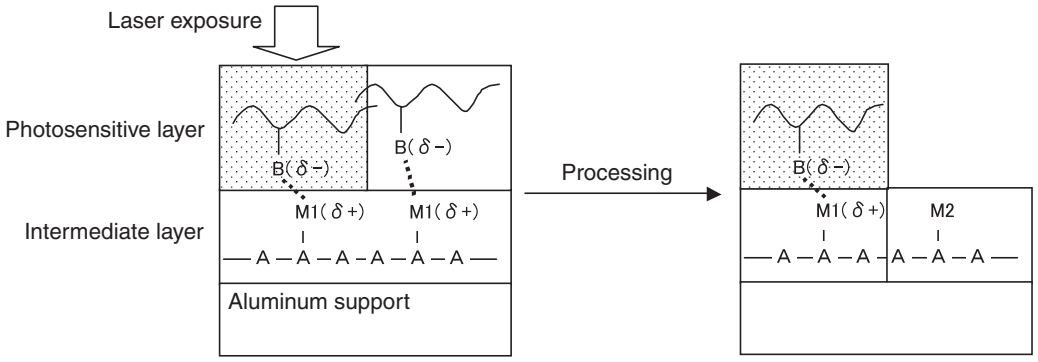

A : Hydrophilic functional group
B : Polar functional group of photosensitive layer components
M1 : Electrostatically interacting functional group
M2 : Hydrophilic functional group (converted from M1 to M2 by processing)

Fig. 5 Control mechanism of interface between photosensitive layer and intermediate layer.

systems (Fig. 6). The system provides stable processing without replenishment of a processing solution. The consumption of processing chemicals is reduced about 75% compared with the conventional CTP systems, assuming 1000 m^2 of plates are processed per month for 8 hours a day for 20 days a month (Fig. 7).

4.2 Quality

4.2.1 Tone Reproduction

Fig. 8 shows the tone reproducibility of a plate exposed for imaging with the Luxel plate setter Vx9600 and made with the PRO-V system (plate: PRO-V, processing solution: LC-V and automatic processor: FCF-125V). Fig. 9 shows enlarged photographs of the dots on the plates exposed and made in the same way as above with AM screening (200 lpi, 2438 dpi) and FM screening (20 μm, 2438 dpi). The tone reproduction curve is linear and the reproducibility is good. The result indicates that the system can form sharp dots suitable for high-definition FM screening.

4.2.2 Processing Stability

Fig. 10 shows how the processing solution pH and the tone reproducibility change when the PRO-V system under the same conditions above has processed plates at 20 m^2/L. It indicates that, without replenishment, the processing solution remains insusceptible to fatigue due to repeated processing or fatigue with age by carbon dioxide generated during operation/stand-by hours of the automatic processor. Both the physical properties of the processing solution and the processing ability are stable. Moreover, no sludge is generated and the automatic processor is easy to clean.

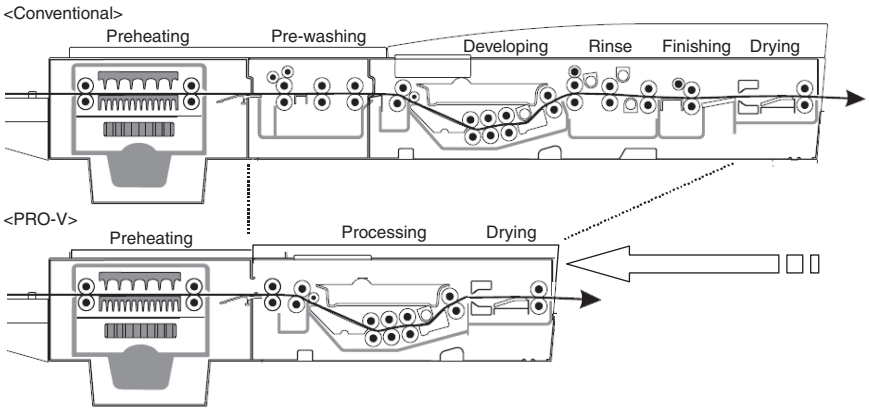

Fig. 6 Comparison between the conventional type and PRO-V type processors.

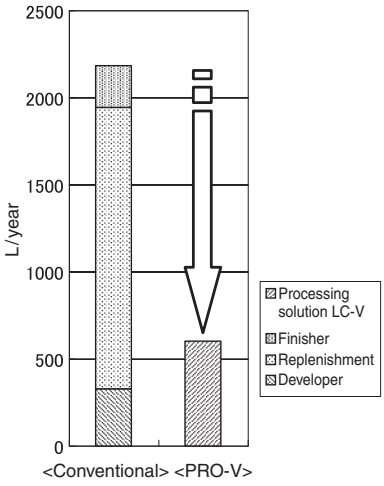

Fig. 7 Comparison of treatment solution consumption between the conventional type and PRO-V type.

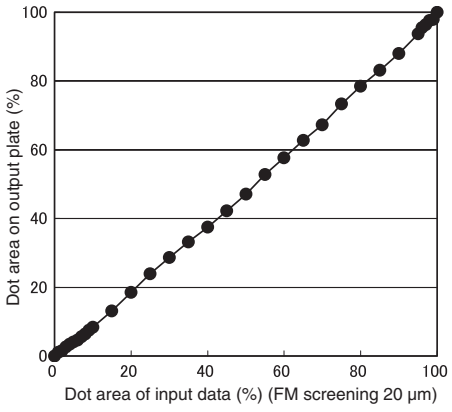

Fig. 8 Tone reproduction curve.

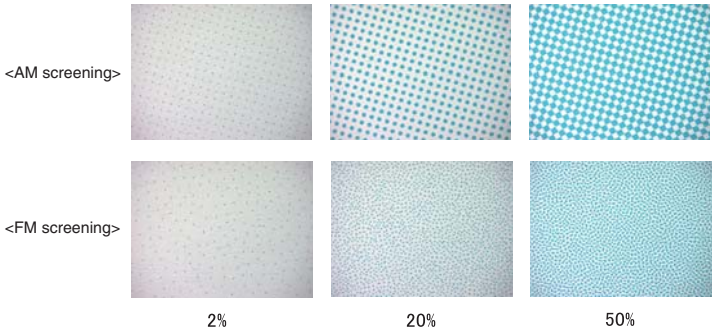

Fig. 9 Dot quality on plate.

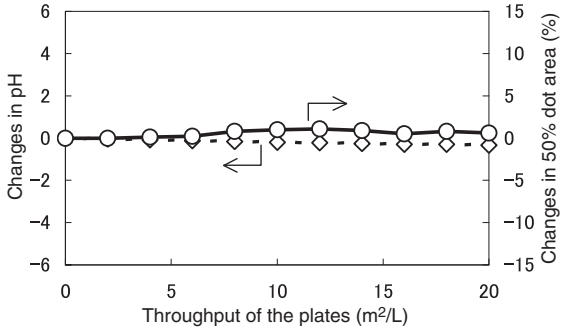

Fig. 10 Fluctuation of solution pH and dot area reproduction in running treatment.

5. Conclusion

The simple-process photopolymer CTP system, PRO-V/PRO-VN, is the product of the high-sensitivity polymer technology and the processless thermal plate technology Fujifilm has developed for CTP. It is an environmentally friendly system that has the same level of capabilities as the conventional photopolymer CTP. We are launching this system in Europe. The new system is very well received for its ease of maintenance, processing stability and low effluents. As people are getting more and more ecologically aware, we hope that this system, which provides above-mentioned benefits to customers, will spread in the market and contribute to printing solutions.

References

1) Oda, Akio; Mitsumoto, Tomoyoshi; Endo, Akihiro; Kunita, Kazuto; Ohashi, Hidekazu. Development of Process-less Thermal CTP Plate "PRO-T". FUJIFILM RESEARCH & DEVELOPMENT. No.52, 34-37 (2007).

(In this paper, "Brillia" is a registered trademark of FUJIFILM Corporation.)

UDC 621.382+621.3.032.35+544.523

Development of Efficiency and Stability of Phosphorescent Organic Electroluminescent Devices

Wataru SOTOYAMA*, Tasuku SATOH*, Masaru KINOSHITA*, Manabu TOBISE*, Kouji KAWATO**, Toshihiro ISE***, Hiroo TAKIZAWA***, and Seiji YAMASHITA*

Abstract

We developed stable and efficient blue phosphorescent materials for organic electroluminescent (EL) devices on the basis of the evaluation of their stability under UV irradiation. Structures of organic EL devices with the above-stated materials were improved with the aid of a method to estimate the site distribution of exciton formation in the emissive layer by doping it with a small amount of fluorophore at varied positions. The improved blue phosphorescent organic EL devices showed high external quantum efficiency (7.9%) with a half life of 10,000h at a practical luminance (360 cd/m^2).

1. Introduction

Organic electroluminescent (EL) devices have many favorable properties for application in displays, such as fast response, thin and lightweight appearance. They are now used for mobile terminals and small TV displays, and are expected to use as solid-state lighting.

An organic EL device consists of two flat electrodes and a 100-nm-level organic thin film sandwiched by the electrodes. Its light-emitting mechanism is similar to that of an inorganic semiconductor LED. Holes and electrons injected from the electrodes move through their respective transport layers into the emissive layer (EML). The recombination of the holes and electrons in the EML causes the generation of molecular excited states (excitons) and light emission (Fig. 1). Due to random combination of spin state of the holes and electrons, it is estimated that 25% of the formed excitons are singlet and 75% are triplet. A fluorescent EL device uses singlet excitons to emit light and thus the internal quantum efficiency is limited to a maximum of 25%.

On the other hands, a phosphorescent EL device, which emits light from triplet excitons, utilizes the 75% triplet excitons formed by the direct recombination of holes and electrons, as well as the residual 25% triplet excitons that are converted from the 25% singlet excitons by energy transfer. Theoretically, the upper limit of the internal quantum efficiency of a phosphorescent EL device is 100%. However, ordinary organic materials that contain no heavy atoms do not emit phosphorescent light at room temperature. Recently, phosphorescent EL devices have been developed, using room-temperature-phosphorescent complexes of heavy metals, such as iridium or platinum, as emitters [1-2]. The device structures are designed to provide the internal quantum efficiency close to 100%, which have been verified in principle[3-4].

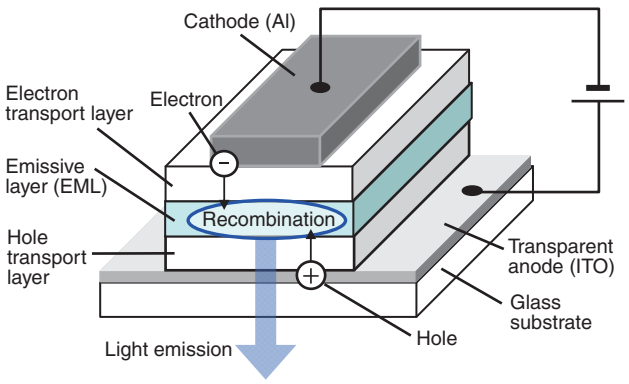

Fig. 1 Structure of a typical organic EL device.

The phosphorescent EL devices are intensively investigated for practical applications by many institutes. Their properties need improvement for practical devices in all the three primary colors: red, green and blue; which are required for displays and white light sources. Especially, for blue phosphorescent EL devices, it is essential to increase the efficiency and durability. We have worked on development of phosphorescent materials and phosphorescent EL devices,

Original paper (Received December 11, 2009)
* Frontier Core-Technology Laboratories
Research & Development Management Headquarters
FUJIFILM Corporation
Ushijima, Kaisei-machi, Ashigarakami-gun, Kanagawa 258-8577, Japan
** Analysis Technology Center
Research & Development Management Headquarters
FUJIFILM Corporation
Ushijima, Kaisei-machi, Ashigarakami-gun, Kanagawa 258-8577, Japan
*** Synthetic Organic Chemistry Laboratories
Research & Development Management Headquarters
FUJIFILM Corporation
Ushijima, Kaisei-machi, Ashigarakami-gun, Kanagawa 258-8577, Japan

utilizing our molecular design and synthesis technology for functional materials, as well as our film forming and analysis technology. This report provides our two methods effective for development of EML materials and EL devices: (1) Evaluation of stability of EML materials under ultraviolet (UV) irradiation and (2) Estimation of the distribution of excitons formed in the EML.

2. Development of EML Materials with High Stability under UV Irradiation

2.1 Degradation and Decomposition of EML Materials by UV Light

One of the biggest drawbacks of organic EL devices to practical use is a fall in the EL luminance efficiency during the operation. Degradation of the EML is considered as the major factor of the operational degradation of organic EL devices, since the fall in the EL luminance efficiency correlates closely with the fall in photoluminescence (PL) efficiency of the EML[5-6]. Chemical analysis before and after the degradation of organic EL devices shows that the faster decomposition of EML materials than the other layers. Furthermore, it is indicated that the holes or electrons alone have little effect to the decomposition, meanwhile, the excitons facilitate the decomposition seriously[7]. In order to increase the durability of an organic EL device, it is important to develop EML materials stable against excitons. We evaluated stability of EML materials against excitons by irradiating the EML film with UV light and comparing a decrease in PL efficiency with the irradiation dose. At the same time, we measured the UV-visible absorption spectrum of the EML film and checked the change in absorption intensity to determine the degree of decomposition of the EML materials.

Each sample was prepared by depositing a layer of a host containing a phosphorescent emitter as a dopant (50 nm), followed by an Al layer (100 nm) on a quartz substrate, and then encapsulating it with a desiccant in N_2 atmosphere. The Al layer was introduced to make the environment of the organic layer in each sample close to that of the layer in a usual organic EL device. A typical emitting layer consists of a host material, i.e., the chief ingredient, and a luminescent material (guest), i.e., the minor ingredient. In this study, we used N,N-dicarbazolyl-3,5-benzene (mCP) widely used as the host material and bis[2-(4,6-difluorophenyl) pyridinato-N,C2'] iridium picolinate (Firpic), a typical blue phosphorescent material, as the reference materials. A film of mCP doped with 10% Firpic was irradiated by UV light with a wavelength of 365 nm at 220 mW/cm^2. Fig. 2 shows the PL spectra of the film at various UV irradiation time. The PL intensity falls in proportion to the irradiation dose. It is reduced to 75% of the initial intensity after 120-minute irradiation. Fig. 3 (A) shows the absorption spectra of the mCP (host)/Firpic (guest) film, and the neat films of Firpic and mCP before UV irradiation. The absorption peaks of the mCP/Firpic film at shorter wavelengths than the absorption edge of the host (360 nm) show the absorption of the host, on the other hands, those at longer wavelengths show the absorption of the guest. The irradiated UV light is mostly absorbed by the guest. Fig. 3 (B) shows the differential absorption spectrum (result of deducting the spectrum after irradiation from that before irradiation) of the mCP/Firpic film before and after 120-minute irradiation. The differential absorption spectrum shows that the absorbance of both host and guest has fallen. The decrease is considered to indicate decomposition of each material by UV irradiation.

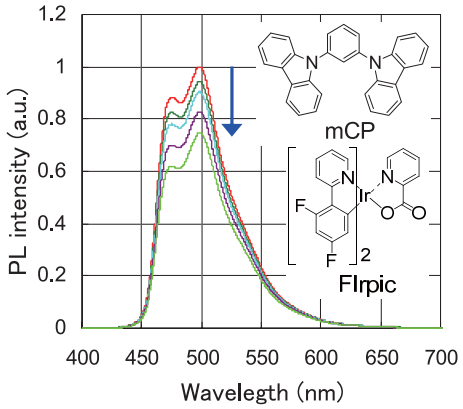

Fig. 2 PL spectra of mCP-10% FIrpic film at various UV irradiation times (0, 10, 30, 60, 120 min). (Inset ; structures of mCP and FIrpic).

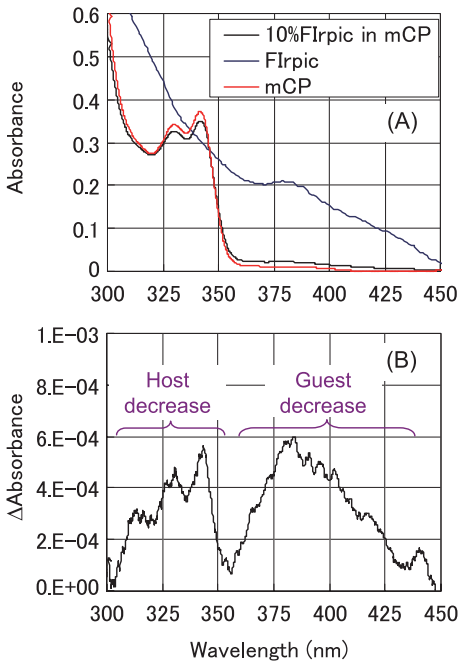

Fig. 3 (A) Absorption spectra of films (50 nm-thick) of 10% FIrpic in mCP before UV irradiation (black), FIrpic (blue), and mCP (red). The arrow indicates the wavelength of UV light (365 nm). (B) Differential absorption spectrum of 10% FIrpic in mCP film between the spectra of before and after UV irradiation (120 min).

The decomposition percentage of each material can be estimated by comparing the amount of decrease in absorbance with the initial absorbance. Fig. 4 shows changes in PL intensity by the UV irradiation dose and the decomposition percentages of the host and guest. The UV irradiation dose is calculated from the irradiation time and intensity corrected with the absorbance of the film at the UV wavelength. When the PL intensity is reduced to 75%, the decomposition rates of the host and guest are 0.12% and 2.3%, respectively. Considering the number of molecules of the host in the film is approximately 10 times of that of the guest, it is deduced that the nearly same number of molecules have decomposed in both materials.

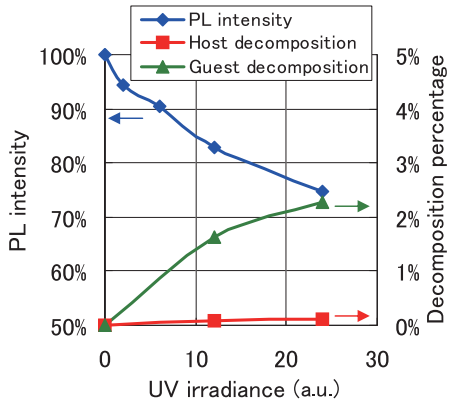

Fig. 4 Plot of PL intensities (blue diamond), decomposition percentages of host (red square) and guest (green triangle) vs. UV irradiance of films of 10% FIrpic in mCP.

2.2 PL Properties of Developed Materials

To develop materials highly stable against UV light, we made molecular design using theoretical chemical calculation. As for the candidates for the gust, we designed organic metal complexes with strengthened bonds between the central metal and the ligands to prevent their dissociation. We also eliminated the structurally weak part of ligands in complexes. We have then come up with a new blue phosphorescent gust material BG-1. As for the host, we have developed a material BH-1, which has a structure with weak bond eliminated.

Fig. 5 shows the PL spectra of the BH-1/BG-1 film and the mCP/Firpic film (guest content 10%). Table 1 shows the PL properties. Compared with the mCP/FIrpc film, the emission spectrum of the BH-1/BG-01 film has peaks in a short wavelength range and shows small spectral width. That indicates the color purity for blue light emission is improved. The PL quantum yield of this film is also high. These results indicate that BH-1 and BG-01 are a promising candidate for materials for high-efficiency high-color-purity blue phosphorescent EL devices.

Table 1 PL properties of FIrpic in mCP and BG-1 in BH-1.

Film	PL peak wavelength (nm)	Full width at half maximum (nm)	PL quantum yield (%)
10% FIrpic in mCP	470	51	88
10% BG-1 in BH-1	467	46	93

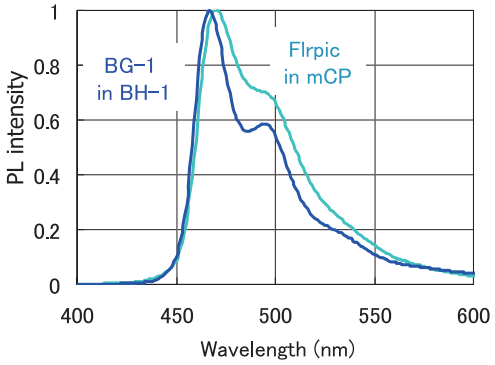

Fig. 5 PL spectra of films of 10% BG-1 in BH-1 and 10% FIrpic in mCP.

2.3 UV Stability Evaluation of a Film Made of the Newly Developed Material

Using the mCP/Firpic film as a reference, we examined the rate of decrease in PL intensity of films made of different materials compared with the UV dose. The content of the gust was 10%. As shown in Fig. 6, the mCP/BG-1 film is three times more resistant to UV light than the mCP/Firpic film, when the UV doses at the same PL decrease rate are compared. The BH-1/BG-1 film has double the resistance of the mCP/BG-1 film. The combination of BH-1 as the host and BG-1 as the guest will form an EML highly stable against excitons. Organic EL devices using this combination of materials are expected to give high operational stability.

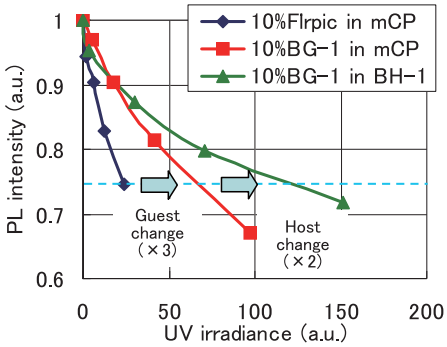

Fig. 6 Plot of PL intensities vs. UV irradiance for films of 10% FIrpic in mCP (blue diamond), 10% BG-1 in mCP (red square) and 10% BG-1 in BH-1 (green triangle).

3. EL Device Structure Design Based on Estimation of Site Distribution of Exciton Formation in EML

3.1 Comparing the Properties of EL Devices Made of the New Material and the Reference Material

We have made an EL device using the BH-1/BG-1 for its EML. We compared the properties of the device with those of an EL device with mCP/Firpic EML. Fig. 7 shows the structure of fabricated devices. The two devices have a same structure except for the EML materials. We call this structure of a device Structure 1. Table 2 shows the properties of the two devices (Devices A and B). The operational time to half luminance of Device B (BH-1/BG-1 EML) at a constant current is more than 30 times longer than that of Device A (mCP/Firpic EML). This result indicates that the durability of an EL device during operation will be drastically increased by using materials enhanced in stability against excitons for the EML. [This increase (more than 30 times) is larger than the increase in resistance against UV light (about 6 times) by using the same material in Section 2.3 above. One of the possible reasons is that there is combined degradation due to combinations of excitons with holes or with electrons.] However, the external quantum efficiency [= internal quantum efficiency multiplied by extraction efficiency (approx. 20%)] of Device B is lower than that of Device A. It is much lower than a theoretical limit [= 93% × 20% ≈ 18%] projected from the PL quantum yield. Next section will discuss our development for enhancing the external quantum efficiency.

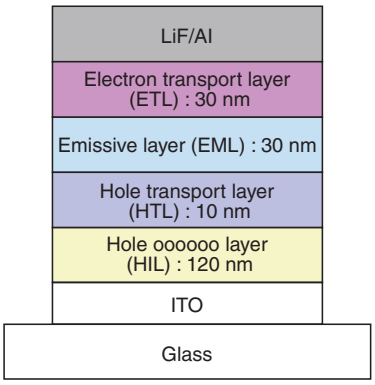

Fig. 7 Structure of a fabricated device.

3.2 Improvement in Device Structure Based on the Distribution of Exciton Formation

In an organic EL device, excitons are formed by the recombination of the holes and electrons in the EML. The excitons formed in the EML often dissipate into the hole transport layer and the electron transport layer adjacent to the EML. That is considered one of the causes to lower the EL luminance efficiency. It will be desirable that more excitons form in the center of the EML and that less form near the interfaces with the adjacent layers. To improve the device structure in this regard, we need to know the distribution of excitons formed in the EML. For this purpose, we have devised a method to estimate the distribution of the sites where excitons are formed by extra fluorophore doping in the EML.

We will explain the method in detail while referring to Fig. 8. Assume the EML is 30 nm thick and the distribution is determined in four parts of the layer.

(A) A regular EL device (Device 0) and test devices (Devices 1-4) were fabricated with the same structure except that a small amount of fluorophore (rubrene) was doped in the EMLs of Devices 1-4 with variation of the doping position,

(B) The EL spectra of Devices 1-4 were measured and compared with that of Device 0.

(C) The site distribution of exciton formation in the EML of Device 0 was estimated on the basis of the fluorescence intensities of Devices 1-4.

We estimated the distribution in Device B as shown in Table 2. Many excitons have been formed near the interfaces,

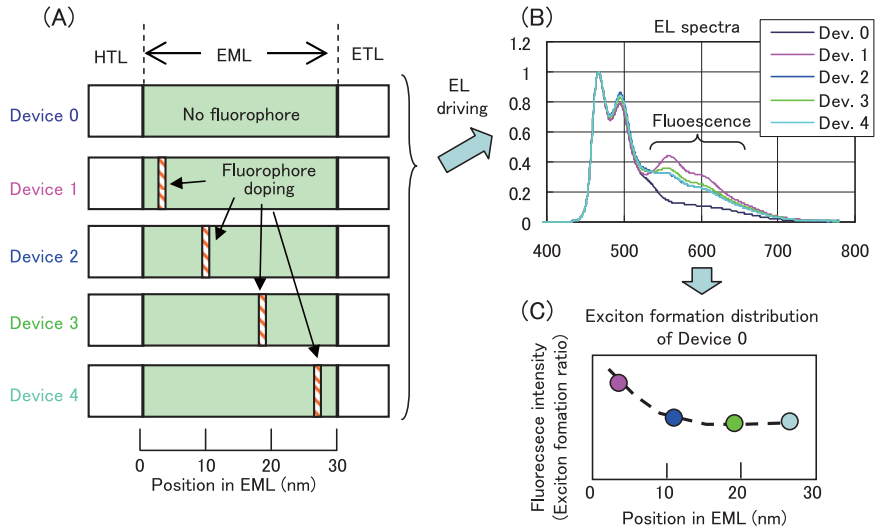

Fig. 8 Concept of estimation of exciton formation distribution in emissive layer by fluorophore doping. (A) Emissive layer structure of test devices. (B) EL spectra of the test devices when driven. (C) Estimated exciton formation distribution of Device 0 by fluorescence intensities of the test devices.

Table 2 EL characteristics of fabricated devices (@360 cd/m^2).

Device	Host/Guest	Structure	Driving voltage(V)	External quantum efficiency (%)	Operational time to half luminance (h)	CIE (x, y)
A	mCP/FIrpic	Structure 1	7.2	7.2	110	(0.15, 0.29)
B	BH-1/BG-1	Structure 1	7.9	6.8	4,000	(0.17, 0.27)
C	BH-2/BG-1	Structure 2	5.3	7.9	10,000	(0.20, 0.28)

especially near the hole transport layer. That suggests a decline in efficiency is attributed to moving of excitons into the adjacent layers (curve with blue circles in Fig. 9).

While estimating the exciton distributions of devices with various structures, we sought ways of enhancing the EL properties of Device B.

(1) To reduce the driving voltage, we increased the carrier density and enhanced the charge mobility by doping a charge generating material to the hole injection layer and the electron transport layer (Structure 1).

(2) We modified BH-1 and made an improved host material BH-2 to enhance the hole mobility in the EML and thereby concentrating the distribution of excitons in the center of the EML, which was near the hole transport layer in Structure 1. In the BH-2/BG-1 device in Structure 2 (Device C), it is likely that exciton formation is decreased near the interfaces of the EML, especially one with the hole transport layer, and that excitons are evenly distributed in the EML (curve with red squares in Fig. 9).

Looking at the EL properties of Device C (Table 2), the external quantum efficiency has been improved from Device B and the dissipation of excitons through the both interfaces of the EML has been reduced. Furthermore, the durability has been also improved. It is considered that the even distribution of excitons prevents local degradation of the EML. We have finally come up with a blue phosphorescent organic EL device that attains the time to half luminance of 10,000 hours at a practical brightness (360 cd/m^2). As for external quantum efficiency, there is still room for improvement. We are studying for further improving the distribution of exciton formation.

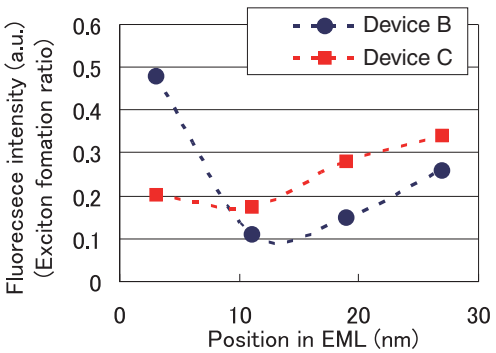

Fig. 9 Change in exciton formation distribution by improvement of HIL, ETL and host.

4. Conclusion

We have developed a high-efficiency, high-durability blue phosphorescent organic EL device and its materials. We used two methods during the development: stability evaluation of EML materials under UV irradiation and estimation of the distribution of exciton formation in the EML of newly developed EL devices. Finally, we have achieved good efficiency and durability by improving the distribution of exciton formation and finding the host and guest materials that exhibit high stability against UV light.

We have been also carrying out development of red and green phosphorescent EL devices and their materials using the same methods. Table 3 shows the properties of our latest phosphorescent EL devices in those three colors. Not only blue but green and red EL devices are almost achieving high efficiency and durability. We will continue our efforts in development of materials and devices to launch phosphorescent organic EL devices as soon as possible.

Table 3 EL characteristics of blue-, green-, and red-emitting devices.

Device	Driving voltage (V)	External quantum efficiency (%)	Operational time to half luminance (h)
Blue (@360cd/m^2)	5.3	7.9	10,000
Green (@1,000cd/m^2)	4.1	15.0	>50,000
Red (@300cd/m^2)	3.5	14.1	>100,000

References

1) Baldo, M. A.; O'Brien, D. F.; You, Y.; Shoustikov, A.; Sibley, S.; Thompson, M. E.; Forrest, S. R., Nature **395**, 151-154 (1998).

2) Baldo, M. A.; Lamansky, S.; Burrows, P. E.; Thompson, M. E.; Forrest, S. R., Appl. Phys. Lett. **75**, 4-6 (1999).

3) Ikai, M.; Tokito, S.; Sakamoto, Y.; Suzuki, T.; Taga, Y., Appl. Phys. Lett. **79**, 156-158 (2001).

4) Adachi, C.; Baldo, M. A.; Thompson, M. E.; Forrest, S. R., J. Appl. Phys. **90**, 5048-5051 (2001).

5) Popovic, Z. D.; Aziz, H.; Hu, N. -X.; Ioannidis, A.; dos Anjos, P. N. M., J. Appl. Phys. **89**, 4673-4675 (2001).

6) Giebink, N. C.; D'Andrade, B. W.; Weaver, M. S.; Mackenzie, P. B.; Brown, J. J.; Thompson, M. E.; Forrest, S. R., J. Appl. Phys. **103**, 044509-1−044509-9 (2008).

7) Kondakov, D. Y.; Lenhart, W. C.; Nichols, W. F., J. Appl. Phys. **101**, 024512-1−024512-7 (2007).

UDC 544.722.122+621.795

Development of the Organic-inorganic Hybrid Super-hydrophilic Layer

Sumiaki YAMASAKI*, Satoshi TANAKA*, Makoto FUKUDA*, Yuuichiro MURAYAMA**, Yoshiaki KONDO**, Hideki OGASAWARA**, and Osamu UCHIDA***

Abstract

FUJIFILM Corporation has developed a novel super-hydrophilic layer using organic-inorganic hybrid technology. Different from phtocatalyst TiO_2, our hydrophilic layer shows super-hydrophilicity when stored in a dark room for a long time, and has various properties such as anti-clouding, self-cleaning, and hard surface. In addition, it can be applied to various materials (glass, resin metal), and has many other uses.

1. Introduction

A super hydrophilic surface is a "surface extremely wettable by water" with a contact angle of 10 degrees or less (Fig. 1). One of the most commonly known examples is a coating material using a photocatalyst (TiO_2). This material exhibits super hydrophilicity under UV light. It is attracting attention as an anti-stain material that is easily cleaned with water because of its super hydrophilicity[1]. In addition to anti-stain quality, hydrophilicity is known to bring about many effects. More and more hydrophilic products are being launched for various applications (Fig. 2).

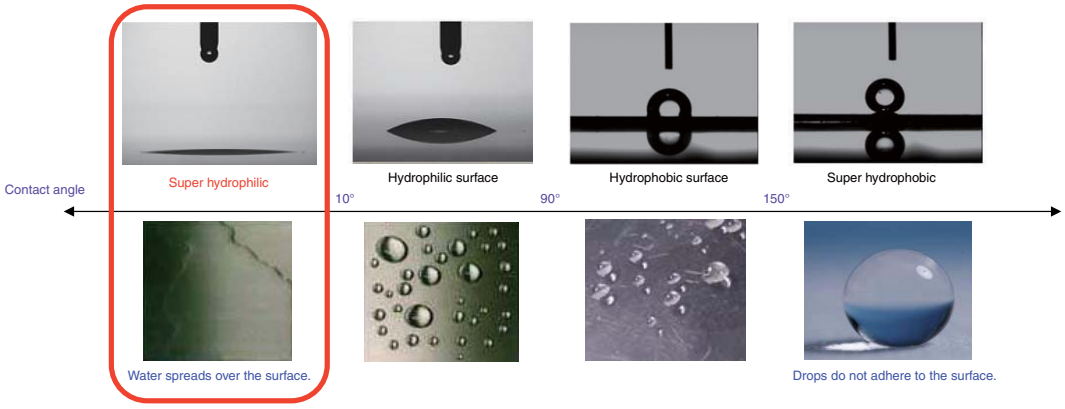

Fig. 1 Comparison between hydrophilic surface and hydrophobic surface.

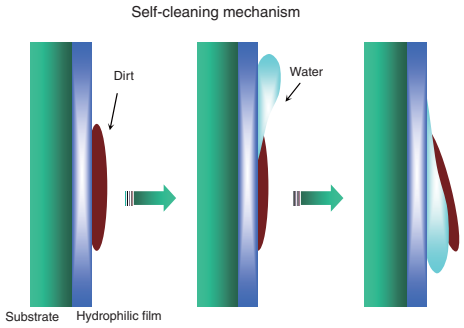

Effects of hydrophilicity
(1) Anti-fog (Prevents fogging)
(2) Self-cleaning / easy-cleaning (Cleans dirt)
(3) Quick dry (Drops spread)
(4) Cooling (Takes the heat of vaporization)
(5) Draining / water distribution (Very thin water film)
(6) Water absorptive (Enhanced wettability)
(7) Resistant to snow and ice accretion
(8) Biocompatible
(9) Antistatic
(10) Enhancement in coating material performances

Fig. 2 Hydrophilic effects.

Original paper (Received November 19, 2009)
* Synthetic Organic Chemistry Laboratories
Research & Development Management Headquarters
FUJIFILM Corporation
Nakanuma, Minamiashigara, Kanagawa 250-0193, Japan
** Industrial Products Division
FUJIFILM Corporation
Ohgi-cho, Odawara, Kanagawa 250-0001, Japan
*** Procurement Division
FUJIFILM Corporation
Akasaka, Minato-ku, Tokyo 107-0052, Japan

FUJIFILM has developed an original "super hydrophilic film that has a strong molecular bridge structure"[2], making the most of its functional polymer design/synthesis technology honed in the development and manufacturing of graphic materials and nanocomposite technology.

This report describes the method of making the super hydrophilic film, its structure, features of the properties, and uses of the features.

2. Structure of Super Hydrophilic Film

The super hydrophilic film has an "elaborate molecular bridge structure" inside the film. The hydrophilic group is oriented toward the outermost surface by delicate hydrophilicity/hydrophobicity control (Fig. 3). This structure gives the film the following features.

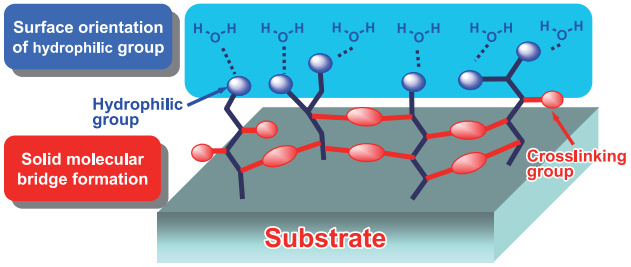

Fig. 3 Image of super-hydrophilic layer.

(1) As the hydrophilic group is oriented toward the outermost surface, a free water layer is easily formed on the surface. Although the mechanism is yet to be defined, an additive controls the surface hydrophilicity (Fig. 4). When a hydrophilic film does not contain an additive, the initial contact angle of a water droplet is around 40 degrees. As immersed in water for a long time, the hydrophilic group is oriented toward the surface and super hydrophilicity is exhibited. When a hydrophilic film contains an additive, it exhibits super hydrophilicity without immersion in water. The additive is considered to help to orient the hydrophilic group toward the surface.

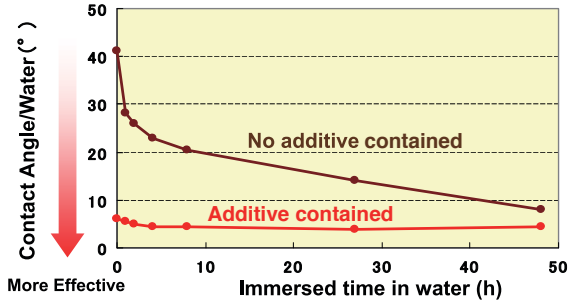

Fig. 4 Effect of additive.

(2) The elaborate molecular bridge structure makes a strong film that will not be swollen by water.

Organic and inorganic materials fused into a hybrid form the elaborate molecular bridge structure, which makes a high-strength film.

3. Making Super Hydrophilic Film

To make the super hydrophilic film, we apply a water-based coating liquid to a substrate and harden it with heat. The coating liquid contains a high-hydrophilic polymer developed by our functional polymer design technology. The procedure consists of the three steps below (Fig. 5).

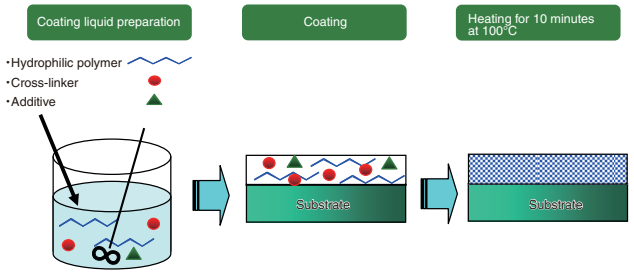

Fig. 5 Production method of super-hydrophilic layer.

(1) Preparing coating liquid

Mix the hydrophilic polymer, cross-linker and additive and agitate the solution for two hours at room temperature. That produces a sol precursor of an organic-inorganic hybrid.

(2) Film making

The coating liquid can be applied to various substrates in various thicknesses. The thickness ranges from several tens of nanometers to several micrometers utilizing our precise coating technique.

(3) Hardening

Heating and drying for 10 minutes at 100°C accelerates the hardening and results in a nanocomposite of the organic-inorganic-hybrid super hydrophilic film.

4. Features

We have found that our super hydrophilic film has greater hydrophilicity than other companies' hydrophilic films using organic materials, such as photocatalyst and polyacrylic acid. We will explain its significant features as below with the experiment data.

(1) Sustainability of surface hydrophilicity

Photocatalysts exhibit hydrophilicity in sunlight but they cannot keep the hydrophilicity in the dark. Our super hydrophilic film, different in mechanism from a photocatalyst (TiO_2), keeps the super hydrophilicity

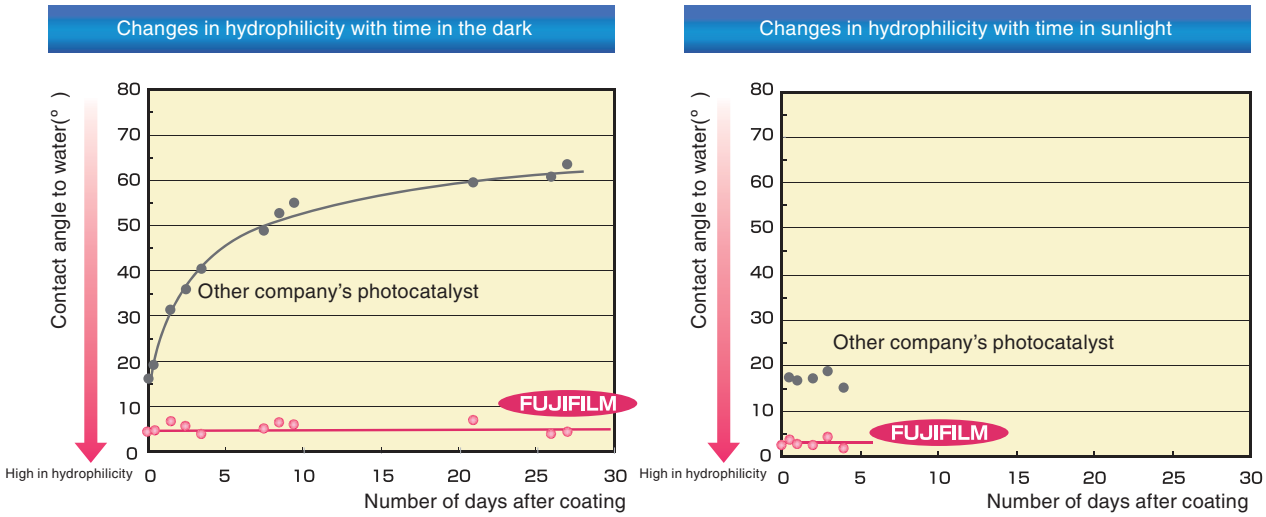

Fig. 6 Change of hydrophilicity under a dark room condition.

Fig. 7 Super-hydrophilic effect.

in the dark for at least one month (Fig. 6). And, the contact angle of our film does not exceed 10 degrees. Our film will be suitable for indoor applications, which are difficult for photocatalysts.

(2) Anti-fog quality and ease of cleaning

Fogging on glass or mirror is generally caused by very small water droplets on the surface. The droplets form acute angles to the surface. They reflect and diffuse light and the surface looks as if it is fogged. Our super hydrophilic film has high anti-fog quality. It does not fog even when water vapor of a humidifier is directly blown on the film (Fig. 7). The film also has high easy-cleaning quality. Oil and grease are easily washed off the film with water (Fig. 7). We infer that this is because the hydrophilic group is oriented toward the outermost surface of the film and that a uniform water layer is easily formed on the surface.

(3) Coating film strength

Another feature of our film is the high coating film strength. Our film is harder than other companies' organic hydrophilic polymers (Fig. 8). We presume that the strength comes from the elaborate molecular bridge structure of the nanocomposite.

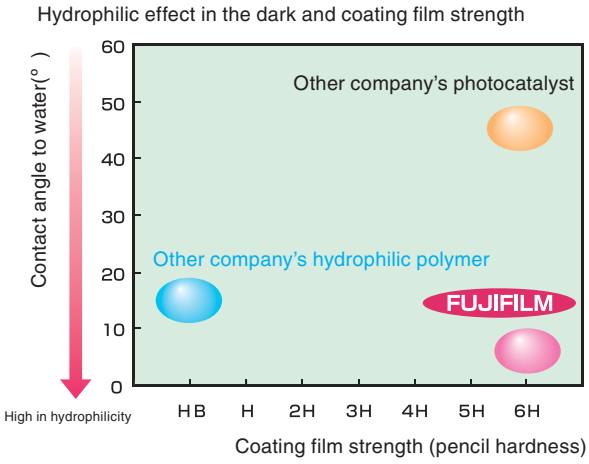

Fig. 8 Comparison with other hydrophilic products.

Unlike photocatalyst, our film does not decompose the substrate. That means our film can be used for a wide variety of substrate materials, such as glass, resin and metal,

although it needs a primer layer suitable for the substrate material (Table 1).

Table 1 Typical physical properties applied to various substrates.

Substrate	Contact angle to water		Hydrophilic properties			
	Untreated	Treated	Pensile hardness		Adhesion	Scratch resistance
			Untreated	Treated		
Glass plate	14°	≦5°	≧9H	6H	Good (no peeled off)	Good (no scratch)
Tile	14°	≦5°	≧9H	6H	Ditto	Ditto
Polycarbonate plate	89°	≦5°	≦6B	≦6B	Ditto	Ditto
Acrylic plate	67°	≦5°	B	HB	Ditto	Ditto
PET film	67°	≦5°	≦6B	H	Ditto	Ditto
SUS plate	99°	≦5°	2B	B	Ditto	Ditto

◊ Adhesion: 180-degree peel test using adhesive tape
◊ Scratch resistance: Rub the surface back and forth with a wet cloth 1,000 times and perform visual check. Load of 500 g at 5,000 mm/min.

5. Applications

Table 2 shows the functions and possible application fields of our super hydrophilic film.

Table 2 List of properties and corresponding anticipated applications for super-hydrophilic layer.

Functions	Applications (examples)
Anti-fog	Mirror, window, showcase and lens
Self-cleaning / easy-cleaning	Washbasin, sink, exterior wall and car body
Quick dry	Bathroom floor, sanitary ware and glass dishes
Cooling	Warehouse roof and asphalt
Draining / water distribution	Fuel battery and air-conditioner aluminum fan
Water absorptive	Fiber and filter
Resistant to snow and ice accretion	High-voltage power line and road safety mirror
Biocompatible	Contact lens and catheter
Antistatic	Display monitor and plastic component
Enhancement in coating material performances	Enhancement in wettability and ease of coating

6. Conclusion

We have developed a super hydrophilic film with a strong molecular bridge structure. We have made the film using delicate hydrophilicity/hydrophobicity control of the film surface and making the most of the functional polymer design/synthesis technology honed in the development and manufacturing of graphic materials and nanocomposite technology. It provides super hydrophilicity based on its mechanism different from that of photocatalyst. One of the features is the coating film strength higher than other hydrophilic polymers. To launch the super hydrophilic film, we need further study tailored to the requirements of individual applications. We are planning to start technological development for those requirements.

References

1) Fujimoto, Noboru. The control of Wetting and water repellent, Hydrophophilic technology -Practical application, Surface treatment, Test & evaluation, and Product development-. Tokyo, Technical Information Institute (2007).
2) a) Yamasaki, Sumiaki; Kawamura, Koichi. FUJIFILM Corporation. Surface Hydrophilic Member. JP2002-361800A. 2002-12-18.
b) Tanaka, Satoshi; Fukuda, Makoto; Hoshi, Satoshi. FUJIFILM Corporation. Hydrophilic Composition and Hydrophilic Member. JP2008-222998A. 2008-9-25.

UDC 613.49

Development of Functional Cosmetics "ASTALIFT WHITENING ESSENCE"

Fumi KUSUDA*, Toshiaki KUBO*, Yukio SUDO*, Tatsuo KAWABUCHI**,
Atsushi ORIKASA***, and Yoshisada NAKAMURA*

Abstract

Skin blemishes are big problems. We focused particular attention on "everlasting blemishes". We developed "ASTALIFT WHITENING ESSENCE", which contains Astaxanthin. Astaxanthin regulates cytokine levels during the production of melanin, and along with vitamin C, inhibits excessive melanin production. The "ASTALIFT WHITENING ESSENCE" combines substances that control formation of normal blemishes with other substances to act on "everlasting blemishes". We found this product moisturizes the skin and makes the skin more elastic. It also not only reduces the number and the size of blemishes, but inhibits the forming of wrinkles.

1. Introduction

FUJIFILM is seeking to be a total healthcare company covering "therapy" and "prophylaxis" in addition to our conventional expertise, "diagnosis," such as x-ray image diagnosis and hemodiagnosis. In the field of prophylaxis, we have launched functional food and functional cosmetics (skin care cosmetics) described below since 2006.

"Anti-aging" tops the list of cosmetic functions women look for, beating "moisturizing" and "whitening". Skin aging is largely attributed to UV radiation and resultant active oxygen, rather than genes considered to cause natural aging. The decline in the skin functions and changes in the skin structure by light are called photoaging. It is the main target of anti-aging care. Especially, age spot is the biggest skin complaint.

The ASTALIFT WHITENING ESSENCE (Fig. 1) launched in February 2009 has been designed to combat the age spot.

Fig. 1 ASTALIFT WHITENING ESSENCE.

2. What is Age Spot?

Production and Discharge of Melanin, Cause of Age Spot

Melanin pigment responsible for age spots is produced by the pigment cells (melanocyte) in the epidermis. The melanin pigment is transferred from the pigment cells to the surrounding epidermal keratinocytes and it protects DNA in the cells from harmful UV radiation.

Melanin pigment is normally discharged from the body as scurf with the metabolism (turnover) of keratinocytes. The rates of the production and the discharge are balanced to maintain the skin complexion[1].

When skin is exposed to UV radiation or other external stimulus or it suffers internal stimulus including stress, melanin pigment production is accelerated. The excessive production causes suntan and age spots. With the turnover, melanin pigment is gradually discharged and the skin restores its complexion. But, that is not always the case.

Age spots may result when melanin production does not stop or when some melanin pigments do not go with the turnover. We call the latter "everlasting blemish". The whitening essence in this report targets that type of age spot (Fig. 2).

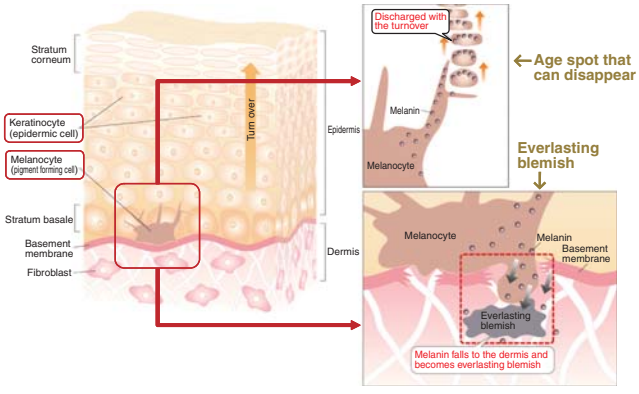

Fig. 2 Mechanism of blemish production.

Original paper (Received November 20, 2009)
* Life Science Research Laboratories
Research & Development Management Headquarters
FUJIFILM Corporation
Ushijima, Kaisei-machi, Ashigarakami-gun, Kanagawa 258-8577, Japan
** Life Science Products Division
Healthcare Business Headquarters
FUJIFILM Corporation
Nishiazabu, Minato-ku, Tokyo 106-8620, Japan
*** New Business Development Office
Life Science Products Division
Healthcare Business Headquarters
FUJIFILM Corporation
Akasaka, Minato-ku, Tokyo 107-0052, Japan

The "everlasting blemish" is caused when melanosomes containing melanin produced by melanocyte fall through a hole in the basement membrane into the dermis and they are not carried with the turnover.

Mechanism of Melanin Production

Melanin pigment that causes age spots is produced by the following mechanism of action (Fig. 3).

When stimulated by UV radiation or resultant singlet oxygen, keratinocytes produce a cytokine called IL-1α (interleukin-1α). And then, the keratinocytes also produce cytokines which give melanocytes a command to produce melanin, including ET-1 (endothelin-1) and SCF (stem cell factor), and proinflammatory cytokines such as PGE2 (prostaglandin E2). --- Fig. 3 (1)

The fibroblasts in the dermis produce cytokines including HGF (hepatocyte growth factor) and SCF. These cytokines stimulate melanocytes. --- Fig. 3 (1)

The stimulated melanocytes synthesize melanin pigment from tyrosine as the starting ingredient through oxidation polymerization inside melanosomes (a type of endoplasmic reticulum in a cell) provided with a substrate, e.g., tyrosine, and an enzyme, e.g., tyrosinase. --- Fig. 3 (2)

The melanosomes containing melanin pigment are normally carried through a dendritic projection of melanocytes and taken up by keratinocytes by their phagocytosis.

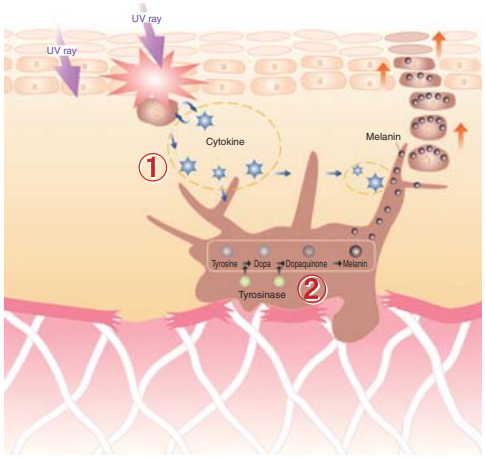

Fig. 3 Normal blemish generation mechanism.

2.1 Everlasting Blemish

Melanophage, the Culprit of Everlasting Blemish

Melanosomes that have not taken up by keratinocytes to fall into the dermis through a hole in the basement membrane are captured by macrophages in the dermis.

Macrophages provide cell immunity. They migrate and phagocytose foreign bodies. Macrophages in the dermis phagocytose melanosomes as foreign bodies. A macrophage that has phagocytosed a melanosome is called melanophage. Once turned into melanophage, the cell loses mobility, although it is unknown why. The melanin captured in a melanophage and remaining in the skin is the culprit of the everlasting blemish[2].

The left photo in Fig. 4 shows melanosomes containing melanin in a pigment cell on the basement membrane. The photo also shows a hole in the basement membrane near the cell. The right photo shows a melanophage that phagocytosed melanosomes.

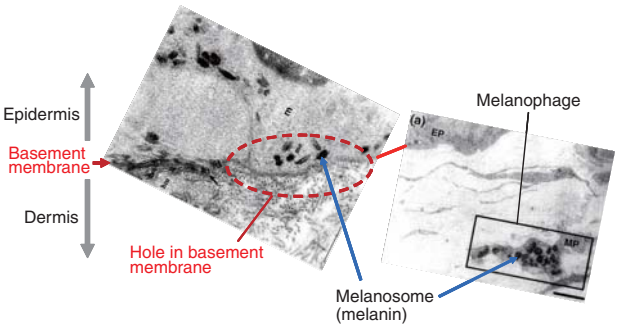

Fig. 4 Melanophage[2].

2.2 Breakage of Basement Membrane

What is Basement Membrane? Why is it Broken?

The basement membrane located between the epidermis and the dermis. It joins the relatively hard epidermis packed with cells and the relatively soft dermis mostly made of extracellular matrices. It also has something to do with keratinocyte division. This membrane is a sheet-like structure mainly made of type IV collagen.

Exposure to UV radiation increases production of MMP (matrix metalloproteinase) that degrades collagen as well as producing singlet oxygen in the keratinocytes in the epidermis and fibroblasts in the dermis. --- Fig. 5 (4)

When exposed to UV radiation, keratinocytes produce proinflammatory cytokines. They also increase production of MMP. --- Fig. 5 (3)

The MMP accelerates degradation of type IV collagen in the basement membrane and makes a hole in the basement membrane. --- Fig. 5 (5)

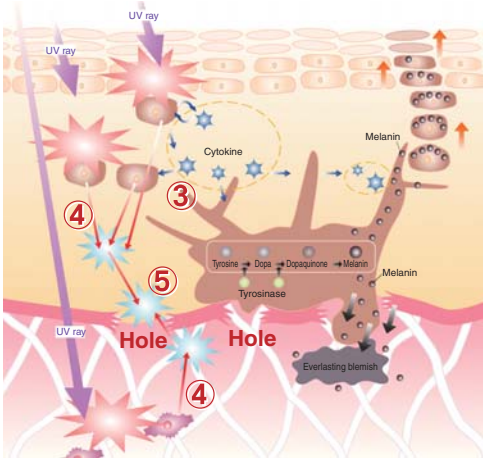

Fig. 5 Everlasting blemish generation mechanism.

3. Development of ASTALIFT WHITENING ESSENCE

Product Concept

The recently developed ASTALIFT WHITENING ESSENCE aims at combating the everlasting blemish. To achieve the aim, the essence is designed to control the melanin pigment production triggered by UV radiation and resultant singlet oxygen based on the above-described mechanism and to prevent the basement membrane from breakage and repair it.

3.1 Controlling Age Spot Formation

Protecting Against UV Radiation and Eliminating Singlet Oxygen

The first step to control production of melanin is protection against UV radiation. For this purpose, the ASTALIFT series has Day Protector containing UV inhibitor.

The next step is to eliminate singlet oxygen that is produced by UV radiation. We have focused on astaxanthin[3]. Astaxanthin eliminates singlet oxygen 1,000 times faster than CoQ10 the antioxidant effect of which is used for cosmetics (Fig. 6).

Astaxanthin

Astaxanthin is a type of carotenoid pigment derived from algae, such as Haematococcus pluvialis. Prawns, crabs, salmon and other water animals contain astaxanthin via food chain[4].

Astaxanthin inactivates singlet oxygen by taking its energy. Unlike inactivation by redox, repeated elimination counts performed by astaxanthin are 1,800 times more than those done by CoQ10.

Controlling Cytokine Production

We have found that astaxanthin has the effect of inhibiting production of cytokines that play an important role in the melanin production mechanism. Fig. 7 shows astaxanthin's effect of inhibiting IL-1α that is produced by UV radiation to human keratinocytes. Controlling IL-1a will help control melanin production. IL-1α is an upstream cytokine which commands melanin production.

We have also found that astaxanthin inhibits production of PGE-2 in keratinocytes, a proinflammatory cytokine that also commands transfer of melanosomes from melanocytes to keratinocytes (Fig. 10).

Controlling Melanin Production

We have confirmed that astaxanthin inhibits melanin production in melanocytes like APM does (Fig. 8). Fig. 9 shows effects of astaxanthin and APM, which inhibit melanocytes from producing melanin. It shows that astaxanthin has the similar effect to that of APM although they do not produce a synergetic effect.

Astaxanthin is thus effective for controlling age spots, inhibiting all the steps toward melanin production. To help

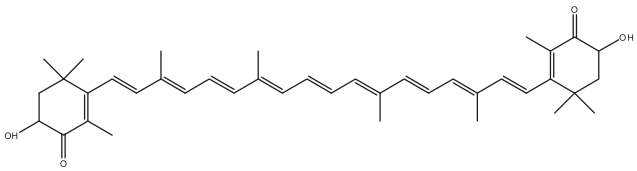

Fig. 6 Structure of Astaxanthin.

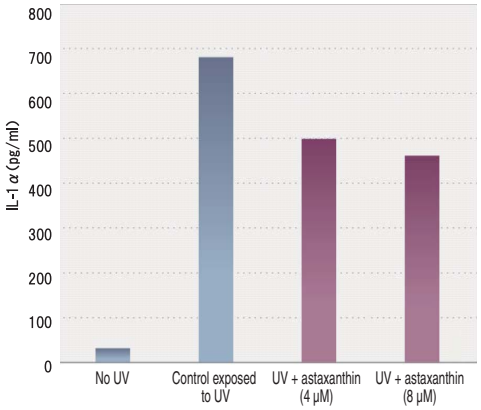

Fig. 7 Generation inhibition of IL-1α by Astaxanthin.

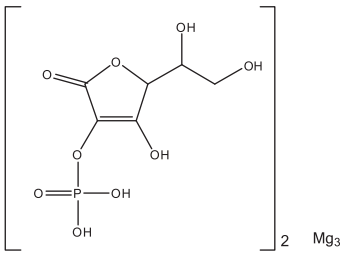

Fig. 8 Structure of the APM, "ascorbic acid manganese phosphate".

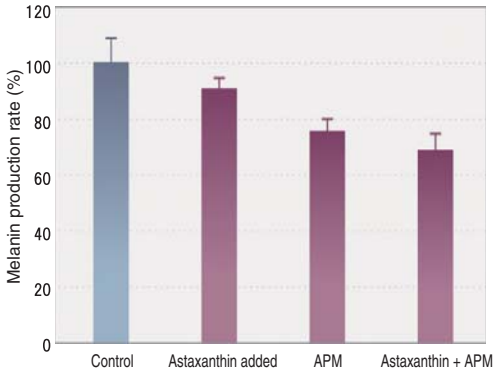

Fig. 9 Melanin production inhibition by Astaxanthin and APM.

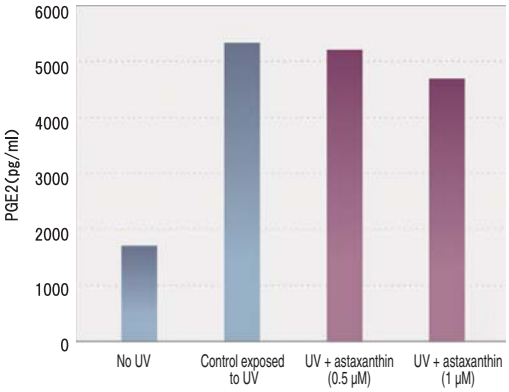

Fig. 10 Generation inhibition of PGE2 by Astaxanthin.

astaxanthin reach the depth of skin while keeping it effective, we have developed approximately 50-nm emulsion[5] making the most of our emulsifying and dispersion technology accumulated for photographic films.

3.2 Preventing Hole in Basement Membrane

The whitening essence contains an ingredient to prevent a hole in the basement membrane that is a cause of the everlasting blemish.

Preventing Breakage of Basement Membrane

MMP accelerates the creation of a hole in the basement membrane. Production of MMP is accelerated by singlet oxygen generated by UV radiation. As stated above, astaxanthin not only eliminates singlet oxygen but also inhibits cytokine production (Fig. 10) and thus it inhibits production of MMP.

Regeneration of Basement Membrane

The basement membrane is basically made of collagen. Pico-Collagen (acetyl hydroxyproline) and APM contained in the collagen whitening essence act on fibroblasts and accelerate production of collagen that forms the membrane structure.

Acetyl hydroxyproline is a derivative of hydroxyproline that specifically abounds in collagen protein. It becomes hydroxyproline in the skin. When hydroxyproline, a decomposed material of collagen protein, abounds, fibroblasts accelerate production of collagen.

3.3 Product Evidence

We have conducted four-week test for continued use of the whitening essence that contains an ingredient effective for all the steps of melanin production attributable to age spots and an ingredient preventing a hole in the basement membrane attributable to the everlasting blemishes.

We asked 49 women in their 40s to 60s to use the ASTALIFT WHITENING ESSENCE after their regular skin care in the morning and evening. We checked the skin condition before after the test. Fig. 11 shows a change in the number of age spots by continued use of the essence for four weeks. Fig. 12 shows a change in the average area of age spots of the 49 women. Both figures show a decrease.

Fig. 13 shows an example of a reduced age spot. The spot is reduced in area and lightened.

4. Conclusion

Development of Photographic Technology

We have developed the ASTALIFT WHITENING ESSENCE as a functional cosmetic with well-designed ingredients based on age spot mechanism, making the most of our accumulated technology developed for photographic films (Fig. 14). Specifically, the emulsifying and dispersion technology achieves highly functional fine particles (nanotechnology). The antioxidation technology helps utilize various antioxidants. Collagen material technology is common to skin and photographic film.

We will continue to study the science of skin care and put in our original technologies to develop functional cosmetics that provide new values for customers.

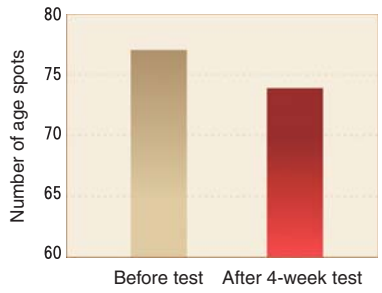

Fig. 11 Decrease in the number of blemishes after four weeks of continuous use.

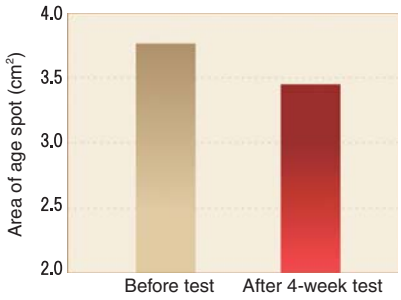

Fig. 12 Decrease in the size of blemishes after four weeks of continuous use.

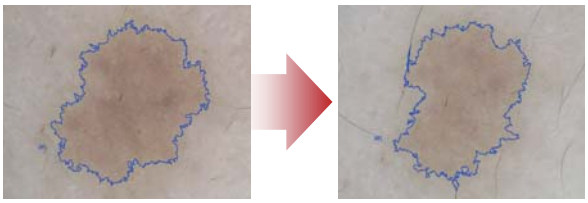

Fig. 13 Example of decrease in the color density of blemishes after four weeks of continuous use.

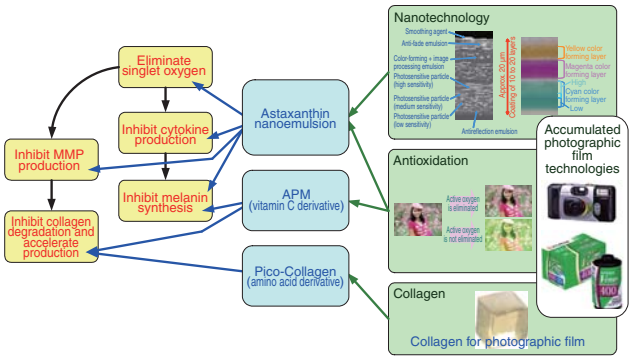

Fig. 14 Development of the photographic technology.

References

1) Advanced Cosmetic Dermatology. Imayama, Shuhei et al., eds., Tokyo, Nankodo (2008).
2) a) Bacharach-Buhles, M.; Lubowietzki, M.; Altmeyer, P. Dose-Dependent Shift of Apoptotic and Unaltered Melanocytes into the Dermis after Irradiation with UVA 1. Dermatology **198** (1), 5-10 (1999).
   b) Ünver, N.; Freyschmidt-Paul, P.; Hörster, S.; Wenck, H.; Stäb, F.; Blatt, T.; Elsässer, H-P. Alterations in the epidermal–dermal melanin axis and factor XIIIa melanophages in senile lentigo and ageing skin. British Journal of Dermatology **155** (1), 119-128 (2006).
3) Carotenoid –the Diversity and Bioactivity–. Takaichi, Shinichi ed., Tokyo, Shokabo Publishing, (2006).
4) Mori, Junichi et al. In-vivo Measurement of Antioxidant Ability of Astaxanthin. Japanese Society for Astaxanthin, reported on 2007-9-12.
5) Ogawa, Manabu; Sato, Masao; Suzuki, Keiichi. Development of Astaxanthin Nano Emulsion with Improved Shelf Life and Enhanced Absorbability. FUJIFILM RESEARCH & DEVELOPMENT. No.52, 26-29 (2007).

UDC 616-074+577.113

Development and Application of DNA Array (GD-700) for Congenital Anomaly Syndromes

Yoshihide IWAKI*, Yasuyuki ISHII*, Dai UJIHARA*, Junya YOSHIDA*,
Hayato MIYOSHI*, Tomoko MORI*, Hideyuki KANEHARA**,
Masayuki KURAMITSU***, and Kaoru TERASHIMA*

Abstract

The recent development of the Comparative Genomic Hybridization (CGH) method enables the comprehensive analysis of the fine structure of human chromosomal abnormalities. The causes of many congenital anomaly syndromes in newborns and children are difficult to be determined. Therefore, it is significantly important to clarify the syndromes and to apply the CGH method for a practical diagnosis.

Professor Inazawa of Tokyo Medical and Dental University established a well reproducible CGH method that enables quantitative analysis of the change in the copy number of the genome. Furthermore, his team prepared the Genome Disorder Array (GD-700) with BAC DNA for congenital anomaly syndromes. From 2005, FUJIFILM has collaborated with Prof. Inazawa, has proven this GD-700 to be practical, and developed an original analysis method "Dual Hybridization method" this year. In this paper, we introduce the design of this array and its original method.

1. Introduction

The conventional analysis of genomic aberration leading to congenital anomaly syndromes is carried out mostly by chromosomal test. As the Comparative Genomic Hybridization (CGH) method has been recently developed, it is now possible to analyze anomalies in the microscopic structure of a human chromosome[1)]. Causes of many congenital anomaly syndromes in newborns and young children are unknown. To determine the causes and diagnose with the CGH method are very important to this field of medical care.

Professor Inazawa at Tokyo Medical and Dental University has established a quantitative analysis method that detects loss or gain in a single copy of a chromosome with high reproducibility[2)]. The professor also made Genome Disorder Array (GD-700) for diagnosis of congenital anomaly syndromes. FUJIFILM started joint research with Professor Inazawa's team in 2005. We have worked with Professor Inazawa, who conducted practicality test on more than 500 cases, and the consortium for practical application of array CGH diagnosis method, which is led by, Professor Inazawa and BML, Inc. At the same time, we have developed Dual Hybridization, our original analysis method suitable for clinical examination. As a result, we have found a new examination system suitable for clinical use based on GD-700 and Dual Hybridization.

This paper reports on the product design and performance of the GD-700 and on the Dual Hybridization, the new analysis method (Fig. 1).

Fig. 1 The appearance of "GD-700".

Original paper (Received November 24, 2009)
* Life Science Research Laboratories
Research & Development Management Headquarters
FUJIFILM Corporation
Ushijima Kaisei-machi Ashigarakami-gun, Kanagawa 258-8577, Japan
** Frontier Core-Technoligy Laboratories
Research & Development Management Headquarters
FUJIFILM Corporation
Ushijima Kaisei-machi Ashigarakami-gun, Kanagawa 258-8577, Japan
*** Film Materials Production Division
Fujinomiya Factory
FUJIFILM Corporation
Ohnakazato, Fujinomiya, Shizuoka 418-8666, Japan

2. Launching GD-700

2.1 Design Policy of GD-700

The chromosomal test has been said to be difficult to simplify. It requires such processes as cell culturing, specimen preparation and microscopic observation using G-banding, which are time and effort consuming. It also requires a highly skilled technician to identify a chromosomal anomaly. Using GD-700 with the Dual Hybridization, copy number anomalies of microscopic chromosomes can be detected simply and accurately.

The GD-700 uses the highly reliable RP-11[3], a BAC (Bacterial Artificial Chromosome) library widely used in the Human Genome Project across the world. Specifically, it employs 712 BAC clones that have regions relating to congenital anomaly diseases registered in the human genome database. Using the resource, it is possible to analyze anomalies in genome copy number at once including 30 types of microdeletion/microduplication syndromes, 41 subtelomeres (excluding the p-arms of 13, 14, 15, 21, 22 and Y chromosomes) and 42 pericentromeres. It is significant to be able to analyze subtelomeres with the G-700. Subtelomeres, difficult to analyze with the conventional chromosomal test, is drawing attention as a possible cause of mental retardation (Table 1).

2.2 Production Method

As for the 712 BAC clones comprising the GD-700, we have confirmed that stable signals are obtained in the FISH (Fluorescence in situ hybridization) method and that there is no mishybridization to other chromosomes. We isolated high-purity BAC DNA from the selected BAC clones using the plasmid purification column. We amplified the BAC DNA in the adapter ligation PCR technique to make probe DNA. The 712 probe DNAs are spotted onto a glass slide for DNA array (made by Matsunami Glass Ind., Ltd.) using a non-contact inkjet spotter GENESHOT (made by NGK Insulators, Ltd.) to ensure they are all aligned and uniform in concentration, diameter, shape, and position. Through these processes, we have succeeded in making a BAC array that enables stable detection of genome copy number anomalies[4] (Fig. 2).

Table 1 The list of congenital anomaly syndromes tested by "GD-700".

Syndrome	DNA	Deletion/duplication	Remarks
van der Woude syndrome	*IRF6*	1q32-q41 anomaly (deletion)	
Mowat-Wilson syndrome	*ZFHX18*	2q22.3 anomaly (deletion)	
BPES syndrome	*FOXL2*	3q22.3 deletion	
4p- syndrome	*Multiple*	4p16.3 deletion	
5p- syndrome	*Multiple*	5p15.3-p15.2 deletion	
Sotos syndrome	*NSD1*	5q35 deletion	5q35 duplication syndrome
Saethre-Chotzen syndrome	*TWIST1*	7p21.1 deletion	
Williams syndrome	*ELN*	7q11.23 deletion	7q11.2 duplication syndrome
Langer-Giedion syndrome	*EXT1,TRPSI*	8q24.11-q24.13 deletion	
Beck with-Wiedeman syndrome	*IGF2*	11p15.5 deletion/ duplication	
WAGR syndrome	*WT1,PAX6*	11p13 deletion	
Potocki-Shaffer syndrome	*ALX4,EXT2*	11p11.2 deletion	
Pallister-Killian syndrome	*Multiple*	i(12p) duplication	
Prader Willi syndrome	*SNRPN*	15q11-q13 deletion	15q11-q13 duplication syndrome
Angelman syndrome	*UBE3A*	15q11-q13 deletion	
Rubinstein-Taybi syndrome	*CREBBP*	16p13.3 deletion	
Miller-Dieker syndrome	*LIS1*	17p13.3 deletion	
Charcot-Marie-Tooth 1A	*PMP22*	17p12 duplication	HNPP
Smith-Magenis syndrome	*RAI1*	17p11.2 deletion	Potocki-Lupski syndrome
Neurofibromatosis I	*NF1*	17p11.2 deletion	
Diamond-Blackfan syndrome	*RPS19*	19q13.2 anomaly (deletion)	
Alagille syndrome	*JAG1*	20p12.2 deletion	
Down syndrome	*Multiple*	21q22 duplication	
Cat eye syndrome	*Multiple*	22q11.2 duplication	
22q11.2 deletion syndrome	*TBX1*	22q11.2 deletion	22q11.2 duplication syndrome
X-linked ichthyosis	*STS*	Xp22.31 deletion	
Kallmann syndrome type I	*KAL1*	Xp22.31 deletion	
Duchenne Muscular Dystrophy	*DMD*	Xp21.2 deletion/ duplication	
Pelizaeus–Merzbacher disease	*PLP1*	Xq22.2 deletion/ duplication	
MECP2 duplication syndrome	*MECP2*	Xq28 duplication	

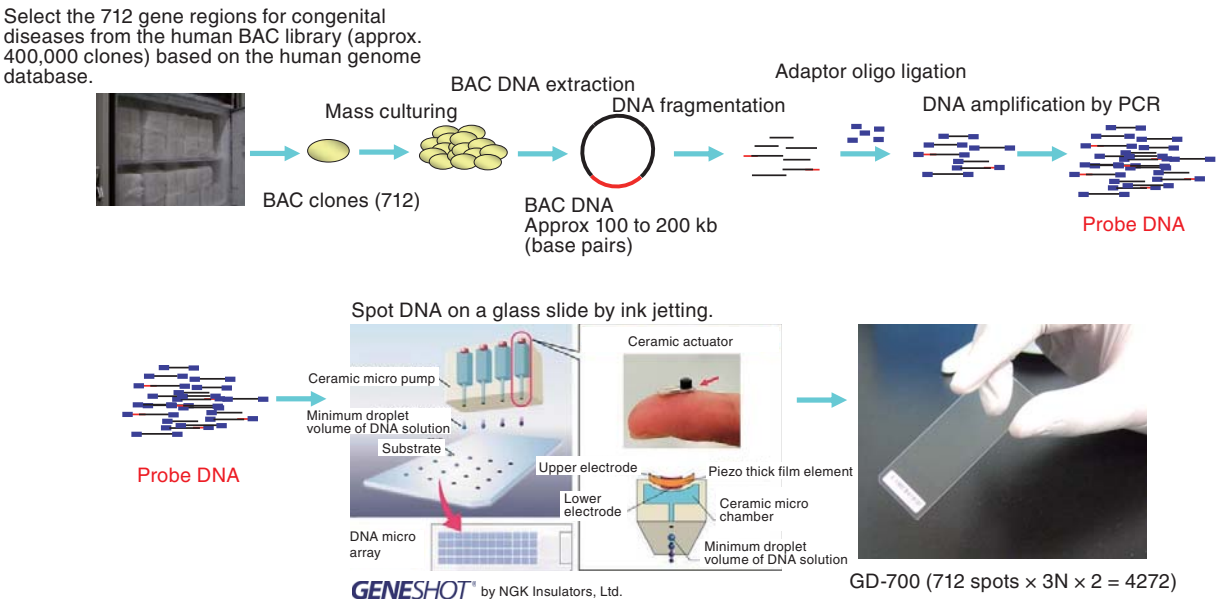

Fig. 2 The flow of "GD-700" production.

3. Development of Analysis Method

3.1 Overview

Fig. 3 shows the principle of a typical array CGH method (one color method). The test sample and the reference sample are labeled with fluorescent molecules (it must have been confirmed that the samples have no genetic aberrations). Each sample is hybridized to the probes on the BAC array. The fluorescence intensities of hybridized DNA on the array are measured to calculate the ratio of test to reference samples in fluorescence intensity. The result shows whether there is deletion or amplification in the sample genome (Fig. 3).

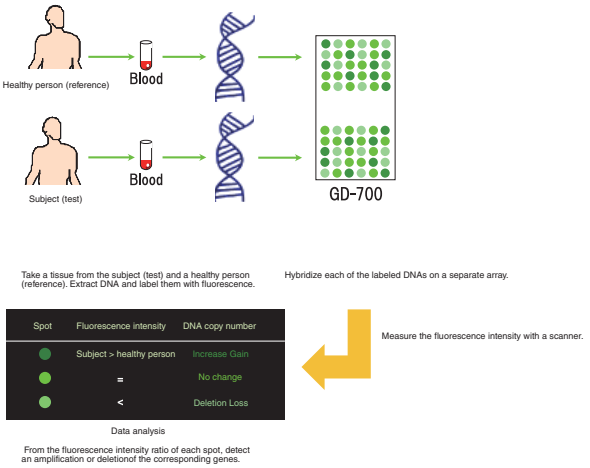

Fig. 3 The principle of CGH array method.

In the conventional one-color method, the test and reference samples have to be hybridized separately on different arrays. That means the test result may vary depending on hybridization condition: for example, composition of the hybridization liquid, temperature, agitation condition, and the amount of immobilized DNA in the probes. We have developed a new array CGH, Dual Hybridization, less subject to the hybridization conditions.

3.2 Principle of Dual Hybridization

In the Dual Hybridization, each of the test and reference samples is mixed with florescence-labeled internal standard DNA before hybridized on a CGH array. As the internal standard DNA, we used one in a quantity large enough to be hybridized to all the probe DNAs on the CGH array.

The fluorescence intensities of the hybridized test and reference probe DNAs and those of the internal standard DNAs are measured. The fluorescence intensity is corrected by dividing the test (reference) fluorescence intensity by that of the internal standard DNA. The ratio of the corrected test and reference fluorescence intensities is calculated. This correction solved the problem of varying data due to hybridization on separate arrays, which is inherent in the conventional one-color method (Fig. 4).

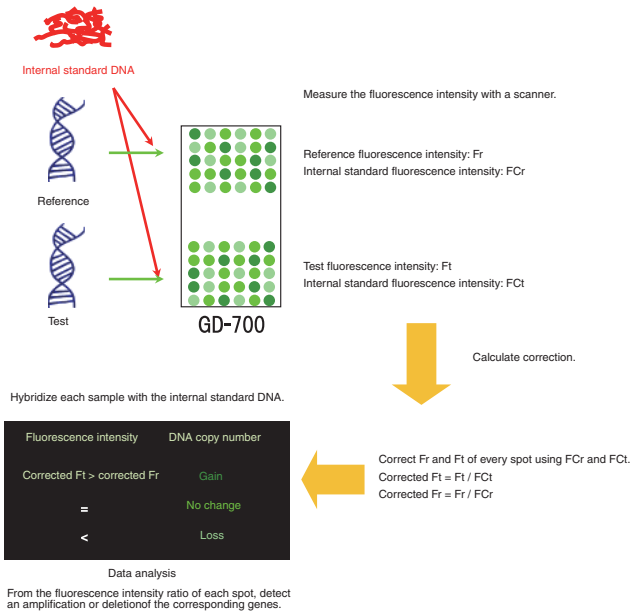

Fig. 4 The principle of Dual Hybridization.

4. Evaluation of GD-700

To evaluate the GD-700, we have carried out sex chromosome comparison (fundamental evaluation) using standard genomes available on the market (male/female by Promega KK) and Dual Hybridization using genomes with chromosome anomalies (positive sample).

4.1 Evaluation Using Standard Genomes

In the evaluation using standard genomes, we set the two criteria below. (1) The fluorescence intensity ratios of the autosomes shall fall within the range from 0.75 to 1.25. Even if there are some data outside the range, they shall not be continuous. (2) When a male genome is used as the reference and a female as the test sample, the X-chromosome, a sex chromosome, shall be different from autosomes. There shall be a difference of 0.5 or more between the X-chromosome average and the autosome average. As a result of the evaluation (n = 4), we have confirmed that both criteria were met concerning all the samples.

4.2 Evaluation Using Chromosomally Aberrant Genomes

For this evaluation, we used six DNA samples with congenital anomaly diseases and three DNA samples with miscarriage and stillbirth.

The DNA samples with congenital anomaly disease had known abnormal chromosome regions: Sample No. 1 (2p25.3 Gain/5p15 Loss), No. 2 (15q26.3 Gain), No. 3 (22q13.31 Loss), No. 4 (16p13.3 Gain), No. 5(22q11.21 Gain), No. 6 (2p25.3 Gain/10p15.3 Loss). We carried out array CGH analysis of those samples in the Dual Hybridization to see whether the regions would be correctly detected. All the regions were detected properly.

All the DNA samples with miscarriage and stillbirth had a trisomy: trisomies 13, 16 and 21. All the trisomies were detected (Fig. 5 and Fig. 6).

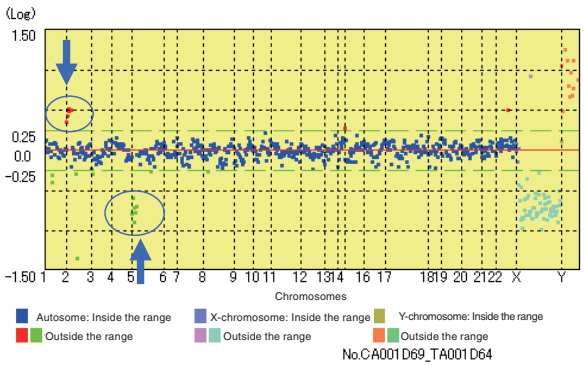

Fig. 5 The result of sample No.1 (2p25.3 Gain/5p15 Loss).

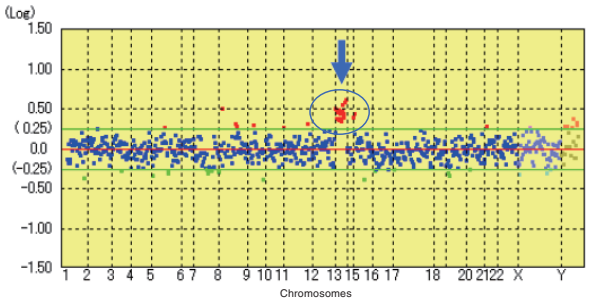

Fig. 6 The result of sample No.7 (13q Gain (trisomy)).

In both evaluations, chromosome anomalies are clearly detected. The combination of the GD-700 and the Dual Hybridization is effective for chromosomal testing (Table 2).

Table 2 The results of positive samples.

Detection of congenital anomaly disease samples		
Sample No.	Abnormal chromosome region	Result
No.1	2p25.3 Gain/5p15 Loss	○ Succeeded
No.2	15q26.3 Gain	○ Succeeded
No.3	22q13.31 Loss	○ Succeeded
No.4	16p13.3 Loss	○ Succeeded
No.5	22q11.21 Gain	○ Succeeded
No.6	2p25.3 Gain/10p15.3 Loss	○ Succeeded
Detection of miscarriage and stillbirth samples		
Sample No.	Abnormal chromosome region	Result
No.7	13q Gain (Trisomy 13)	○ Succeeded
No.8	16q Gain (Trisomy 16)	○ Succeeded
No.9	21q22 Gain (Trisomy 21)	○ Succeeded

* The symbols for abnormal chromosome regions: Example 2p25.3 Gain(Loss)

Chromosome No. (p: long arm, q: short arm) | Sub-band in chromosome | Gain: amplification, Loss: deletion

5. Conclusion

We have succeeded in commercializing the GD-700, a new array for congenital anomaly syndrome detection and developing the Dual Hybridization, the analysis method for the array. We have demonstrated that samples with known abnormal chromosome regions are accurately detected using this array and the method. We believe this method and the array will be widely used and replace or complement the conventional chromosome testing technology. And, they will be applied as genome analysis and diagnosis tools for congenital anomaly diseases of unknown cause, mental development disorders, autism and cancers, behind which chromosome and genome anomalies lie.

6. Acknowledgement

We would like to thank Professor Inazawa at Tokyo Medical and Dental University and people at BML, Inc. for their great cooperation in commercialization of the GD-700 and development of the Dual Hybridization.

References

1) Pinkel, D. et al. Nat. Genet., **20** (2), 207-211 (1998).
2) Imoto, Issei; Inazawa, Johji. Protein, Nucleic Acid and Enzyme, **50** (16), 2134-2139 (2005).
3) Osoegawa, K. et al. Genome Res., **11** (3), 483-96 (2001).
4) Array CGH diagnosis handbook. Inazawa, Johji et al. eds., Osaka, Iyaku (Medicine and Drug) Journal (2008).

UDC 582.766.5+612.017+575.113.1

Investigation by Microarray Analysis of the Immunostimulatory Function of an Extract of the Genus Plant Salacia in the Small Intestine of Rats

Yuriko ODA*, Fumitaka UEDA*, Chihaya KAKINUMA**,
Takaaki NAKAMURA**, and Yoshisada NAKAMURA*

Abstract

In our previous studies, Salacia extracts demonstrated beneficial effects on the enteric environment of the rat, as represented by decrease in ammonia and other products decomposed by enteric microorganism. In the present study, we showed that the expression of immunologically relevant genes increased in the epithelium of the small intestine from the rat orally dosed with Salacia extracts. T-RFLP analysis (Nagashima method) revealed altered composition of intestinal flora. Salacia extracts reportedly inhibit enzymatic degradation of polysaccharides, hence blocking the intestinal absorption of polysaccharides. These results taken together suggested that unabsorbed polysaccharides may affect the intestinal flora environment through the enteric immune system of the rat.

1. Introduction

It is known that extracts of plant in the genus Salacia, such as Salacia reticulata and Salacia oblonga, contain salacinol, kotalanol, mangiferin, catechin and many other components although not all the components those extracts contain are identified yet[1].

Some in-vitro experiments have proved that salacinol and kotalanol extracted from plant in the genus Salacia plants have been shown to exert an inhibitory effect *in vitro* on both α-glucosidase activity and blood glucose elevation in glucose-loaded rats[2]. It has been also proved that extracts of the genus Salacia improve conditions of diabetic patients and rat models of diabetes[3].

The small intestine, where α-glucosidase is secreted, is a vital organ. It takes in nutrients and eliminates foreign bodies by its immune function. It is considered to be the area where Salacia extracts work. But, it is yet to be determined how they work in the intestinal tract.

Another report says that catechin and mangiferin, also extracted from plant in the genus Salacia, have an antiobesity effect[4]. Other findings on the genus Salacia have been also reported[5-6]. However, most of the findings are effects on diabetes and obesity. There are few findings on other effects or the mechanism of function in a living body. The action of several components of a Salacia extract has not been defined.

This study aims at finding out the physiology of plant in the genus Salacia in the small intestine, which is the area where the extract inhibits sugar absorption and which has absorption, removal of foreign bodies and various other functions. In the experiment, we gave an extract of plant in the genus Salacia to rats and conducted gene expression analysis using a microarray and profiled the intestinal flora using T-RFLP. In the lower part of the small intestine, the administration of a Salacia extract accelerated expression of several immune-related genes, especially those relating to Th1, which contributes to cell immunity. In the large intestine, it increased bacteria that have an immune function. A Salacia extract caused changes in intestinal flora.

2. Experiments

2.1 Preparing an Extract Powder of Plant in the Genus Salacia

We used a species of plant in the genus Salacia (Salacia reticulata) that grew in Sri Lanka and dried the stem and root to make chips. The well-dried chips were left them in hot water for an hour and then filtered out. Resultant liquid was cooled to be reduced to powder using a spray dryer ADL-310 (Yamato Science Co., Ltd., Tokyo, Japan), and kept at 4 °C.

Original paper (Received November 20, 2009)
* Life Science Research Laboratories
Research & Development Management Headquarters
FUJIFILM Corporation
Ushijima, Kaisei-machi, Ashigarakami-gun, Kanagawa
258-8577, Japan

** Drug Discovery Research Laboratories
Research & Development Management Headquarters
FUJIFILM Corporation
Ushijima, Kaisei-machi, Ashigarakami-gun, Kanagawa
258-8577, Japan

2.2 Animal

We bought 6-week-old male Sprague Dawley® rats (SD rats) (CLEA Japan, Inc., Shizuoka, Japan) and kept them for one week for quarantine and habituation in the following environment: room temperature of 23 ± 2 °C, relative humidity of 50±10%, ventilation of 15 times per hour and artificial lighting for 12 hours a day. We gave the rats a solid feed sterilized with irradiation CRF-1 (Oriental Yeast Co., Ltd., Tokyo, Japan), letting them eat it freely. For drinking water, we gave city water that complies with the water quality requirements by the Water Supply Act after filtering (50 μm and 5 μm) (AION Co., Ltd., Osaka, Japan) and sterilizing with UV radiation, through an automatic watering nozzle to let them drink freely. One week later, we divided the rats into two groups of 10 at random.

We dissolved the Salacia extract powder in an injection solvent (Otsuka Pharmaceutical Co., Ltd., Tokyo, Japan) to make an 80 mg/ml solution. Using a metal gastric tube, we forced oral administration of the Salacia extract solution into the stomach of the test group until they were given 20 mg/kg in the weight of extract powder. To the control group, we gave the injection solvent only. The administration was repeated once a day for 13 weeks. We fasted the rats for 16 hours from the evening of the day of last administration. After anesthetizing the rats with pentobarbital sodium, we sampled the blood and euthanized them by exsanguinations. We dissected the rats, weighed the respective organs and observed the conditions. We took out the ileum, removed the epithelium and kept the epithelium in ISOGEN (NIPPON GENE Co., Ltd., Tokyo, Japan). We also sampled feces from the lower part of the large intestine and froze them with dry ice.

During the dissection, we also sampled blood from the posterior aorta and added an anticoagulant, EDTA-2K, to the blood to conduct biochemical test.

We tested the blood on these items: white blood cell count (WBC), red blood cell count (RBC), hemoglobin content (HGB), hematocrit level (HCT), mean corpuscular volume (MCV), mean corpuscular hemoglobin (MCH), mean corpuscular hemoglobin concentration (MCHC), platelet count (PLT), reticulocyte count (Reti), prothrombin time (PT), activated partial thromboplastin time (APTT), total protein (TP), albumin level (ALB), A/G, triglyceride (TG), total cholesterol (T-CHO), blood urea nitrogen (BUN), creatine (Cre), Calcium (Ca), inorganic phosphorus (IP), AST activity (AST), ALT activity (ALT), CPK activity (CPK), total bilirubin (T-BIL), sodium (Na), potassium (K), and chlorine (Cl).

We measured WBC, RBC, HGB, HCT, MCV, MCH, MCHC, PLT and Reti using a comprehensive hematology analyzer, XT-2000iV (Sysmex Co., Ltd., Hyogo, Japan). To measure PT and APTT, we used a fully automated coagulation and fibrinolysis analyzer, STA Compact (Roche Diagnostics K.K., Tokyo, Japan). We used an automatic biochemical blood analyzer, H7070 (Hitachi Ltd., Tokyo, Japan), for measurement of TP, ALB, A/G, Glu, TG, T-CHO, BUN, Cre, Ca, IP, AST, ALT, GGT, ALP, CPK, T-Bil, Na, K and Cl.

We verified the weights of the rats and their organs (absolute weights and relative weights) and biochemical test data of blood as below.

We first conducted F-test to test the equality of variance and then checked for significant differences using Student's t-test. The tissues were preserved and fixed in 10% neutral buffered formalin. We made specimen slices of the tissues, stained them with hematoxylin-eosin (HE) stain, and observed them with an optical microscope. We did not do verification concerning the general conditions, pathoanatomical test result or histopathological test result.

All of the animal experiments were approved by the Animal Care and Use Committee for Fujifilm.

2.3 RNA Extraction and DNA Microarray Analysis

From the preserved rat ileum cells, we extracted total RNA by the standard procedure using ISOGEN and then purified the total RNA using the RNeasy Mini Kit (QIAGEN, Hilden, Germany). We chose four rats with a weight closest to the average from each of the Salacia extract-treated group and the control group. From the total RNA of those rats' ilea, we synthesized cDNA, synthesized and labeled cRNA, and fragmented labeled cRNA, using an Affymetrix kit in accordance with the Affymetrix protocol. To check the quality of RNA, we used the Agilent 2100 bioanalyzer (Agilent Technologies Japan, Ltd., Tokyo, Japan) and confirmed that cRNA was elongated sufficiently. The fragmented cRNA was hybridized to GeneChip® Rat Genome 230 2.0 Array (Affymetrix Inc., CA, USA) at 45 °C for 16 hours in the Hybridization Oven 640 (Affymetrix Inc., CA, USA) and then washed and stained using the GeneChip® Fluidics Station 450. We scanned the cRNA with the GeneChip® Scanner 3000 and measured the gene expression levels. The acquired data were normalized in the Distribution Free Weighted (DFW) method using Bioconductor version 2.2 with the R version 2.7.2. We conducted Rank Products analysis to compare the results of the two groups and extracted a probe set with significant changes in gene expression that had a false discovery rate (FDR) below 0.05[7-11].

We classified the extracted probe set by biological function while referring to the Gene Ontology tool, Bingo 2.3 (Cytoscape 2.6) (http://www.psb.ugent.be/cbd/papers/BiNGO/index.htm) to draw a tree structure[12-13].

2.4 Analysis of Intestinal Flora (T-RFLP)

We outsourced the analysis of intestinal flora using the rat feces to TechnoSuruga Laboratory Co., Ltd., (Shizuoka, Japan). The analysis was conducted using T-RFLP (Nagashima method)[14]. The following are alterations made to the procedures in the reference literature.

The frozen feces were suspended in a GTC buffer (100 mM Tris-HCl [pH 9.0], 40 mM Tris-EDTA [pH 8.0] and 4M Guanidine Thiocyanate). The feces in the solution were lysed with zirconium beads (at 5 m/s for 5 minutes by the FastPrep FP100A Instrument (MP Biomedicals, CA, USA). From the 100-µl suspension, DNA was extracted using an automatic nucleic acid extractor (Precision System Science, Chiba, Japan). The reagent used for the automatic nucleic acid extraction was GC series Genomic DNA whole blood (Precision System Science, Chiba, Japan). The primer for the PCR, FAM-labeled 516F was used instead of HEX-labeled 516F as specified in the reference. The PCR products were purified with the MultiScreen PCRµ96 plate (Millipore, Billerica, MA, USA).

The fragment analysis was conducted with the ABI PRISM 3130x1 genetic analyzer (Applied Biosystems, CA, USA) using an analysis software, Gene mapper (Applied Biosystems, CA, USA). As a size standard marker, the MapMarker® X-Rhodamine Labeled 50-1000bp (BIOVENTURES, TN, USA) was used. Using a ratio of the peak area of each OTU (operational taxonomic unit) to the total peak area, hierarchical cluster analysis (using the pvclust function) was carried out to measure the similarity in flora pattern.

3. Results

3.1 Biochemical Test Results

No significant differences were found between the Salacia extract-treated group (20 mg/kg) and the control group after 13 weeks of continuous administration in weight (541.2 ± 47.8 g vs 578.2 ± 76.0 g) or biochemical blood test (WBC, RBC, HGB, HCT, MCV, MCH, MCHC, PLT, Reti, TP, ALB, A/G, Glu, TG, T-CHO, BUN, Cre, Ca, IP, AST, ALT, GGT, ALP, CPK, T-Bil, Na, K and Cl). Concerning all the individual rats, we weighed the brain, pituitary, thymus, lung, liver, kidney, spleen, heart, adrenal gland, testicle, epididymis, seminal vesicle and prostate gland (ventral lobe). WE then fixed the liver in a 10% neutral buffered formalin, stained the specimen slices with hematoxylin-eosin, and observed them with an optical microscope.

As a result, we found no changes that indicated toxicity under the test conditions above.

3.2 Microarray Analysis

After we confirmed there are no findings indicating toxicity, we chose four rats with a weight closest to the average from each group and conducted the microarray analysis. We extracted a probe set of 237 genes with increased expression and 111 genes with decreased expression in the test group compared with the control group.

3.2.1 Genes with Increased Expression

The gene ontology result acquired by the analysis above shows that genes relating to oligopeptide transport, defense response, response to nutrient levels, antigen processing and presentation of peptide or polysaccharide antigen via MHC class II have been concentrated. Taking a close look at the genes with increased expression, many of them are genes relating to biological defense including immune-related genes, and genes relating to transport and metabolism (Fig. 1).

Among the MHC class II genes involved in antigens recognition, the genes with increased expression are Cathepsin E (Ctse), RT1 class II, locus Ba (RT1-Ba), HLA class II histocompatibility antigen, and DM beta chain precursor (MHC class II antigen DMb, Hla-dmb)[15].

Among the genes relating to biodefense (immunity), changes have been made in tumor necrosis factor alpha (Tnfα), Clusterin (Clu), Chemokine (C-C motif) ligand 5 (Ccl5, Rantes), Adenosine deaminase (Ada), Apolipoprotein

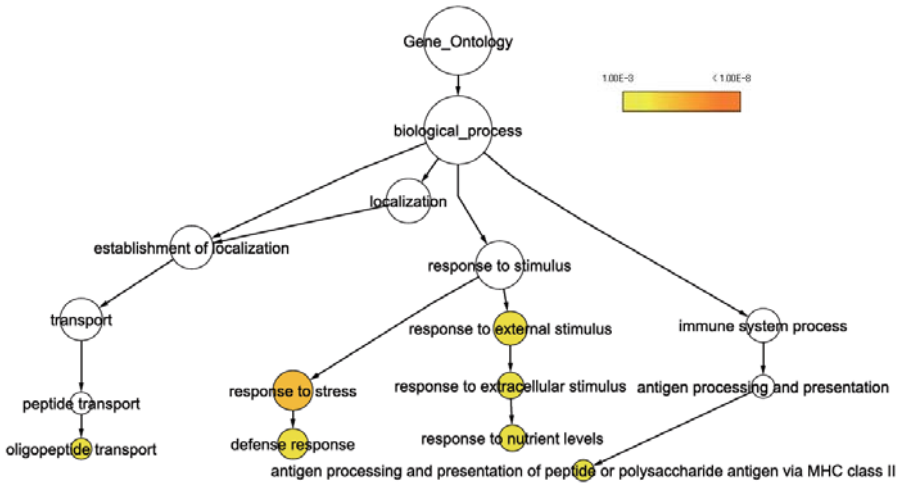

Fig. 1 Significant gene ontology categories (P < 0.001) were extracted from 237 genes showing increased expression.

A-IV (Apoa5), Chemokine (C-X-C motif) receptor 4 (Cxcr4), Apolipoprotein H (Apoh), Membrane-spanning 4-domains, subfamily A, member 1 (Ms4a1), Dipeptidyl-peptidase 4 (Dpp4, Cd26), Protein tyrosine phosphatase (Ptprc, Cd45), T cell receptor beta locus (Tcrb), and Apoptotic peptidase activating factor 1 (Apaf1).

Among cholesterol- and ketone-body-metabolism genes, the expression of 3-hydroxy-3-methylglutaryl-Coenzyme A synthase 2 (Hmgcs2) has increased. Among transport genes, the genes with increased expression are Solute carrier family 15 (oligopeptide transporter) and member 1 (Slc5a1) (Table 1).

3.2.2 Genes with Decreased Expression

Genes with decreased expression included urea cycle and lipid metabolic process. Among urea cycle related genes, the genes with decreased expression are Arginase, type II (Arg2), Ornithine carbamoyltransferase (Otc), and carbamoyl-phosphate synthase 1 (Cps1). Among the genes relating to lipid transport and metabolism, the genes with decreased expression are peroxiredoxin 6 (Prdx6) and Peroxisome proliferator-activated receptor gamma (Ppar γ) (Fig. 2 and Table 2).

Table 1 Genes showing increased expression (P < 0.001, Gene ontology categories extracted using BiNGO).

【response to stress】		
Gene name	Definition	UniGene ID
Tnf	tumor necrosis factor	Rn.2275
Aldob	aldolase B	Rn.98207
Clu	clusterin	Rn.1780
Atp6v1g2	ATPase	Rn.158487
Abhd2	abhydrolase domain containing 2	Rn.136611
Sfn	stratifin	Rn.145079
RT1-Ba	RT1 class II, locus Ba	Rn.25717
Ccl5	chemokine (C-C motif) ligand 5,	Rn.8019
Hla-dmb	major histocompatibility complex	Rn.5892
Ada	adenosine deaminase	Rn.12689
RT1-Aw2	RT1 class Ib, locus Aw2	Rn.40130
Apoa4	apolipoprotein A-IV	Rn.15739
RatNP-3b	rat neutrophil peptide-1	Rn.114810
Alb	albumin	Rn.202968
Cxcr4	chemokine (C-X-C motif) receptor 4	Rn.44431
Gsn	gelsolin	Rn.103770
Apoh	apolipoprotein H (beta-2-glycoprotein I)	Rn.1824
Ms4a1	membrane-spanning 4-domains	Rn.16385
Creb3l3	cAMP responsive element binding protein 3-like 3	Rn.20059
Cfd	complement factor D (adipsin)	Rn.16172
Dpp4	dipeptidyl-peptidase 4 (CD26)	Rn.91364
Car3	carbonic anhydrase 3	Rn.1647
Ptprc	protein tyrosine phosphatase	Rn.90166
Bmp2	bone morphogenetic protein 2	Rn.90931
Si	sucrase-isomaltase	Rn.10057
Ephx2	Epoxide hydrolase2	Rn.54495
Tcrb	T cell receptor beta locus	Rn.34871
Adipoq	adiponectin, C1Q and collagen domain containing	Rn.24299
Defa-rs1	defensin alpha-related sequence 1	Rn.122020
Cyp4f5	cytochrome P450 4F5	Rn.10171
Abcc2	ATP-binding cassette	Rn.10265
Apaf1	apoptotic peptidase activating factor 1	Rn.64522
Prnp	prion protein	Rn.3936
Ta4sf4	transmembrane 4 L six family member 4	Rn.13425
【response to external stimulus】		
Gene name	Definition	UniGene ID
Suox	sulfite oxidase	Rn.25720
Bmp2	bone morphogenetic protein 2	Rn.90931
Tnf	tumor necrosis factor	Rn.2275
Si	sucrase-isomaltase	Rn.10057
Clu	clusterin	Rn.1780
Aldob	aldolase B	Rn.98207
Ephx2	Epoxide hydrolase2	Rn.54495
Abhd2	abhydrolase domain containing 2	Rn.136611
Ccl5	chemokine (C-C motif) ligand 5,	Rn.8019
Adipoq	adiponectin, C1Q and collagen domain containing	Rn.24299
Ada	adenosine deaminase	Rn.12689
Apoa4	apolipoprotein A-IV	Rn.15739
Coro1a	coronin	Rn.6990
Apoa1	apolipoprotein A-I	Rn.10308
Cyp4f5	cytochrome P450 4F5	Rn.10171
Hmgcs2	3-hydroxy-3-methylglutaryl-Coenzyme A synthase 2	Rn.29594
Gsn	gelsolin	Rn.103770
Alb	albumin	Rn.202968
Ms4a1	membrane-spanning 4-domains	Rn.16385
Apoh	apolipoprotein H (beta-2-glycoprotein I)	Rn.1824
Cfd	complement factor D (adipsin)	Rn.16172
Tm4sf4	transmembrane 4 L six family member 4	Rn.13425
Smpd2	sphingomyelin phosphodiesterase 2	Rn.16572

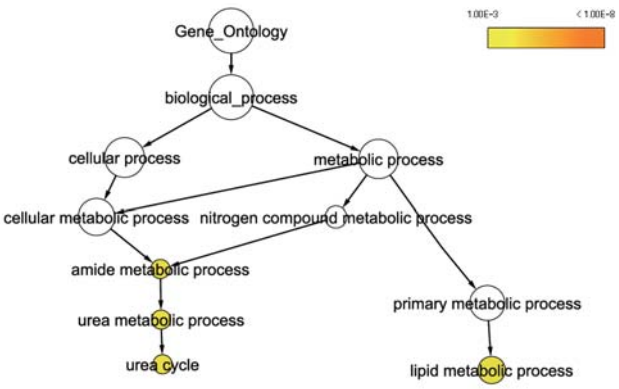

Fig. 2 Significant gene ontology categories (P < 0.001) were extracted from 113 genes showing decreased expression.

【defense response】		
Gene name	Definition	UniGene ID
Ptprc	protein tyrosine phosphatase	Rn.90166
Bmp2	bone morphogenetic protein 2	Rn.90931
Tnf	tumor necrosis factor	Rn.2275
Ephx2	Epoxide hydrolase2	Rn.54495
Tcrb	T cell receptor beta locus	Rn.34871
RT1-Ba	RT1 class II, locus Ba	Rn.25717
Ccl5	chemokine (C-C motif) ligand 5,	Rn.8019
Hla-dmb	major histocompatibility complex	Rn.5892
Defa-rs1	defensin alpha-related sequence 1	Rn.122020
Ratnp-3b	rat neutrophil peptide-1	Rn.114810
Apoa4	apolipoprotein A-IV	Rn.15739
Cyp4f5	cytochrome P450 4F5	Rn.10171
Ms4a1	membrane-spanning 4-domains	Rn.16385
Apaf1	apoptotic peptidase activating factor 1	Rn.64522
Cfd	complement factor D (adipsin)	Rn.16172
【response to nutrient levels】		
Gene name	Definition	UniGene ID
Apoa4	apolipoprotein A-IV	Rn.15739
Suox	sulfite oxidase	Rn.25720
Bmp2	bone morphogenetic protein 2	Rn.90931
Apoa1	apolipoprotein A-I	Rn.10308
Hmgcs2	3-hydroxy-3-methylglutaryl-Coenzyme A synthase 2	Rn.29594
Gsn	gelsolin	Rn.103770
Alb	albumin	Rn.202968
Si	sucrase-isomaltase	Rn.10057
Aldob	aldolase B	Rn.98207
Adipoq	adiponectin, C1Q and collagen domain containing	Rn.24299
Ada	adenosine deaminase	Rn.12689
【oligopeptide transport】		
Gene name	Definition	UniGene ID
Slc15a1	solute carrier family 15 (oligopeptide transporter)	Rn.10500
RT1-Ba	RT1 class II, locus Ba	Rn.25717
Hla-dmb	major histocompatibility complex	Rn.5892
【response to extracellular stimulus】		
Gene name	Definition	UniGene ID
Apoa4	apolipoprotein A-IV	Rn.15739
Suox	sulfite oxidase	Rn.25720
Bmp2	bone morphogenetic protein 2	Rn.90931
Apoa1	apolipoprotein A-I	Rn.10308
Hmgcs2	3-hydroxy-3-methylglutaryl-Coenzyme A synthase 2	Rn.29594
Gsn	gelsolin	Rn.103770
Alb	albumin	Rn.202968
Si	sucrase-isomaltase	Rn.10057
Aldob	aldolase B	Rn.98207
Adipoq	adiponectin, C1Q and collagen domain containing	Rn.24299
Ada	adenosine deaminase	Rn.12689
【antigen processing and presentation of peptide or polysaccharide antigen via MHC class II】		
Gene name	Definition	UniGene ID
Ctse	cathepsin E	Rn.92738
RT1-Ba	RT1 class II, locus Ba	Rn.25717
Hla-dmb	major histocompatibility complex	Rn.5892

Table 2 Genes showing decreased expression (P < 0.001, Gene ontology categories extracted using BiNGO).

【urea cycle】		
Gene name	Definition	UniGene ID
Arg2	arginase	Rn.11055
Otc	ornithine carbamoyltransferase	Rn.2391
Cps1	carbamoyl-phosphate synthase 1	Rn.53968
【urea metabolic process】		
Gene name	Definition	UniGene ID
Arg2	arginase	Rn.11055
Otc	ornithine carbamoyltransferase	Rn.2391
Cps1	carbamoyl-phosphate synthase 1	Rn.53968
【amide metabolic process】		
Gene name	Definition	UniGene ID
Arg2	arginase	Rn.11055
Otc	ornithine carbamoyltransferase	Rn.2391
Cps1	carbamoyl-phosphate synthase 1	Rn.53968
【lipid metabolic process】		
Gene name	Definition	UniGene ID
Phlpb	phospholipase B	Rn.91079
Cubn	cubilin (intrinsic factor-cobalamin receptor)	Rn.3236
Hsd3b6	hydroxy-delta-5-steroid dehydrogenase, 3 beta- and steroid delta	Rn.109394
Prdx6	peroxiredoxin 6	Rn.42
Pparg	peroxisome proliferator-activated receptor gamma	Rn.23443
Hsd11b2	hydroxysteroid (11-beta) dehydrogenase 2	Rn.10186
Aldh1a7	aldehyde dehydrogenase family 1, subfamily A7	Rn.74044
Srd5a1	steroid-5-alpha-reductase	Rn.4620
Comt	catechol-O-methyltransferase	Rn.220
Pcca	propionyl Coenzyme A carboxylase	Rn.6033
Pck1	phosphoenolpyruvate carboxykinase 1	Rn.104376

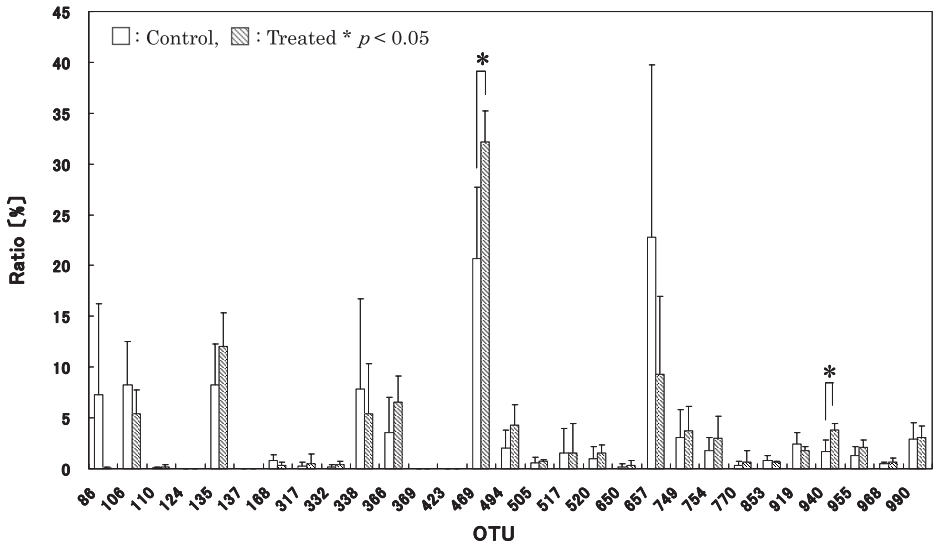

Fig. 3 Fecal specimens were analyzed by T-RFLP analysis (Nagashima method) and presented as the intestinal bacterial flora composition by OTU.

3.3 Intestinal Flora Analysis

The gene expression analysis showed that many immune-related genes were up-regulated in the ileal epithelium of animals administered the *Salacia* extract. Therefore, we have also analyzed the intestinal flora, which is considered to have effect on expression of immune-related genes in intestines.

For the analysis, we used the feces taken from the lower part of the large intestine during the dissection. As the large intestine contains many bacteria difficult to culture, we used T-RFLP analysis to measure the composition ratio of the intestinal flora. T-RFLP analysis profiles intestinal flora accurately without culturing. Based on the composition ratio, we performed clustering using R and drew a phylogenetic tree to measure the similarity in flora pattern. The profiles of the intestinal flora of the test group were different from those of the control group (Fig. 3).

Compared with the Salacia extract-treated group, the intestinal flora of the control group varies largely from rat to rat. They are also distant from one another in the phylogenetic tree, which show little similarity. The profiles of the test group are all similar. All the rats are very close to one another in the phylogenetic tree. These indicate that intake of plant in the genus Salacia results in similar intestinal flora (Fig. 4).

When categorized by phylum, a significant decrease in the ratio of Firmicutes (OTU: 106, 110, 168, 332, 338, 369, 423, 494, 505, 517, 520, 650, 657, 749, 754, 919, 940, 955, 990) was observed, with a significant increase in the ratio of Bacteroidetes (OTU: 366, 469, 853) in the Salacia plant extract-treated group (Fig. 5). That indicates the administration of a Salacia extract has made changes not only in the expression of immune-related genes but in the intestinal flora.

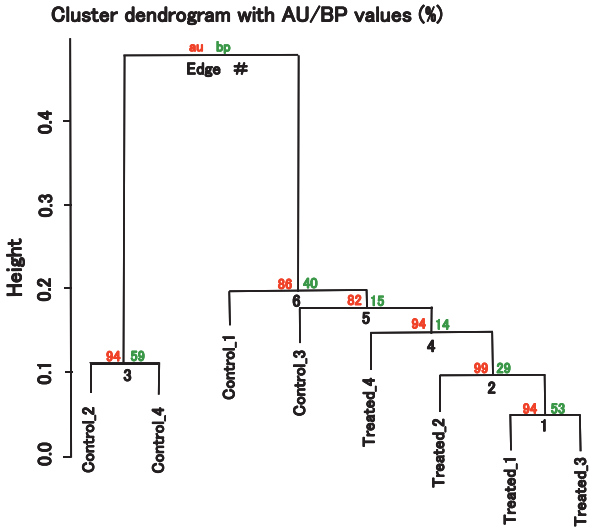

Fig. 4 Cluster analysis was performed on the intestinal bacterial flora composition data determined by T-RFLP analysis (Nagashima method) to construct a phylogenetic tree (au=Approximately Unbiased, bp=Bootstrap Probability).

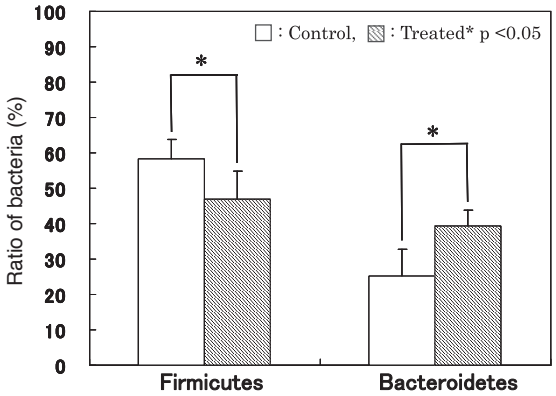

Fig. 5 Proportions of Bacteroidetes and Firmicutes relative to the entire intestinal flora population in the fecal extract administration.

4. Discussion

It has been known that plant in the genus Salacia has many useful effects. This research has been conducted to find out its physiology in the small intestine. As a result, we have found that Salacia makes changes in the expression of many genes in the ileum epithelium. That shows that the genus Salacia has many effects on the intestinal tract. Above all, the changes in the expression of immune-related genes have been found for the first time by this research and the effect is significant. Accordingly, the following discussion will focus on the immune function of Salacia.

Examining the genes with increased expression closely, we have found that they include many genes relating to foreign body recognition, immune system and host defense, especially those relating to Th1 cells. More specifically, they are Ptprc (Cd45)[16] considered to inhibit production of IgE that causes allergies, Th1 related gene Cd26 (Dpp4)[17] contributing to cell immunity, IgG2a[18], which suppresses the invasion of pathogens including various bacteria and viruses, e.g., the influenza virus, and exerts an allergy-suppressive effect, and MHC class II-related genes. Based on the genes identified as showing elevated expression, a possible mechanism of action is proposed, which may operate in the vicinity of Th1 cells (Fig. 6)[19].

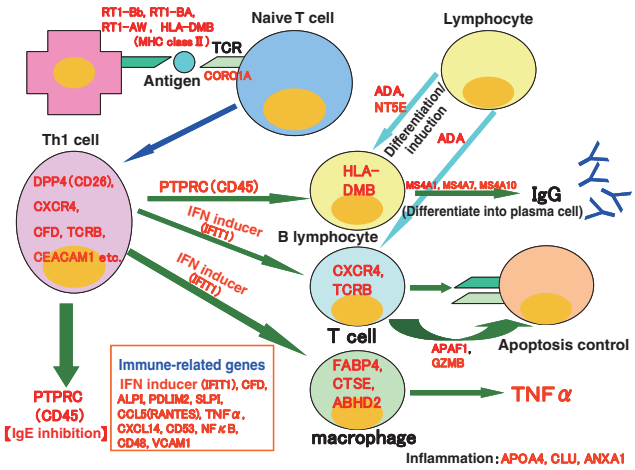

Fig. 6 Possible mechanism of action speculated from the genes identified as showing increased expression in the vicinity of the Th1 cells (genes listed in Table 1 are shown in red, genes identified among the 237 genes showing increased expression but not used in the functional categorization by BiNGO are presented in black).

In our previous study, we found that Salacia extracts had the effect of decreasing putrefied products and ammonia in intestines. We infer that the decrease of ammonia in the intestines by a Salacia extract has resulted in a decrease in the expression of urea cycle related genes (Cps1, Arg2 and Otc) in the epithelium of small intestine[20].

The types of bacteria and their composition in intestinal flora are closely connected with intestinal immunity. In our analysis of the intestinal flora, the flora patterns that varied from rat to rat have become similar to one another due to the administration of a Salacia extract. The percentage of Bacteroides has increased. The immunostimulatory function of this phylum of bacteria is attracting attention. They exhibit a stronger immune function than lactic acid bacteria well known for their immune activation. It has been found that Bacteroides increase production of a cytokine relating to IgA and biodefense[21-22]. In our experiment, two OTUs of Bacteroides (366 and 469) drastically increased in percentage. We studied the homology using the base sequences obtained by cloning. The result shows that it is highly possible that the two OTUs include Bacteroides acidofaciens, one of the Bacteroides having particularly high immune activation effect. Also, some research shows LPS existing in the cell walls of Bacteroides has the immune activation effect[23].

All these indicate that a Salacia extract has effects on intestinal flora and that the changed flora acts on the immune system of the lower part of the small intestine. In this research, expression of many transport and metabolism related genes has also changed. These genes work closely with the liver. We would like to continue study on these genes.

The result of this research may not necessarily hold true for humans. We have conducted the experiment on the rats in clean environment and under strictly managed conditions, such as the temperature and feed. There are no bifidobacteria, which exist in large quantity in human intestines[24]. However, we have confirmed that a Salacia extract does make changes in human intestinal flora. We believe there is great possibility it acts on human immune functions. We would like to verify its functions on humans.

Although plant in the genus Salacia has been used in Ayurveda for many years, not much about its functions is known. However, the biological regulation through intestinal immunity is connected with many diseases that are said to be improved by Salacia extracts. We are convinced that this research has revealed some of the functions of Salacia extracts.

We launched functional food containing a Salacia extract, Metabarrier (Fig. 7), in 2007. Through research of functionality of food ingredients to develop products using still more highly functional ingredients, we will continue our efforts to help enhance people's quality of life.

Fig. 7 Metabarrier.

References

1) Yoshikawa, M.; Shimoda, H.; Nishida, N.; Takada, M.; Matsuda, H. *Salacia reticulata* and Its Polyphenolic Constituents with Lipase Inhibitory and Lipolytic Activities Have Mild Antiobesity Effects in Rats. J. Nutr., **132** (7), 1819-1824 (2002).
2) Matsuura, T.; Yoshikawa, Y.; Masui, H.; Sano, M. Suppression of Glucose Absorption by Various Health Teas in Rats. YAKUGAKU ZASSHI, **124** (4), 217-223 (2004).
3) Im, R.; Mano, H.; Matsuura, T.; Nakatani, S.; Shimizu, J.; Wada, M. Mechanisms of blood glucose-lowering effect of aqueous extract from stems of Kothala himbutu (*Salacia reticulata*) in the mouse. J. Ethnopharmacol., **121** (2), 234-240 (2009).
4) Nair, P. S.; Shyamala, Davi, C. S. Efficacy of mangiferin on serum and heart tissue lipids in rats subjected to isoproterenol induced cardiotoxicity. Toxisology, **228** (2-3), 135-139 (2006).
5) Muraoka, O.; Ying, S.; Yoshikai, K.; Matsuura, Y.; Yamada, E.; Minematsu, T.; Tanabe, G.; Matsuda, H.; Yoshikawa, M. Synthesis of a Nitrogen Analogue of Salacinol and Its α-Glucosidase Inhibitory Activity. Chem. Pharm. Bull., **49** (11), 1503-1535 (2001).
6) Im, R.; Mano, H.; Nakatani, S.; Shimizu J.; Wada, M. Safety Evaluation of the Aqueous Extract Kothala Himbutu (*Salacia reticulata*) Stem in the Hepatic Gene Expression Profile of Normal Mice Using DNA Microarrays. Biosci. Biotech. Biochem., **72** (12), 3075-3083 (2008).
7) The R Development Core Team. R : A Language and Environment for Statistical Computing. R Foundation for Statistical Computing, Vienna, Austria (2006).
8) Gentleman, R. C.; Carey, V. J.; Bates, D. M.; Bolstad, B.; Dettling, M.; Dudoit, S.; Ellis, B.; Gautier, L.; Ge, Y.; Gentry, J.; Hornik, K.; Hothorn, T.; Huber, W.; Iacus, S.; Irizarry, R.; Leisch, F.; Li, C.; Maechler, M.; Rossini, A. J.; Sawitzki, G.; Smith, C.; Smyth, G.; Tierney, L.; Yang, J. Y. H.; Zhang, J. Bioconductor : open software development for computational biology and bioinformatics. Genome Biol., **5** (10), R80.1-R80.16 (2004).
9) Chen, Z.; McGee, M.; Liu, Q.; Scheuermann, R.H. A distribution free summarization method for Affymetrix GeneChip arrays. Bioinformatics., **23** (3), 321-327 (2007).
10) Breitling, R.; Armengaud, P.; Amtmann, A.; Herzyk, P. Rank products : a simple, yet powerful, new method to detect differentially regulated genes in replicated microarray experiments. FEBS Lett., **573** (1-3), 83-92 (2004).
11) Motoyama, K.; Nakai, Y.; Miyashita, T.; Fukui, Y.; Morita, M,; Sanmiya, K.; Sakakibara, H.; Matsumoto, I.; Abe, K.; Yakabe, T.; Yajima, N.; Shimoi, K. Isolation stress for 30 days alters hepatic gene expression profiles, especially with reference to lipid metabolism in mice. Physiol. Genomics, **37** (4), 79-87 (2009).
12) Shannon, P.; Markiel, A.; Ozier, O.; Baliga, N.S.; Wang, J.T.; Ramage, D.; Amin, N.; Schwikowski, B.; Ideker, T. Cytoscape : A Software Environment for Integrated Models of Biomolecular Interaction Networks. Genome Res., **13** (11), 2498-2504 (2003).
13) Maere, S.; Heymans, K.; Kuiper, M. *BiNGO* : a Cytoscape plugin to assess overrepresentation of Gene Ontology categories in Biological Networks. Bioinformatics., **21** (16), 3448-3449 (2005).
14) Nagashima, K.; Mochizuki, J.; Hisada, T.; Suzuki, S.; Shimomura, K. Phylogenetic Analysis of 16S Ribosomal RNA Gene Sequences from Human Fecal Microbiota and Improved Utility of Terminal Restriction Fragment Length Polymorphism Profiling. Biosci. Microflora., **25** (13), 99-107 (2006).
15) Renard, C.; Hart, E.; Sehra, H.; Beasley, H.; Coggill, P.; Howe, K.; Harrow, J.; Gilbert, J.; Sims, S.; Rogers, J.; Ando, A.; Shigenari, A.; Shiina, T., Inoko, H. Chardon, P.; Beck, S. The genomic sequence and analysis of the swine major histocompatibility complex. Genomics, **88** (1), 96-110 (2006).
16) Yamada, T.; Zhu, D.; Saxon A.; Zhang, K. CD45 Controls Interleukin-4-mediated IgE Class Switch Recombination in Human B Cells through Its Function as a Janus Kinase Phosphatase. J. Biol. Chem., **277** (32), 28830-28835 (2002).
17) Hoshimoto, K.; Ohta, N.; Ohkura, T.; Inaba, N. Changes in Plasma Soluble CD26 and CD30 during Pregnancy : Markers of Th1/Th2 Balance? Gynecol. Obstet. Invest., **50** (4), 260-263 (2000).
18) Hovden, A. -O.; Cox, R. J.; Haaheim, L. R. Whole influenza virus vaccine is more immunogenic than split influenza virus vaccine and induces primarily an IgG2a response in BALB/c mice. Scand. J. Immunol., **62** (1), 36-44 (2005).
19) Umesaki, Y.; Okada, Y.; Matsumoto, S.; Imaoka, A.; Setoyama, H. Segmented filamentous bacteria are indigenous intestinal bacteria that activate intraepithelial lymphocytes and induce MHC class II molecules and fucosyl asialo GM1 glycolipids on the small intestinal epithelial cells in the ex-germ-free mouse. Microbiol. Immunol., **39** (8), 555-562 (1995).
20) Mouillé, B.; Robert, V.; Blachier, F. Adaptative increase of ornithine production and decrease of ammonia metabolism in rat colonocytes after hyperproteic diet ingestion. Am. J. Physiol. Gastrointest Liver Physiol., **287** (2), G344-G351 (2004).

21) Tsuda, M.; Hosono, A.; Yanagibashi, T.; Hachimura, S.; Hirayama, K.; Itoh, K.; Takahashi, K.; Kaminogawa, S., Prior stimulation of antigen-presenting cells with *Lactobacillus* regulates excessive antigen-specific cytokine responses in vitro when compared with *Bacteroides*. Cytotechnology, **55** (2-3), 89-101 (2007).
22) Yanagibashi, T.; Hosono, A.; Oyama, A.; Tsuda, M.; Hachimura, S.; Takahashi, Y.; Itoh, K.; Hirayama, K.; Takahashi, K.; Kaminogawa, S. *Bacteroides* Induce Higher IgA Production Than *Lactobacillus* by Increasing Activation-Induced Cytidine Deaminase Expression in B Cells in Murine Peyer's Patches. Biosci. Biotechnol. Biochem., **73** (2), 372-377 (2009).
23) Humphries, H. E.; Triantafilou, M.; Makepeace, B. L.; Heckels, J. E.; Triantafilou, K.; Christodoulides, M. Activation of human meningeal cells is modulated by lipopolysaccharide (LPS) and non-LPS components of *Neisseria meningitidis* and is independent of Toll-like receptor (TLR) 4 and TLR2 signalling. Cell Microbiol., **7** (3), 415-430 (2005).
24) Bouhnik, Y.; Raskine, L.; Simoneau, G.; Paineau, D.; Bornet, F. The capacity of short-chain fructo-oligosaccharides to stimulate faecal bifidobacteria : a dose-response relationship study in healthy humans. Nutr. J., **5**:8, 1-6 (2006).

UDC 621.395.721.5+621.397.3+681.3.06

High Quality Document Viewer on Mobile Phones

Hiroshi OHTANI*, Naoki IKEYA**, Eiji UESUGI**, Arito ASAI*,
Hideo SEGAWA*, and Norihisa HANEDA*

Abstract

We have developed a document viewer named “GT-Document” for various non-PC mobile devices. “GT-Document” displays high quality document images converted from the original documents by our document converter engine. “GT-Document” shows the best performance at document downloading or opening speed and fidelity of the original documents compared with pre-installed document viewers on mobile devices.

“GT-Document” is incorporated into “Keitai Remote” service which helps you to securely access office network data such as e-mails, schedules and files via mobile phones.

1. Introduction

As data throughput of mobile terminals is increasing and their communications band is expanding, many mobile terminals are now capable of processing document, image and movie files that are usually processed on computers.

Mobile terminals, such as cell phones and smartphones, have potential to be a business tool, replacing laptops. There are two reasons for that. One reason is that with growing concern about information security, more and more cell phones and smartphones are being equipped with the remote lock function to prevent leak of information from stolen or misplaced phones. The other reason is that the remote access function, as well as the emergency contact function, is drawing attention as part of measures against the new flu pandemic or the earthquake disaster, which is projected to have a serious impact on business activities. The remote access function allows the user to do his or her job accessing an office computer from anywhere.

Under these circumstances, we have concluded that there is growing demand for a mobile terminal function that allows the user to view documents in an office computer on his or her mobile terminal securely. And, we have developed document viewer software for mobile terminals, GT-Document or GT-Doc for short.

2. Overview

The GT-Doc system consists of the GT-Doc server that converts documents to images and the GT-Doc viewer, the client application that acquires the images from the server via the Internet and displays them on a mobile terminal. GT-Doc hereinafter refers to the GT-Doc viewer.

The GT-Doc viewer runs on the so-called third generation (3G) mobile terminals of NTT Docomo, KDDI and SoftBank Mobile including iOS (iPhone/iPad) and Android devices. Fig. 1 shows how document images are displayed on a mobile terminal.

Fig. 1 GT-Doc viewer showing a document image.

Quite many recent models of mobile terminals come with other company’s document viewer. But most old models don’t. The GT-Doc runs comfortably on such old models, which are often low in throughput. As of April 22, 2011, the GT-Doc supports some 400 models of those three carriers mentioned above.

Original paper (Received December 29, 2009)
* Internet Buisiness Development Division
FUJIFILM Corporation
Nishiazabu, Minato-ku, Tokyo 106-8620, Japan

** FUJIFILM Software Co., Ltd.
Shinyokohama, Kouhoku-ku, Yokohama, Kanagawa 222-0033, Japan

Since most mobile terminals are equipped with image processors, it is easier for mobile terminals to handle image files than document files.

Table 1 Japanese mobile network operators, their service brands, applications, application platforms and the number of phones on which our GT-Doc viewer works.

Carrier	NTT Docomo	KDDI	SoftBank Mobile
Brand	docomo	au	SoftBank
Application	i-appli	EZ appli	S! appli
Platform	DoJa, STAR	BREW	MIDP
Number of supported models	179	128	89

Table 2 Global smartphone platform providers, their platforms and the versions of platforms on which our GT-Doc viewer works.

Provider	Apple	Google
Platform	iOS	Android
Supported versions	4.x	2.1, 2.2, 2.3, 3.0

Just like other applications for mobile terminals, the GT-Doc can be launched from the mobile browser. Clicking on the link on the web page, the program is downloaded and at the same time installed or started (Fig. 2). Therefore GT-Doc can be integrated with web application or system.

Fig. 2 Launching GT-Doc viewer from hyperlink in a browser on a mobile phone.

Even if a mobile terminal does not have a document viewer, the user can download the GT-Doc and view various types of document files, provided the user has signed up for a service package comprising the GT-Doc. For details about the services, see below.

Table 3 shows the document and image file formats viewable on the GT-Doc as of November 27, 2009.

Table 3 Supported document formats on GT-Doc viewer.

Application	Extension
Microsoft Office	doc
	xls
	ppt
Microsoft Office 2007	docx
	xlsx
	pptx
Adobe Acrobat	pdf
Fuji Xerox DocuWorks	xdw
JustSystems Ichitaro	jtd
JustSystems Hanako	jhd
(Plain text file format)	txt
(Versatile image file format)	jpeg
	jpg
	gif
	png

The GT-Doc is also compatible with the Net Print Service by Fuji Xerox. The GT-Doc can output a document to a multi-function printer at one of the 7-Eleven stores in Japan.

The communications between the viewer and the server is encrypted and the documents are transmitted as images. That makes it difficult to sniff the data on the network or copy and paste them on the viewer. Also, the viewer does not save the document images on a nonvolatile memory or a disk. That eliminates chances of leak of the documents as image files either.

3. Technology

3.1 System configuration

Fig. 3 shows the configuration of the GT-Doc system. As mentioned above, it is a client-server system. The GT-Doc server consists of the document conversion server (hereinafter referred to as conversion server) that receives a request to view a document directly from the viewer and the document conversion engine (hereinafter referred to as conversion engine) that converts a document to an image, controlled by the document conversion server. The conversion server, besides controlling the conversion engine, acquires documents from other servers and manages print reservation with the Net Print Service.

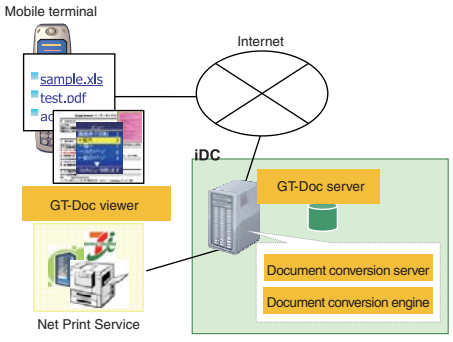

Fig. 3 The structure of GT-Doc system.

3.2 Document conversion engine

Besides converting documents sent from the conversion server to images, the document conversion engine processes converted images. For example, it crops a part of a document image.

We will first talk about the processing to convert documents to images. The conversion engine has its original document processing application and printer driver installed. On the application program, it looks like a virtual printer exists. The virtual printer prints a document as an image via the application. That creates a document image. The quality of the document image is as good as that of a computer printout of a document. The document image thus acquired is then returned to the conversion server. The conversion server saves it in the cache temporarily.

Next, we will talk about the processing of a part of a document image. When the user chooses to move, enlarge or reduce a document image on the GT-Doc viewer, the GT-Doc viewer requests the processing server for the area of the image to display. Upon receipt of the request, the processing server sends the converted document image to the processing engine again. The processing engine crops the requested area from the document image, reduces it in area size if necessary, and returns it to the conversion server. The conversion server sends this cropped image area to the GT-Doc viewer.

For the cropping and reducing, we use the very high speed codec[1)] we have been developing. While reducing the load on the conversion engine, it achieves the image with quality and data size that best suits display on a mobile terminal.

3.3 Document conversion server

The conversion server has Web APIs for our or your web systems and viewer applications.

The conversion server sends and receives documents and converted images to and from the conversion engine, sends and receives cropped image areas to and from the GT-Doc viewer, and manages the conversion engine states relating thereto.

The conversion server is also responsible for transmission of original documents. The server downloads a document from an external web server or uploads a document to the Net Print Service.

As a common protocol, HTTP(S), is used for data transmission, the GT-Doc system can link with the Net Print Service and other web services and other service providers can integrate the GT-Doc system into their systems.

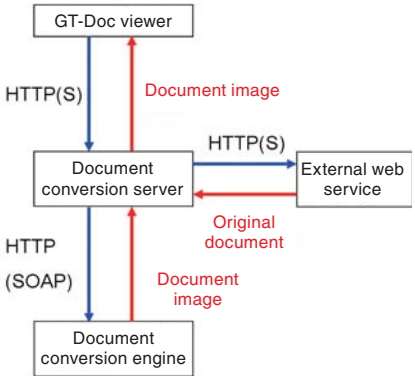

Fig. 4 The data flow in the GT-Doc system.

3.4 GT-Doc viewer

The viewer receives document images from the conversion server and displays them on the mobile terminal display. Using the arrow key, the user can move the image up and down and right and left. Number keys are used to enlarge or reduce the image, turn and return to the page, and move to thumbnail of the page list. The menu has options to reserve the Net Print Service, cancel the reservation, and display Help.

On most mobile terminals supporting touch panel operation, the above operations can be done by a touch panel, which allows intuitive operation.

It is ensured that the GT-Doc runs on diversified mobile terminals. The GT-Doc is designed to keep no data at all. These are the key features of the GT-Doc.

4. Evaluation

This section provides the result of performance comparison between the GT-Doc and other companies' document viewers installed on cell phones and smartphones.

4.1 Reproducibility

Fig. 5 shows the images of the same PowerPoint file displayed on the GT-Doc and a viewer built in a mobile terminal. The image on the built-in viewer has changed from the original in layout and design. The image on the GT-Doc is true to the original.

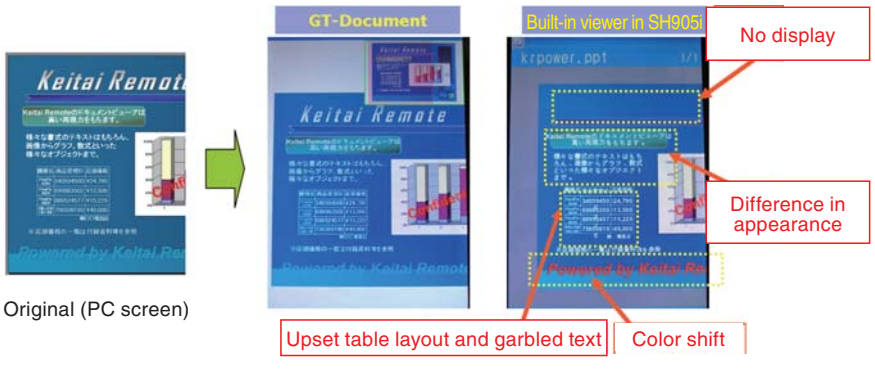

Fig. 5 Fidelity comparison between GT-Doc viewer and PDF viewer pre-installed on the mobile phone, SH905i.

4.2 Speed

Fig. 6 shows the measurements of speeds of downloading a document and displaying it. We used a PDF file of a one-page A4 size document with approximately 1 MB. We measured the downloading time (blue) from when the start link of the GT-Doc is clicked to when the document image appears on the screen. We also measured the opening time (dark red) from when a page is selected on the thumbnail screen to when the image of the page appears on the screen.

As shown by Fig. 6, it is apparent that the GT-Doc is better in download speed and opening speed than other document viewers.

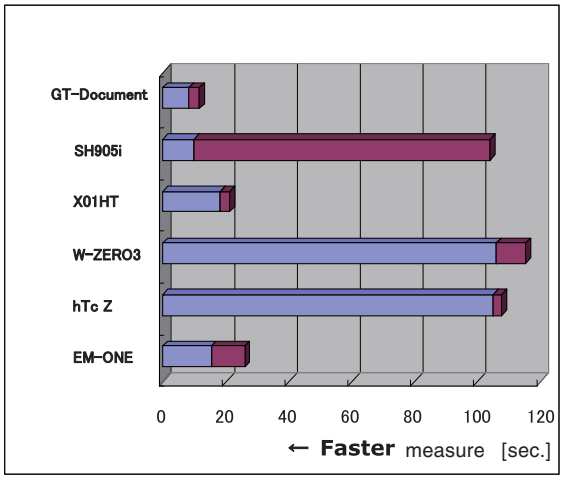

Fig. 6 Speed comparison with GT-Doc viewer and other document viewers (a blue portion: downloading time, a dark red portion: opening time).

5. Product example

5.1 beat Keitai Remote Service

The beat Keitai Remote Service is provided as an option in Fuji Xerox's beat/basic Service. It is the first service that incorporates the GT-Doc system.

For the beat/basic Service, an appliance server built by Fuji Xerox called beat-box is installed in the network of the client company. Keitai Remote Basic system is linked with the beat-box and makes it possible to view on a mobile terminal emails and files saved on the beat-box. The GT-Doc is used to display documents attached to those emails and document files saved in the shared folder on the beat-box.

5.2 Keitai Remote Mail Access NS/ES

While the beat Keitai Remote Service targets small and midsize firms, the Keitai Remote Mail Access NS/ES targets midsize and big businesses. We launched this service on December 3, 2009 as our original service.

While the beat Keitai Remote Service is connected to Fuji Xerox's beat-box, the Keitai Remote Mail Access NS/ES is connected to IBM's Lotus Notes Server and Microsoft's Exchange Server to enable sending and receiving of emails and viewing and editing of schedules on mobile terminals. The GT-Doc is used to view the files attached to emails and schedules.

5.3 GT-Document for Dropbox

GT-Document for Dropbox is distributed via iTunes App Store and Android Market as a free application running on iOS and Android devices. This application behaves as a file browser (or a file manager) and a document viewer and enables you to browse a file list and the content of a document file in your share folders on Dropbox which is one of the largest online storage service in the world.

6. Conclusion

The GT-Document provides an environment in which documents on an office PC can be viewed securely at home or any other remote locations. Books and newspapers are expected to go digital further. And it will become a way of life to view documents on mobile terminals. We will continue our effort to narrow differences in function and appearance between documents on a PC and those on a mobile terminal. We will also seek to improve the viewer to be a user-friendlier program that makes the most of the user interface specific to mobile terminals.

References

1) Arito Asai, Ta thi Quynh Lien, Shunichiro Nonaka and Norihisa Haneda. Very High Speed JPEG Codec Library. FUJIFILM RESEARCH & DEVELOPMENT. No.53, 13-17 (2008).

UDC 621.397.3-681.3.06

Development of New Image Processing Framework by the Collaboration of FUJIFILM and Fuji Xerox

Kazuyuki ITAGAKI*, Takashi IGARASHI*, Keiichi MORITA*, Mayuko IKUTA*,
Shin HAMAUZU*, Yuuki CHIBA*, Yusuke SUGIMOTO*,
Takashi NAGAO**, and Yukio KUMAZAWA**

Abstract

We developed a new image processing framework for different kinds of commercial products to reduce the development time and cost. Many of those products were independently designed for efficiency but without satisfying consumability and reusability, which have became increasingly important these days. To satisfy these requirements which have not been well considered, we have designed a new software framework based on the Pipes and Filters architectural pattern to orchestrate various combination of image processing modules. The framework provides a unified interface to easily develop modules to be orchestrated an flexibly customize the combination of modules in response to the various user requirements without significant performance degradation. It has been adopted by more than 20 products in the first two years and significantly reduced their development time and cost.

1. Introduction

To FUJIFILM (hereinafter referred to as FF), image processing technology is the source of product differentiation in photography, printing, medical care and various other fields. It is the fundamental technology and core technology to gain a competitive edge[1]. Achievements by those technologies are put into a group of our digital image processing software, called "Image Intelligence". The Image Intelligence has added values to our products[2].

Digital image processing technology is also the core technology for Fuji Xerox (hereinafter referred to as FX). FX has honed the technology for many years and created various added values particularly in the general office equipment market[3].

FF and FX have decided that both could beef up the competitiveness and development efficiency by utilizing each other's image processing technology. And, we have promoted a collaboration. However, the two companies' technologies differ in specification and structure. To evaluate fairly and make the most of each other's technology, we need to have a common basis for software to use as a mutually-agreed unified standard.

What is most required of the common software basis is versatility. The versatility here means applicability to the various business domains of both FF and FX. The existing technology of either company could not achieve sufficient versatility because of the following problems and trade-offs in pursuing versatility.

(1) Scalability of common software basis

It is difficult to expand common software basis to meet changes in operation environment or form of use. Such expansion requires a wide range of modifications.

(2) Ease of implementation of image processing functions

The structure is complicated and difficult to learn. It imposes a heavy workload on the developers in implementation.

(3) Efficiency and speed

If versatility is prioritized, an excess overhead and a decrease in speed may result, exceeding the tolerance level.

To solve the problems stated above and achieve versatility, we jointly developed the new common software basis, "FF/FX common image processing framework"[4]. A framework is a method of achieving reusability of software and a mechanism that provides the developers with a unified basis[5].

In this report, Section 2 describes the software structures of FF and FX's conventional technologies. Section 3 describes the structure of the FF/FX common image processing framework. Section 4 provides the evaluation of this framework on the problems stated above. Section 5 gives examples of application in products to show how much versatility is achieved.

Original paper (Received December 24, 2009)

* Software Research & Development Center
Research & Development Management Headquarters
FUJIFILM Corporation
Shin-yokohama, Kouhoku-ku, Yokohama, Kanagawa 222-0033, Japan

** System Technology Laboratory
Research & Technology Group
Fuji Xerox Co., Ltd.
Sakai, Nakai-machi, Ashigarakami-gun, Kanagawa 259-0157, Japan

2. Conventional Software Structure

Many of FF and FX's existing image processing software programs (frameworks) employ the Pipes and Filters architectural pattern[6]. Similar patterns are widely used in other companies' existing technologies. This report focuses on FF and FX's existing technologies and aims at improving those technologies.

In many conventional technologies using this pattern, performance is put before versatility in order to solve the problem (3) mentioned in Section 1. The problems (1) and (2) have not been sufficiently taken into consideration. Especially the problem (2) is significant. As a result of pursuing efficiency and speed, the structure has become complicated and imposed a heavy workload on the developers.

Many of these conventional technologies are optimized for particular purposes. They conflict with the versatility we pursue.

3. Structure of FF/FX Common Image Processing Framework

3.1 Design Policy

As described in Section 2, the Pipes and Filters architectural pattern, which is used for many conventional technologies, is effective for a system that handles data as a stream. It is suitable for image processing, however, it also has a drawback. Because data are handled as a stream, if an error occurs during processing, it is difficult to resume processing (error reset). However, the drawback rarely seems to be a critical problem, since the architectural pattern has been used in many of FF and FX's products and has shown successful results.

We have decided to use this Pipes and Filters architectural pattern for our new framework to achieve versatility by designing so as to solve the problems as described in Sections 1 and 2.

3.2 Overall Structure

Fig. 1 shows the structure of the new framework. The buffer module is the pipe and the image processing module is the filter of the Pipes and Filters architectural pattern. These are combined to build an image processing pipeline that does required processing. Next section provides detailed description of the main components of the framework shown in Fig. 1.

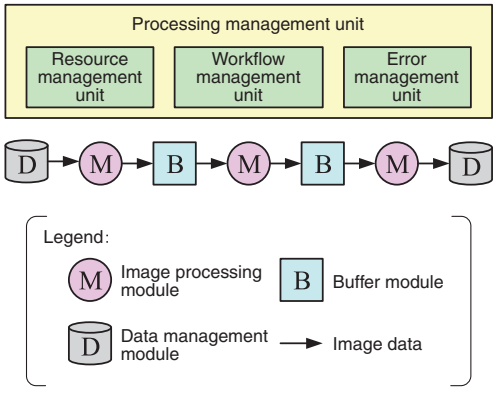

Fig. 1 Structure of developed framework.

3.3 Component

3.3.1 Image Processing Module

If encapsulating an image processing task to be finally implemented as a module, we won't be able to achieve versatility. Instead, we divide a required task into several single-function processing steps in accordance with the Pipes and Filters architectural pattern. We implement a series of image processing by combining those processing steps. Each of these processing steps is called the image processing module. Table 1 shows examples of image processing modules.

Table 1 Example of image processing module.

Classification	Functions
FF/FX common functions	Image format reading/writing (JPEG, TIFF, BMP, PNG, …), geometric transformation, color conversion, gradation conversion, composition, filtering, compression, decompression, …
FF function	Automatic image correction, facial skin smoothing, …

Combining several of the image processing modules according to the purposes, image processing is implemented.

Each image processing module carries out processing for the set unit data size. The unit data size is freely set to suit the type of processing the module implements, for example, data for one pixel, one line, several lines or the whole image. We call this data size a block. Because each image processing module does processing block by block, optimization for each individual purposes is possible, for example, increase in speed and reduction in memory usage. That makes the internal structure simpler and imposes a less workload on the developers in implementation. The image processing modules, after processing block by block, accomplishes processing of the whole image.

3.3.2 Buffer Module

The buffer module controls data exchange between the adjacent processing modules. The buffer module supplies or stores only the block the image processing modules request. The blocks image processing modules process vary from module to module. However, image processing modules with different block settings can coexist in the same image processing pipeline, thanks to the buffer module. Encapsulating complicated data control in the buffer module eases the workload on the developers and makes the image processing module flexible and reusable.

3.3.3 Processing Management Unit

The processing management unit consists of the resource management unit, the error management unit and the workflow management unit. The resource management unit controls securing and releasing of memory space for each module. The error management unit controls information on

the errors caused during processing and action against those errors. The workflow management unit controls flow of the processing by the image processing modules. The processing management unit covers the whole image processing pipeline.

The management and control methods of each management unit are not fixed. They can be expanded to suit the user's intension or the operation environment without having to make any changes in the program of the image processing module. The workflow management unit will be a good example. The following are examples of workflow management methods.

(1) Block-by-block workflow

Each image processing module passes over data for a block to next image processing module.

(2) Image-by-image workflow

Each image processing module processes data for the whole image and pass them to next image processing module.

(3) Parallel module workflow

The buffer module employs exclusion control. Each image processing module is assigned to a thread of execution and the image processing modules do processing in parallel.

4. Evaluation

We have evaluated this framework to see whether it overcomes the problems of the conventional technology described in Sections 1 and 2.

4.1 Scalability of Common Software Basis (Framework)

This framework has the processing management unit (resource, error and workflow management units) which covers the whole image processing pipeline, which the conventional technology does not have. These processing management unit makes it possible to expand the framework to meet changes in operation environment or form of use without any changes in the program of the image processing module.

4.2 Ease of Implementation of Image Processing Functions (Image Processing Module)

In the conventional technology, the block for the image processing module is fixed for the convenience of designing. That leads to a heavy workload on the developers in implementation. The image processing module of this framework is not subject to the restriction on block setting. The developers can select block setting freely. That helps keep the structure simpler. That also makes the implementation and optimization less demanding and reduces the workload on the developers in implementation of image processing modules.

4.3 Efficiency and Speed

As stated in Section 3, the image processing module and the buffer module of this framework are designed more versatile than the conventional modules. It is possible that the data control between these modules causes excess overhead and that a decrease in speed results, exceeding the tolerance level.

To check the overhead of data control between the image processing module and the buffer module, we have measured the processing time of several NOP (No OPeration) image processing modules linked together. Table 2 shows the two experiment environments. Fig. 2 shows the results of measurements using experiment images (a) and (b).

Table 2 Experimental environment.

Item	Configuration	
	Environment A	Environment B
CPU	Intel Core2Quad Q6700 2.66 GHz	Intel Pentium 4 Prescott 3.20 GHz
Memory	3.25 GB	2.00 GB
OS	Windows XP Professional SP2	
Compiler	Visual C++ 2005 SP1	

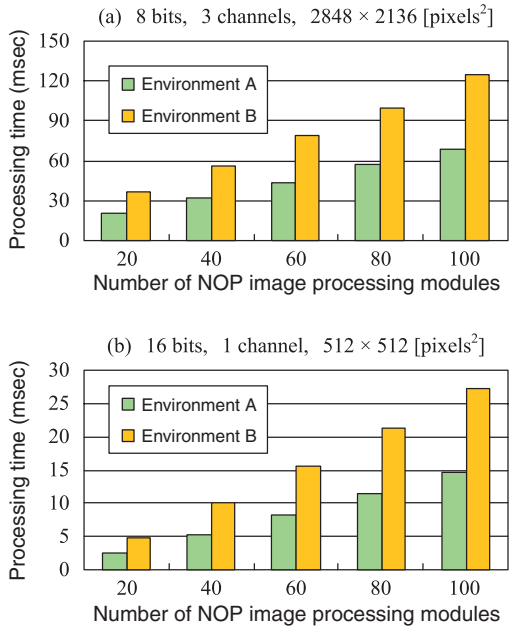

Fig. 2 Measurement results of data control overhead.

In the design of the framework, we have assumed the tolerance of the excess overhead of data control to be below 10 msec for every image processing module in processing of the size of an image as shown in Fig. 2 (a) in the environment B in Table 2. We have calculated the tolerance from the capabilities of FF and FX's conventional technologies and requirements by the product development departments.

As shown in Fig. 2, the excess overhead of data control is several msec. A decrease in the processing speed is within the tolerance.

5. Application in Products

5.1 Examples of Application

To date, this framework has been used in several tens of FF and FX's products, for example, medical diagnostic equipment, color conversion software for printing, digital MFP and document management software. The framework is used for general purposes in a wide range of business fields, such as medical care, printing, photography and documentation. Not only applied in products, the framework is also being increasingly introduced to our core technology research departments. It is gaining ground as a common software basis for FUJIFILM Group.

5.2 Reduction in Development Man-Hours

Introducing this framework will increase reuse of image processing functions (image processing modules) and eliminate redundant development in FF and FX. That will reduce the development man-hours on image processing functions during product development.

We have calculated the development man-hours in product development by FF and FX in fiscal 2008. The number of development man-hours was reduced by approximately 120 man-months. We expect the development efficiency will be enhanced further.

6. Conclusion and Outlook

This paper has reported on the FF/FX common image processing framework, a common basis for image processing software used as FF and FX's unified standard.

With FF and FX's conventional technologies, if pursuing the versatility we require, we will have problems concerning scalability of the common software basis, ease of implementation of image processing functions, and efficiency and speed. To solve these problems, we have come up with a new common software basis, the FF/FX common image processing framework. This framework has been designed in accordance with the proven Pipes and Filers architectural pattern, which is used in the conventional technologies. The new framework has the following features.

* The processing management unit makes it possible to expand the framework to meet changes in operation environment or form of use.
* The processing data size (block) is freely set for each image processing module and reduces a workload on the developers in implementation.
* The excess overhead of data control between the image processing module and the buffer module does not exceed the tolerance level we have assumed. A decrease in speed is small.

The framework is used in FF and FX's products in various business fields, verifying that the versatility has been achieved.

Although we did not go into details in this report, using the workflow management method (3) described in Section 3.3.3, it is possible to operate image processing modules in parallel. That means this framework is capable of working in the multi-core CPU environment, which is now in the mainstream. Further expansion is expected. We are planning to apply this framework in more products and services.

References

1) "Fundamental and Core Technologies". FUJIFILM Holdings Corporation. http://www.fujifilmholdings.com/en/rd/technology/detail/index.html.
2) Takemoto, Fumito; Yoda, Akira. High Quality Image Processing Technology "Image Intelligence". FUJIFILM RESEARCH & DEVELOPMENT. No.49, 49-54 (2004).
3) Saito, Kiyoshi. Digital imaging technology at Fuji Xerox. Fuji Xerox Technical Report No.16, 4-10 (2006).
4) Nagao, Takashi; Kumazawa, Yukio; Seki, Noriaki; Kaneko, Yasuhiko; Kaneko, Junichi. Fuji Xerox Co., Ltd., FUJIFILM Holdings Corporation. Image Processor, Method and Program. JP2006-338498A, JP2006-338505A. 2006-12-14.
5) Johnson, Ralph E. et al. Pattern and Framework. Tokyo, Kyoritsu Shuppan, 1999, 264p.
6) Buschmann, F. et al. Pattern Oriented Software Architecture: A System of Patterns. Tokyo, Kindai Kagaku sha, 2000, 454p.